



Publicly Accessible Penn Dissertations


Spring 5-17-2010

Functions of DNA Damage Response Factors in Lymphocyte Development and Transformation

Bu Yin

University of Pennsylvania School of Medicine, buyin@mail.med.upenn.edu

Follow this and additional works at: <http://repository.upenn.edu/edissertations>

 Part of the [Cancer Biology Commons](#), [Immunity Commons](#), and the [Molecular Biology Commons](#)

Recommended Citation

Yin, Bu, "Functions of DNA Damage Response Factors in Lymphocyte Development and Transformation" (2010). *Publicly Accessible Penn Dissertations*. 410.

<http://repository.upenn.edu/edissertations/410>

This paper is posted at Scholarly Commons. <http://repository.upenn.edu/edissertations/410>

For more information, please contact libraryrepository@pobox.upenn.edu.

Functions of DNA Damage Response Factors in Lymphocyte Development and Transformation

Abstract

DNA double strand breaks (DSBs) can activate cell cycle checkpoints or apoptosis, and lead to genomic alterations that drive malignant transformation. The H2AX core histone variant is phosphorylated in chromatin around DSBs by kinases such as ATM and DNA-PKcs. However, how H2AX suppresses chromosome breaks and translocations in cells and prevents tumorigenesis in mice and humans is not well understood. V(D)J recombination is a genetically programmed DNA damage and repair process that assembles the variable region exons of antigen receptor genes in developing lymphocytes. Using an inducible V(D)J recombination system, I found that H2AX is phosphorylated along cleaved antigen receptor loci DNA strands, prevents their irreversible separation in G1 phase, and reduces chromosome breaks and translocations in subsequent cell cycles. Consistent with H2AX functions in DSB repair, I also demonstrated that conditional H2AX deletion results in accumulation of genomic instability in cells, but delays tumor onset in a mouse thymic lymphoma model, presumably due to increased death of cells with synthetic loss of multiple repair factors. To further test this possibility, I generated cells and mice deficient in both H2AX and ATM to examine whether ATM-independent H2AX functions downstream of other kinases are essential for proper DSB repair. I found that thymocyte-specific ablation of H2AX in ATM-deficient mice results in a 50% reduction in thymus cellularity but does not accelerate or delay tumorigenesis. My results suggest that the outcomes of functional interactions between DNA damage response factors likely depend on the cellular context. Additionally, I discovered a novel function of ATM in regulating mono-allelic recombination at the immunoglobulin light chain locus. ATM could orchestrate the signaling pathways enforcing allelic exclusion to provide a time window to test whether the rearrangement on the first allele is productive. In summary, my work has provided novel mechanistic insights into how DNA damage and repair factors coordinately regulate V(D)J recombination, lymphocyte development and neoplastic transformation.

Degree Type

Dissertation

Degree Name

Doctor of Philosophy (PhD)

Graduate Group

Cell & Molecular Biology

First Advisor

Craig H. Bassing, PhD

Keywords

DNA Damage and Repair, V(D)J Recombination, H2AX, ATM, Lymphoma, Allelic Exclusion

Subject Categories

Cancer Biology | Immunity | Molecular Biology

FUNCTIONS OF DNA DAMAGE RESPONSE FACTORS IN LYMPHOCYTE
DEVELOPMENT AND TRANSFORMATION

Bu Yin

A DISSERTATION

in

Cell and Molecular Biology

Presented to the Faculties of the University of Pennsylvania

in Partial Fulfillment of the Requirements for the Degree of Doctor of Philosophy

2010

Supervisor of Dissertation

Craig H. Bassing, PhD, Assistant Professor, Pathology and Laboratory Medicine

Graduate Group Chairperson

Daniel S. Kessler, PhD, Associate Professor, Cell and Developmental Biology

Dissertation Committee

Shelley L. Berger, PhD, University Professor, Cell and Developmental Biology

Tom Curran, PhD, FRS, Professor, Pathology and Laboratory Medicine

Zissimos Mourelatos, MD, Associate Professor, Pathology and Laboratory Medicine

Warren S. Pear, MD, PhD, Professor, Pathology and Laboratory Medicine

M. Celeste Simon, PhD, Professor, Cell and Developmental Biology

DEDICATION

I dedicate this thesis to my parents, who raised me, cared for me, and had to get used to living without me being around, just because they love me and have always had faith in me.

ACKNOWLEDGEMENTS

I would like to thank my advisor Dr. Craig H. Bassing for his generous support, without which I would not have achieved what I have now. Thank you for your encouragement in my research, your guidance at and beyond the bench, and your efforts in helping me to become a better scientist and a better person in general. I am indebted to all current and past Bassing lab members, especially Andrea Carpenter, Velibor Savić and Beth Nuskey, for teaching me the essential techniques, Brenna Brady, Natalie Steinel, Marta Rowh and Angela Fusello for discussions, and Katherine Yang-Iott for making the lab feel like home. A lot of thanks also go to the Cancer Biology/Cell and Molecular Biology graduate group at Penn. The excellent faculty members and many exceptional graduate students have been tremendous role models. Among them I would like to acknowledge my thesis committee, Dr. Tom Curran, Dr. Shelley L. Berger, Dr. Warren S. Pear, Dr. Zissimos Mourelatos, and my chair Dr. M. Celeste Simon, for their support and scientific advice. Marisa Juntilla from Dr. Gary Koretzky's lab was instrumental in the work described in Chapter II. Dr. Aaron Gitler has been very supportive in my job search. I would also like to acknowledge my collaborators, Dr. Barry P. Sleckman together with Grace Mahowald, Beth Helmink, Eric Gapud and Andrea Bredemeyer from Washington University at St. Louis. Without their pioneering work and sharing of expertise and reagents, most of my work would not have been possible. I've also enjoyed collaborations with Dr. Jane Skok's lab at New York University, and with Dr. Larry Turka's lab at Penn. I thank Xiaohe Liu from the Turka lab for being a close friend.

ABSTRACT

FUNCTIONS OF DNA DAMAGE RESPONSE FACTORS IN LYMPHOCYTE DEVELOPMENT AND TRANSFORMATION

Bu Yin

Advisor: Craig H. Bassing

DNA double strand breaks (DSBs) can activate cell cycle checkpoints or apoptosis, and lead to genomic alterations that drive malignant transformation. The H2AX core histone variant is phosphorylated in chromatin around DSBs by kinases such as ATM and DNA-PKcs. However, how H2AX suppresses chromosome breaks and translocations in cells and prevents tumorigenesis in mice and humans is not well understood. V(D)J recombination is a genetically programmed DNA damage and repair process that assembles the variable region exons of antigen receptor genes in developing lymphocytes. Using an inducible V(D)J recombination system, I found that H2AX is phosphorylated along cleaved antigen receptor loci DNA strands, prevents their irreversible separation in G1 phase, and reduces chromosome breaks and translocations in subsequent cell cycles. Consistent with H2AX functions in DSB repair, I also demonstrated that conditional H2AX deletion results in accumulation of genomic instability in cells, but delays tumor onset in a mouse thymic lymphoma model, presumably due to increased death of cells with synthetic loss of multiple repair factors. To further test this possibility, I generated cells and mice deficient in both H2AX and ATM to examine whether ATM-independent H2AX functions downstream of other

kinases are essential for proper DSB repair. I found that thymocyte-specific ablation of H2AX in ATM-deficient mice results in a 50% reduction in thymus cellularity but does not accelerate or delay tumorigenesis. My results suggest that the outcomes of functional interactions between DNA damage response factors likely depend on the cellular context. Additionally, I discovered a novel function of ATM in regulating mono-allelic recombination at the immunoglobulin light chain locus. ATM could orchestrate the signaling pathways enforcing allelic exclusion to provide a time window to test whether the rearrangement on the first allele is productive. In summary, my work has provided novel mechanistic insights into how DNA damage and repair factors coordinately regulate V(D)J recombination, lymphocyte development and neoplastic transformation.

TABLE OF CONTENTS

Title Page	<i>i</i>
Dedication	<i>ii</i>
Acknowledgements	<i>iii</i>
Abstract	<i>iv</i>
Table of Contents	<i>vi</i>
List of Figures	<i>viii</i>
List of Tables	<i>x</i>
Chapter I – Introduction	1
DNA Damage and Repair Mechanisms Are Essential for Tumor Suppression	2
DNA Double Strand Break Response and Repair within Chromatin	3
H2AX Phosphorylation Is a Hallmark of Chromosomal DSB Response	9
V(D)J Recombination is a Physiological DNA Damage and Repair Process	15
Novel Cell Line Systems and Mouse Models to Study H2AX Functions	20
DNA Damage Signals and Mono-allelic V(D)J Recombination	26
Chapter II – Histone H2AX Stabilizes Broken DNA Strands to Suppress Chromosome Breaks and Translocations in V(D)J Recombination	35
ABSTRACT	36
INTRODUCTION	37
RESULTS	40
DISCUSSION	54
FIGURES AND FIGURE LEGENDS	59
Chapter III – Cellular Context Dependent Effects of <i>H2ax</i> and <i>p53</i> Deletion Upon Development of Thymic Lymphoma	74
ABSTRACT	75
INTRODUCTION	76
RESULTS	80
DISCUSSION	91
FIGURES, FIGURE LEGENDS AND TABLES	96
Chapter IV – Functional Interactions Between ATM and H2AX in Lymphocyte Development, Recombination and Tumorigenesis	115
ABSTRACT	116
INTRODUCTION	117

RESULTS	119
DISCUSSION	126
FIGURES, FIGURE LEGENDS AND TABLES	130
Chapter V – ATM-dependent DNA Damage Signals Prevents Biallelic Igc Chromosome Breaks	137
ABSTRACT	138
INTRODUCTION	140
RESULTS	143
DISCUSSION	147
FIGURES AND FIGURE LEGENDS	150
Chapter VI – Summary and Discussion	154
Chapter VII – Materials and Methods	164
Chapter VIII – References	170

LIST OF FIGURES

Figure 1. Model for signal propagation and amplification in DDR	30
Figure 2. Model for the chromosomal V(D)J recombination reaction	31
Figure 3. Defective repair of DSB intermediates in V(D)J recombination can lead to chromosome breaks/translocations	32
Figure 4. Inducible V(D)J recombination in the Abelson cell lines	34
Figure 5. H2AX is not required for normal resolution of V(D)J recombination intermediates of chromosomally integrated pMX-INV in G1 abl cells	59
Figure 6. H2AX deficient cells exhibit normal coding join formation within chromosomal substrates	61
Figure 7. No accumulation of J κ coding ends in the absence of H2AX phosphorylation along RAG cleaved Ig κ DNA strands	63
Figure 8. H2AX suppresses separation of RAG cleaved Ig κ locus DNA strands	65
Figure 9. Quantification of Ig κ cutting following STI571 induction of the cell lines used in 2D-2C-FISH	67
Figure 10. H2AX prevents transition of RAG cleaved Ig κ DNA strands into chromosome breaks and translocations during cellular proliferation	68
Figure 11. OP9-DL1 feeder cell metaphases can be separated from lymphocyte spreads	70
Figure 12. H2AX prevents chromosome breaks emanating from un-repaired TCR α/δ locus coding ends in primary thymocytes	71
Figure 13. Models of H2AX function during end-joining repair of chromosomal DSBs	73
Figure 14. Mice with somatic inactivation of <i>H2ax</i> and <i>p53</i> in thymocytes succumb to clonal thymic lymphomas	96
Figure 15. <i>LHP</i> thymic lymphomas harbor translocations that arise from spontaneous and programmed DNA breakage	100
Figure 16. Combined inactivation of <i>H2ax</i> and <i>Artemis</i> in <i>p53</i> -deficient thymocytes reduces the rate of mortality of mice from thymic lymphoma	103
Figure 17. <i>LAP</i> and <i>LAHP</i> thymic lymphomas exhibit distinct patterns of genomic instability	110
Figure 18. <i>LAHP</i> thymic lymphomas exhibit increased genomic instability as compared to <i>LAP</i> and <i>LHP</i> tumors	114
Figure 19. Characterization of thymic and splenic T cell development in <i>LH</i> , <i>LA</i> and <i>LAH</i> mice	130
Figure 20. Genomic instability of stimulated splenic T cells from one <i>LAH</i> mice analyzed by SKY	132

Figure 21. Conditional inactivation of <i>H2ax</i> in <i>Atm</i> -deficient thymocytes does not alter thymic lymphoma development or pattern of genomic instability	133
Figure 22. ATM prevents the biallelic cleavage and dissociation of Igκ coding ends and biallelic chromosome breaks or translocations	150
Figure 23. No single ATM substrates tested fully recapitulates the <i>Atm</i> ^{-/-} phenotype	153
Figure 24. Proposed model to explain delayed tumor development in <i>LAHP</i> mice compared to <i>LAP</i> mice	162

LIST OF TABLES

Table 1. Characterization of <i>LHP</i> Cohort Mice	98
Table 2. SKY Analysis of <i>LHP</i> Tumors	102
Table 3. Characterization of <i>LAP</i> Cohort Mice	106
Table 4. Characterization of <i>LAHP</i> Cohort Mice	108
Table 5. SKY Analysis of <i>LAP</i> Tumors	112
Table 6. SKY Analysis of <i>LAHP</i> Tumors	113
Table 7. Characterization of <i>LckCreAtm^{-/-}</i> Cohort Mice	135
Table 8. Characterization of <i>LckCreAtm^{-/-}H2ax^{F/F}</i> Cohort Mice	136

Chapter I

Introduction

DNA Damage and Repair Mechanisms Are Essential for Tumor Suppression

The existence of most life forms depends on the stability of the genomes and the fidelity of genomic replication, despite constant assaults to the genetic materials by endogenous and exogenous agents (Lindahl and Barnes, 2000). To counter these threats, multiple layers of DNA damage recognition and repair mechanisms have evolved, and defects in these pathways are closely related to cellular and organism survival and aging, and development of human diseases including cancers (Rouse and Jackson, 2002; Harrison and Haber, 2006; Harper and Elledge, 2007; Jackson and Bartek, 2009).

DNA damage is common and constantly occurring. It is estimated that each of the cells in the human body (approximately 10^{13} cells in total) receives thousands of DNA lesions every day (Lindahl and Barnes, 2000). These lesions can arise during DNA replication in S phase, in which abortive topoisomerase activities can lead to DNA strand breaks. They can also arise in any cell cycle phases from exogenous factors like ionizing radiation (IR) and ultraviolet light (UV), or endogenous processes such as oxidative stress and DNA hydrolysis. Attacks on DNA can generate base losses, adducts that impair base pairing, or DNA single-strand breaks (SSBs). In addition, double-strand breaks (DSBs) can result from two SSBs in close proximity, replication through SSBs or other DNA lesions, collapsed replication forks, or endonuclease cleavage. If left unrepaired or erroneously repaired, DNA lesions can block transcription and genome replication, leading to impaired cellular functions, cell cycle arrest or cell death (Figure 1). Such persistent DNA lesions may also result in mutations or large-scale genome aberrations, such as chromosome breaks or translocations, that can confer growth

advantages to incipient cells, leading to their malignant transformation. Indeed, chromosome translocations that activate oncogenes and chromosome deletions that inactivate tumor suppressor genes are frequently found in many human tumors (van Gent et al., 2001; Hoeijmakers, 2001; Thompson and Schild, 2002; Mills et al., 2003; Jackson and Bartek, 2009).

DSBs are among the most hazardous forms of DNA lesions, since liberated DNA ends are difficult to repair and can separate irreversibly or join promiscuously (Khanna and Jackson, 2001). Mutations of DSB repair factors result in increased cellular sensitivity to DSBs, elevated levels of spontaneous genomic instability, and are closely associated with an increased predisposition to cancers in both mice and humans (Mills et al., 2003). In addition, many cancer cells also have subverted the cell cycle checkpoint activation and cell death mechanisms to allow survival and proliferation of premalignant cells and further neoplastic transformation (Dasika et al., 1999). Thus, understanding how the DNA damage response (DDR) coordinates DNA repair with cell fate determination is crucial to better prevent, diagnose and treat human malignancies.

DNA Double Strand Break Response and Repair within Chromatin

DNA in eukaryotic cells is packaged into chromatin, a highly organized and dynamic DNA/protein polymer. Since chromatin is the native environment in which DNA damage and repair must occur, how chromatin dynamics contributes to the initiation, propagation and termination of the DDR has been the focus of recent studies (Downs et al., 2007).

The most basic pattern of chromatin organization is ~147 base pairs of DNA wrapped around a histone octamer core, which is composed of two of each core histones H2A, H2B, H3 and H4, to form a nucleosome (Downs et al., 2007). Each of these histones has a globular core domain, as well as an unstructured N-terminal tail domain that protrude from the nucleosome core. Histones H2A and H2B also possess functionally important C-terminal tails. In higher eukaryotes, each histone subtype, with the possible exception of histone H4, contains a family of genes encoding multiple variants that have altered amino acid sequences that may confer unique functions (Brown, 2001). Core histones, including their variants, can be covalently modified by a myriad of histone marks, including phosphorylation, acetylation, methylation, ubiquitylation and sumoylation (Strahl and Allis, 2000). These covalent modifications can alter chromatin structure via selectively allowing binding of non-histone effector proteins. The combination of the covalent histone marks and the non-covalently bound effector proteins constitute a code that regulates diverse processes such as transcription, DNA replication, and DNA damage and repair (Strahl and Allis, 2000; Downs et al., 2007). Between nucleosomes there are nucleosome-free regions where linker histones and high-mobility group proteins can bind to regulate chromatin configuration and compaction. In addition, a number of chromatin-remodeling complexes can alter histone-DNA contacts by histone eviction, exchange of histone variants, nucleosome sliding and changing the accessibility of particular DNA elements (Downs et al., 2007). Thus, DNA damage within chromatin may elicit chromatin remodeling, unmask constitutive histone marks normally concealed in unperturbed cells, or induce additional histone

modifications, making damaged DNA more accessible and coordinating DNA damage response and repair.

In all mammalian cells, DSBs can arise accidentally following collapse of stalled replication forks during DNA replication, or by exogenous factors such as IR. During lymphocyte development, DSBs are also imperative intermediates during antigen receptor gene rearrangement reactions such as V(D)J recombination (Figure 2) and B cell class switch recombination (CSR), which are essential processes for the generation of fully functional adaptive immune systems (Bassing et al., 2002a; Chaudhuri et al., 2007). Whichever source they are from, DSBs pose a major threat to genome integrity since they can lead to mutations, chromosome deletions and oncogenic translocations. Thus, eukaryotic cells have evolved sophisticated and redundant genome surveillance mechanisms to rapidly signal the presence of DSBs, initiate DNA repair, and coordinate repair with cell cycle progression and cell survival decisions (Figure 1) (Rouse and Jackson, 2002; Harrison and Haber, 2006; Harper and Elledge, 2007; Jackson and Bartek, 2009).

The DDR is executed coordinately by a constellation of sensor, transducer and mediator/effector proteins (Figure 1). While the mechanisms by which DNA breaks are initially sensed remain elusive and may vary depending on the context, the recognition of DNA damages generally leads to rapid activation of the transducer kinases Ataxia Telangiectasia Mutated (ATM) (Andegeko et al., 2001; Burma et al., 2001), DNA-dependent protein kinase catalytic subunit (DNA-PKcs) (Park et al., 2003) and/or

ATM/Rad3-like (ATR) (Furuta et al., 2003; Zou and Elledge, 2003). These three kinases belong to the phosphoinositide 3-kinase (PI3K) superfamily, and optimal kinase activation/function following DNA damage critically depends on their interactions with the DNA ends and/or chromatin and associated factors. Active ATM/ATR/DNA-PKcs kinases can then activate, among others, effector kinases such as Chk1 or Chk2 (Dasika et al., 1999; Matsuoka et al., 2007). Together with ATM and ATR, Chk1 and Chk2 act to reduce cyclin-dependent kinase (CDK) activity by various mechanisms, slowing down or arresting cell cycle progression (Jackson and Bartek, 2009). In mammalian cells, Chk1 is the primary effector to activate intra-S and G2/M phase checkpoints, while Chk2 contributes to intra-S and G1/S checkpoint activation. ATM/Chk2-mediated stabilization of the p53 transcription factor is essential for effective G1/S checkpoint activation (Bartek and Lucas, 2007). The consequences of DDR signaling include cell cycle arrest to allow time for repair of such breaks, or cell death in cases where DSB repair cannot be easily accomplished.

Mammalian cells have evolved distinct yet complementary DSB repair pathways that are conserved among species to ensure genomic stability. DSBs generated in post-replicative cell cycle phases are primarily repaired by homologous recombination (HR), whereas DSBs generated in G1-phase cells are repaired through non-homologous end joining (NHEJ) (Lieber et al., 2003; Rooney et al., 2004b; Wyman et al., 2004). HR involves two major sub-pathways, sister chromatid recombination (SCR) and single strand annealing (SSA). SCR is generally limited to late S and G2 phases of the cell cycle and uses information from sister chromatids, which are readily available homologous

templates, to accurately repair breaks (Wyman et al., 2004). In contrast, NHEJ mediates the joining of DSB ends independent of extensive homology, and is the principle mechanism used in G1 phase although it is functional throughout the cell cycle (Lieber et al., 2003; Rooney et al., 2004b). SSA also involves ssDNA intermediates, but repair proceeds through the annealing of complementary sequences on the same strand with deletion of intervening sequences. Thus, SSA is error-prone; and, as it often utilizes repetitive elements dispersed along a chromosome, SSA deletes much larger genomic sequences than NHEJ. Although both HR and NHEJ are important for the well-being of cells and organisms, only NHEJ is discussed in detail due to the focus of my thesis.

The NHEJ machinery is conserved from yeast to human and consists of factors with functions such as end stabilization, end processing and end ligation. In yeast, the Mre11/Rad50/Xrs2 (MRX) and Ku complexes are among the first to bind DSB ends, where they serve to protect the ends from degradation and bridge the two termini to prevent their irreversible separation (Daley et al., 2005). In vertebrates Ku70/80 forms a trimeric complex with the catalytic subunit DNA-PKcs, and the holoenzyme DNA-PK is activated upon loading onto DSB ends. Besides its DNA end-bridging role, DNA-PK may also recruit, stabilize and stimulate the ligase complex LigIV/XRCC4/XLF and allow end re-joining to occur (Mahaney et al., 2009). It is estimated that approximately 10-15% of IR-induced DSBs are dependent on the exonuclease Artemis, whose endonuclease activity is activated through phosphorylation by DNA-PKcs, to process hairpin-like structures that are incompatible with end-joining (Riballo et al., 2004). Other DNA nucleases and polymerases can also be mobilized to delete or add nucleotides

before ends are ligated, making NHEJ an inherently imprecise way of DNA repair (Lieber et al., 2003).

One of the earliest events and an important component of eukaryotic DSB response is the phosphorylation of the C-terminal SQE motif (phosphorylation site Ser139) on the histone variant H2AX within chromatin around DSB sites, forming γ H2AX that can be visualized microscopically as foci with phospho-specific antibodies or detected by chromatin immunoprecipitation (ChIP) around site specific DSBs (Rogakou et al., 1998; Rogakou et al., 1999; Bonner et al., 2008; Savić et al., 2009). H2AX represents 2-25% of the cellular H2A pool and can be incorporated into nucleosomes together with other core histones (Rogakou et al., 1998; Bewersdorf et al., 2006). H2AX phosphorylation and γ H2AX foci formation is of fundamental importance to further signaling at the break (Figure 1) (Downs et al., 2007; Bonner et al., 2008). An attractive model has been proposed to emphasize the importance of this phosphorylation event. Upon DNA damage, sensors such as the MRE11/RAD50/NBS1 (MRN, homolog of the yeast MRX complex) complex can recognize un-repaired DSBs (Paull et al., 2000; Carson et al., 2003; Difilippantonio et al., 2005; Horejsí et al., 2004; Lee and Paull, 2005; Uziel et al., 2003), to which ATM is recruited and activated within chromatin (Bakkenist and Kastan, 2003). Phosphorylation of H2AX by ATM then provides a binding site for DDR factors including MRN, MDC1 and 53BP1, all of which can be phosphorylated and activated by ATM (Downs et al., 2007; Bonner et al., 2008). The accumulation of these DDR factors and chromatin conformation changes around the breaks may potentiate activation of ATM, which in turn, phosphorylates more H2AX in adjacent chromatin,

leading to a propagation of γ H2AX signal into chromatin around the breaks and amplification of DDR signals (Figure 1) (Lou et al., 2006).

H2AX Phosphorylation Is a Hallmark of Chromosomal DSB Response

Formation of γ H2AX foci after DNA damage has been widely used as an indicator of DSB induction. Recent studies of protein-protein/protein-DNA interactions have started to unravel the molecular architectures of the multi-component complexes within the DNA damage foci. Among the many molecular interactions with γ H2AX, the tandem BRCA1 carboxyl-terminal (BRCT) domain of MDC1 appears to be the primary γ H2AX recognition module in higher eukaryotes (Stucki and Jackson, 2006). MDC1 mediates efficient foci formation by other DDR factors including the MRN complex, BRCA1, PIP and likely also 53BP1 (Stucki and Jackson, 2006; Gong et al., 2009). However, there are factors, such as MCPH1/BRIT1, that form DNA damage-induced foci in an H2AX-dependent but MDC1-independent manner (Wood et al., 2007). In this regard, although H2AX is not required for the initial recruitment of DDR factors, γ H2AX can facilitate DSB repair by retention of repair factors at the breaks sites (Celeste et al., 2003a). The chromatin changes conferred by the γ H2AX-recruited DDR complexes have been proposed to anchor broken DNA ends in proximity, thus function more directly in end joining (Bassing and Alt, 2004). When repair is completed, removal of γ H2AX might be crucial for restarting the cell cycle, and this could be accomplished by nucleosome exchange or eviction from chromatin, or dephosphorylation via phosphatases such as PP2A and PP4 (Chowdhury et al., 2005; Nakada et al., 2008).

The MRN complex is required for the initial detection of DSBs and several effector pathways, in agreement with its role as an upstream activator and a downstream target of ATM (Uziel et al., 2003; Lee and Paull, 2004; Lee and Paull, 2005; Difilippantonio et al., 2005). Although a direct function of ATM in HR remains controversial, the involvement of MRN components in HR has been documented. First, the endonuclease and exonuclease activities of Mre11 might be involved in DNA end processing (D'Amours and Jackson, 2002; Stracker et al., 2004). Second, Rad50 has ATPase and adenylate kinase activities that may be required for DNA tethering (D'Amours and Jackson, 2002; Stracker et al., 2004; Bhaskara et al., 2007). Besides, Rad50 has N- and C-terminal Walker A and B nucleotide binding motifs, respectively, that form a DNA binding domain upon their intra-molecular association. This association also leads to the formation of a central Rad50 hook domain (D'Amours and Jackson, 2002; Stracker et al., 2004), which can facilitate the tethering of two distinct MRN-bound DNA molecules through an inter-molecular interaction of two Rad50 hook domains (Anderson et al., 2001; de Jager et al., 2001; Hopfner et al., 2002; Wiltzius et al., 2005; Moreno-Herrero et al., 2005). Since ATM phosphorylates Mre11, RAD50 and NBS1 in response to DNA DSBs, ATM may modulate HR repair by regulating MRN effector functions (Gatei et al., 2000; Wu et al., 2000; Lim et al., 2000; Matsuoka et al., 2007). So far no enzymatic activities have been attributed to NBS1; nevertheless, it's an essential DDR mediator due to its interactions with γ H2AX, ATM and MDC1, among others. In light of the strikingly different phenotypes of several NBS1 mutants, MRN might mediate checkpoint activation and apoptosis induction in response to DSBs through distinct molecular domains on NBS1 (Difilippantonio et al., 2007; Stracker et al., 2007). Furthermore, the mammalian MRN

complex was recently shown to also play an important role in NHEJ, likely by bridging and stabilizing DSB ends (Helmink et al., 2009; Deriano et al., 2009; Xie et al., 2009; Dinkelmann et al., 2009; Rass et al., 2009).

MDC1 is a major γ H2AX recognition module in higher eukaryotes. MDC1 modulates S-phase and G2/M checkpoint activation after DNA damage and mediates efficient foci formation by other DDR factors (Stucki and Jackson, 2006). Importantly, docking of MDC1 on γ H2AX has been postulated to facilitate the local accumulation of ATM in damaged chromatin, where activated ATM phosphorylates adjacent H2AX, generating a positive feedback loop that leads to γ H2AX spreading into surrounding chromatin and amplification of DNA damage signals (Stucki and Jackson, 2006; Lou et al., 2006). Recent work using an inducible V(D)J recombination system in mammalian cells has show that the γ H2AX densities equilibrate within a fixed distance from break sites, and MDC1 is essential for γ H2AX formation at high densities near DSBs (Savić et al., 2009). This in part could be due to that MDC1 bound to γ H2AX might prevent phosphatase access to the phosphoepitope. Most recently the phosphorylated SDT repeats of MDC1 have been shown to dynamically associate with NBS1 in undamaged cells, and mediate chromatin retention of MRN after concentration of MDC1 around DSB sites (Melander et al., 2008; Spycher et al., 2008; Chapman and Jackson, 2008). These results confirmed a pivotal role of MDC1 in the relay and amplification of DDR signals.

γ H2AX-dependent MDC1 accumulation at the breaks site also orchestrates the subsequent phospho-dependent recruitment of RNF8-dependent proteins, linking histone

phosphorylation with ubiquitylation (Stewart, 2009). RNF8 is an E3 ubiquitin ligase and through its FHA domain, interacts with a conserved TQXF motif on MDC1 following its phosphorylation by ATM in chromatin. Recruitment of RNF8 to phosphorylated MDC1, in conjunction with the E2 ubiquitin conjugating enzyme, UBC13, catalyses poly-ubiquitylation of H2AX and other H2A histones surrounding DSBs (Huen et al., 2007; Kolas et al., 2007; Mailand et al., 2007; Wang et al., 2007). Another E3 ubiquitin ligase RNF168 was recently found to function downstream of RNF8 to ubiquitylate more H2A molecules (Stewart et al., 2009; Doil et al., 2009). The ubiquitylation events around DSB sites may provide binding sites for additional factors, or configure the chromatin into a more accessible conformation, allowing concealed epigenetic marks such as histone methylation to recruit additional, albeit kinetically slower, component of the DDR cascade (Stewart, 2009).

One such component of the DDR response is 53BP1, which is phosphorylated by ATM and contains a potential γ H2AX-binding motif. Curiously, this tandem BRCT domain is not required for its repair function; instead, its tandem Tudor motifs bind to methylated H3K79 or H4K20 and target 53BP1 to sites of DSBs. The chromatin conformational changes following DSB induction, as discussed above, can expose these constitutively methylated histone marks, providing sites for the initial recruitment of 53BP1 (van Attikum and Gasser, 2009). However, 53BP1 foci form at a slower kinetics than those of γ H2AX, MDC1 or NBS1, and absence of any of these factors impairs 53BP1 foci formation (van Attikum and Gasser, 2009), presumably because these factors are necessary to potentiate 53BP1 retention on chromatin, either through direct protein

interaction or exposure of large numbers of methylated histones, or both.

Recently, it was discovered that in addition to the Ser139 phosphorylation, H2AX is also phosphorylated at residue Tyr142. In unstressed cells, Tyr142 is already phosphorylated by the kinase WSTF; upon DNA damage, Tyr142 becomes gradually dephosphorylated through actions of the phosphatases Eya1 and Eya3. Tyr142 dephosphorylation may be required for Ser139 phosphorylation, since the dually phosphorylated H2AX is incapable to retain MDC1 and elicit further signaling. Thus, Tyr142 phosphorylation status determines the relative recruitment of either DNA repair or pro-apoptotic factors to γ H2AX tails, and functions as a switch of repair versus apoptotic responses to DNA damage (Xiao et al., 2009; Cook et al., 2009).

In summary, H2AX phosphorylation, H2A(X) ubiquitylation and other histone modifications surrounding the DNA breaks may be required to cooperatively promote chromatin changes around the DSB sites, efficient DNA repair, effective checkpoint activation, and/or apoptosis decisions.

Consistent with the important roles of H2AX in response to and/or repair of DSBs, cells deficient in H2AX have been shown to display significant growth defects, IR sensitivity, and increased levels of genomic instability (Bassing et al., 2002b; Celeste et al., 2002). The genomic instability of *H2ax*^{-/-} cells could be due to impaired HR and/or NHEJ repair (Bassing et al., 2002b; Celeste et al., 2002; Xie et al., 2004; Franco et al., 2006). In mammalian cells, H2AX Ser139 phosphorylation is important to enforce

efficient HR and prevent the error-prone deletional repair through SSA (Xie et al., 2004). One potential mechanism is provided by studies in yeast post-replicative DSB repair, where cohesin binding to the γ H2AX domains around the break sites ensures sister chromatid cohesion, promoting proper HR that uses the adjacent intact sister chromatid as a template (Unal et al., 2004). This role of H2AX in HR is consistent with the observation of chromatid breaks that accumulate in *H2ax*^{-/-} cells (Bassing et al., 2002b; Celeste et al., 2002). Although H2AX does not seem to be essential for the joining step of NHEJ using an extra-chromosomal V(D)J recombination assay (Bassing et al., 2002b), *H2ax*^{-/-} cells accumulate chromosome breaks either during normal proliferation in culture or following treatment of DNA damaging agents, indicative of compromised pre-replicative DSBs repair that does not depend on extensive homology (Bassing et al., 2002b; Celeste et al., 2002). Furthermore, in CSR where DSB intermediates are joined through the NHEJ pathways, *H2ax*^{-/-} B cells show reduced CSR efficiency and harbor elevated levels of CSR-associated chromosome breaks/translocations independent of the p53-mediated checkpoint, consistent with a role of H2AX in NHEJ (Reina-San-Martin et al., 2003; Franco et al., 2006; Ramiro et al., 2006). In addition, H2AX-deficient cells exhibit impaired G2/M checkpoint activation in response to low, but not high, doses of IR (Fernandez-Capetillo et al., 2002), suggesting checkpoint signaling defects in response to physiological levels of DNA breaks may also have contributed to the accumulation of genomic aberrations in the absence of H2AX. Thus, the delineation of H2AX functions in DSB repair would be facilitated by experimental systems in which break repair could be separated from cell cycle progression.

V(D)J Recombination is a Physiological DNA Damage and Repair Process

Although protocols that induce large amounts of cellular DNA damage have provided important insights into the DDR mechanisms and the rationales of current cancer therapies (chemotherapies and radiotherapies), cell responses to low, physiologically relevant doses of DNA damage and mechanisms of DNA repair may be different and are poorly understood. This knowledge is necessary to understand tumor initiation during which somatic cells rarely receive large, but rather accumulate mutations due to low, amounts of DNA damage. This knowledge may also form the basis for improved cancer prevention strategies. Thus, systems where a few DSBs can be induced and tracked in each cell would be extremely valuable for this purpose. For my thesis, I have been using V(D)J recombination as a model to elucidate the mechanisms of physiological DNA damage and repair.

The ability of adaptive immune systems to recognize and destroy a plethora of pathogens depends on the immense repertoire of antigen receptor specificities of B and T cells. Each antigen receptor is composed of a constant (C) region and a variable region, whose extreme variability allows the antigen-binding site to recognize antigens with specificity. In developing immature lymphocytes, the variable region exons of either T-cell receptor (TCR) or B-cell receptor (BCR) genes are assembled through cutting and pasting of germ line variable (V), diversity (D) and joining (J) gene segments, in a genetically programmed DNA recombination process termed V(D)J recombination (Bassing et al., 2002a).

In humans and mice, there are seven different antigen receptor gene loci that can undergo V(D)J recombination. In B cells, the BCRs or immunoglobulins (Ig) are encoded by the heavy chain (IgH) and light chain κ and λ (Ig κ and Ig λ) loci; in T cells, the TCRs are encoded by the α and β chain loci in $\alpha\beta$ T cells, or the γ and δ chain loci in $\gamma\delta$ T cells. Mature B cell and $\alpha\beta$ T lymphocytes develop through a highly regulated stepwise differentiation program that includes V(D)J recombination and periods of rapid cell proliferation (Bassing et al., 2002a). V(D)J recombination is initiated by the lymphoid specific endonuclease complex RAG1/2 (recombinase activating genes 1 and 2) in the G0/G1 phase of slowly cycling immature lymphocytes. In the bone marrow, for example, pro-B cells assemble IgH V genes and express the IgH μ chains together with the surrogate light chains (VpreB and $\lambda 5$) to form the pre-BCR, resulting in cell proliferation and maturation into the pre-B cells stage. Early large pre-B cells turn off the recombination machinery, and exit the cell cycle following several cell divisions. These G0/G1 phase late small pre-B cells can now undergo IgL (IgL κ or λ) rearrangement, becoming surface IgM⁺ immature B cells. The initial un-selected B cell repertoire contains large numbers of cells with self-reactive antibodies or receptors. Further IgL rearrangements such as secondary V(D)J recombination or receptor editing can occur in these self-reactive B cells to rescue them from being selected against (Jankovic et al., 2007). In parallel, in-frame VDJ β rearrangements in CD4⁻/CD8⁻ (double negative, DN) thymocytes generate TCR β chains that, when expressed and paired up with pre-T α chains to form the pre-TCR on the cell surface, provide survival signals for DN thymocytes and drive rapid cell proliferation and differentiation to the CD4⁺/CD8⁺ (double positive, DP) cell stage. TCR α variable region exons are then assembled in DP

thymocytes. Successful VJ α rearrangements generate TCR α chains that, when expressed on the cell surface with TCR β chains to form the $\alpha\beta$ TCR, rescue DP cells from apoptosis and signal differentiation to CD4 $^+$ or CD8 $^+$ (single positive, SP) thymocytes. V(D)J recombination is an essential component of lymphocyte development, as evidenced by the observations that *Rag1* $^{-/-}$ or *Rag2* $^{-/-}$ mice completely lack mature B and T lymphocytes.

The combinations of joining between different V, J, and sometimes D, gene segments generate the combinatorial diversity, which contributes to the final repertoire of receptor specificities but by itself is not sufficient to account for the immense pool size. Additional diversity is determined by the repair mechanisms of DSB intermediates during V(D)J recombination. As shown in Figure 2, The RAG1/2 complex introduces DSBs at recombination signal sequences (RSSs) that flank V, D and J gene segments. Upon binding to the RSSs RAG proteins introduce a single stranded nick in the DNA and transesterification leads to two types of double strand breaks: blunt, 5' phosphorylated signal ends (SE) and covalently sealed hairpin coding ends (CE) (Fugmann et al., 2000). RAG proteins hold V(D)J intermediates together in a synaptic complex (Agrawal and Schatz, 1997; Lee et al., 2004), facilitating their repair by seven known NHEJ factors, Ku70, Ku86, XRCC4, ligase IV, DNA-PKcs, Artemis and XLF/Cernunnos (Lieber, 2008) (Figure 2). All seven factors are required to process and join CEs together to form coding joins (CJs) that encode antigen receptor exons, while all seven except DNA-PKcs and Artemis are required to join SEs to form signal joins (SJs). In CJ formation, DNA-PKcs phosphorylates Artemis and activates its endonuclease activity, which is required to open

CE hairpins for repair (Ma et al., 2002). Hairpin opening often generates staggered DNA ends from which nucleotides can be trimmed by the DNA-PKcs/Artemis complex (Figure 2). Before ligation of coding ends by the XLF/XRCC4/ligase IV complex, polymerase μ and/or polymerase λ can fill in the gaps in a template-dependent manner (Nick McElhinny and Ramsden, 2004). In addition, terminal transferase (TdT), a lymphocyte-specific template-independent polymerase, can add nucleotides to the CEs. The imprecise nature of NHEJ thus contributes to the junctional diversity.

NHEJ is essential for functional V(D)J recombination in both mice and humans. Most NHEJ-deficient mice lack mature B and T cells due to their inability to form coding joins, which are prerequisites for clonal expansion of B and T cell precursors (Rooney et al., 2004b). In humans, nearly 30% of all T^+B^- SCID (severe combined immunodeficiency) patients show hypersensitivity to IR, because the V(D)J recombination deficiency results from defective NHEJ, rather than mutations in their *RAG1* and/or *RAG2* genes (Revy et al., 2005). The majority of these patients harbor mutations in *ARTEMIS*. Mutations of other NHEJ components are also associated with human immunodeficiencies, including those of the DNA ligase IV gene (*LIG4* Syndrome) and XLF/Cernunnos gene (O'Driscoll et al., 2004; Ahnesorg et al., 2006; Buck et al., 2006). Phenotypes of knockout/mutant mice for Ku70, Ku80, XRCC4 and DNA-PKcs genes suggest their mutations might also lead to SCID in humans (Rooney et al., 2004b). Indeed, van der Burg et al. recently identified a DNA-PKcs mutation that inhibits Artemis activation and NHEJ in a radiosensitive T^+B^- SCID patient (van der Burg et al., 2009). In addition, the existence of RAG mutants that are able to induce

DSBs but are defective in the joining reaction suggests that RAG may play roles in repair itself (such as holding the DNA ends in proximity) or in recruitment of NHEJ DNA repair factors (Agrawal and Schatz, 1997; Lee et al., 2004). In contrast to RAGs in V(D)J recombination, the enzyme that introduces the DSBs in CSR, and the restriction enzymes used in a number of in vitro studies, are not known to hold DSB ends with high affinity.

Not unlike general DSBs, lymphocytes are challenged to properly activate DDR in response to programmed DSBs during V(D)J recombination and CSR (Figure 3). First, γ H2AX and NBS1 form RAG-dependent foci at the *Tcra* locus in developing thymocytes, indicative of ongoing V(D)J DSB induction and/or repair (Chen et al., 2000). Second, RAG-induced breaks are restricted to the G1 cell cycle phase, since the Skp1-Cul1-Skp2 (Skp2-SCF) polyubiquitylates RAG2 for the proteosome-dependent degradation at G1/S transition (Lee and Desiderio, 1999) (Figure 3). Most DSB intermediates are believed to be repaired before S-phase entry, since un-repaired DSBs can activate the G1/S checkpoint, although it has been reported that in at least a small percentage of lymphocytes with un-repaired V(D)J breaks can persist into S phase even in wild type mice (Pedraza-Alva et al., 2006). An even higher percentage of cells with un-repaired V(D)J breaks may be able to start DNA replication in NHEJ-deficient mice, or in the absence of effective G1/S checkpoint activation, such as in *p53*^{-/-} and *Atm*^{-/-} cells (Dujka et al., 2010) (Figure 3). This fraction of DNA breaks can be replicated to form chromosome breaks, or participate in chromosome translocations after illegitimate joining with other breaks such as those generated during collapsed replication forks. Thus, combined deficiencies in NHEJ repair and G1/S checkpoint mechanisms may

result in dramatically elevated genomic instability due to faulty V(D)J recombination (Figure 3).

Consistence with the aforementioned idea, NHEJ-deficient mice rarely develop lymphomas because p53-mediated apoptosis can eliminate DN or pro-B cells with unrepaired RAG-generated DSBs (Rooney et al., 2004b). NHEJ/p53 compound deficiency allows these cells to survive but does not rescue lymphocyte development. Furthermore, most NHEJ/p53-deficient mice rapidly succumb to pro-B lymphomas with IgH translocations, and some *Artemis*^{-/-}*p53*^{-/-} mice also develop thymic lymphomas with potential TCR α/δ translocations (Rooney et al., 2004a, 2004b). Interestingly, over 10% of peripheral T cells from *Atm*^{-/-} mice contain Chr. 14 breaks or translocations that likely involve the TCR α/δ locus, and *Atm*^{-/-} mice invariably die from thymic lymphomas with clonal TCR α/δ translocations (Liyanage et al., 2000). These abnormalities cannot be fully explained by the checkpoint activation or apoptotic functions of ATM, suggesting ATM may in addition function in the joining step of NHEJ, which is discussed later in this chapter.

In summary, V(D)J recombination is highly regulated in a lineage-, developmental stage- and cell cycle-specific manner. This V(D)J recombination program must orchestrate chromatin conformation and DNA damage and repair proteins, in addition to cis-acting DNA elements and trans-acting transcription factors.

Novel Cell Line Systems and Mouse Models to Study H2AX Functions

Whether and how H2AX functions in NHEJ and V(D)J recombination is poorly understood and existing results are contradictory. Similar to *Atm*^{-/-} mice, *H2ax*^{-/-} mice are mildly lymphopenic and their primary αβ T cells harbor potential TCR translocations, although the *H2ax*^{-/-} defects are generally less severe than that of *Atm*^{-/-} mice (Celeste et al., 2002; Liyanage et al., 2000). Despite the dramatic genomic instability of *H2ax*^{-/-} cells, *H2ax*^{-/-} mice are only slightly predisposed to thymic lymphomas, whereas *H2ax*^{-/-} *p53*^{-/-} mice rapidly succumb to immature T and B lineage lymphomas and solid tumors (Celeste et al., 2003b; Bassing et al., 2003). *H2ax*^{-/-} *p53*^{-/-} thymic lymphomas harbor clonal translocations that predominantly do not involve TCR loci and, which, therefore have been proposed to arise through the mis-repair of spontaneous DSBs. Nevertheless, at very low frequencies, *H2ax*^{-/-} and *H2ax*^{-/-} *p53*^{-/-} mice do develop thymic lymphomas with clonal TCR translocations, which are not observed in *p53*^{-/-} mice (Celeste et al., 2003b; Bassing et al., 2003). Moreover, the majority of *H2ax*^{-/-} *p53*^{-/-} pro-B lymphomas contain *Igh/c-myc* translocations, similar to those in NHEJ/p53-deficient pro-B lymphomas (Mills et al., 2003), suggesting a role of H2AX in resolution of DSB intermediates during V(D)J recombination. Indeed, the subset of thymic lymphomas and pro-B lymphomas with clonal antigen receptor translocations are absent in *H2ax*^{-/-} *p53*^{-/-} *Rag2*^{-/-} mice, though RAG2-deficiency does not significantly alter lymphoma development of *H2ax*^{-/-} *p53*^{-/-} mice (Bassing et al., 2008). Thus, among its more general functions as a genome caretaker, H2AX may play a role in suppressing aberrant processing of RAG-initiated DSBs, though compelling experimental evidence assaying the repair of tractable breaks are still lacking.

On the other hand, H2AX-deficient cells support normal signal and coding end formation on transiently introduced extra-chromosomal V(D)J recombination substrates (Bassing et al., 2002b), suggesting H2AX might not be required for NHEJ *per se*, contradicting aforementioned phenotypes of *H2ax*^{-/-} mice. Such discrepancies also existed for the upstream kinase ATM until a novel cell line base system was developed to assay chromosomal V(D)J recombination. Treatment of v-Abl transformed (Abelson) pre-B cells with STI571, a small molecule Abl kinase inhibitor, results in rapidly up-regulation of RAG expression and induction of DSBs at the endogenous Jk locus and within chromosomally-integrated recombination substrates (Figure 4) (Muljo and Schlissel, 2003; Bredemeyer et al., 2006). A concomitant G1 arrest independent of V(D)J recombination provides large populations of synchronized cells. To prevent elimination of DSB-bearing cells through apoptosis, these Abelson cells were also engineered to express the anti-apoptotic Bcl2 protein (Bredemeyer et al., 2006). Thus, RAG-generated chromatin DSBs can be induced with high efficiency, and their repair tracked, in large populations of G1-arrested Abelson cells. Using this system, a previously unappreciated role of ATM was unraveled: dependent on its kinase activity, ATM stabilizes chromosomal V(D)J recombination DSB intermediates, facilitates coding join formation, and prevents broken DNA ends from participating in chromosome deletions, inversions, and translocations (Bredemeyer et al., 2006). This is consistent with both the lymphoid tumor-prone phenotype in ataxia telangiectasia (A-T) patients and the development of thymic lymphomas harboring RAG-dependent *Tcrα/δ* translocations in *Atm*^{-/-} mice (Liyanaage et al., 2000), neither of which could be explained solely by ATM's checkpoint and apoptosis functions. Thus, abrogation of ATM not only impairs end joining, but also

allows immature lymphocytes with un-repaired chromosome breaks to develop and persist into the periphery, where in the case of B cells, these RAG-initiated breaks can join to AID-dependent breaks during CSR (Callén et al., 2007).

Definite evidence that the MRN complex components play a role in NHEJ and V(D)J recombination was also obtained for the first time using the Abelson cells. In humans, mutations of the *ATM* gene cause A-T, mutations of *NBS1* cause Nijmegen breakage syndrome (NBS) and mutations of *MRE11* cause ataxia-telangiectasia-like disease (ATLD), and all three syndromes are genetic disorders exhibiting multiple phenotypes that include genomic instability, immunodeficiency, and increased predisposition to lymphoid malignancies associated with antigen receptor locus translocations. Consistent with the similarities between A-T and NBS/ATLD patient symptoms, MRN also functions in the NHEJ-mediated repair of DNA DSBs generated during V(D)J recombination (Helmink et al., 2009). The defects observed in MRN mutant lymphocytes are strikingly similar to those observed in ATM-deficient lymphocytes, suggesting that MRN and ATM function in the same pathway in NHEJ-mediated repair of RAG-mediated DSBs in G1-phase cells. Both ATM and NBS1 localize to V(D)J DSB ends and may function to tether ends in proximity in addition to the RAG complex (Chen et al., 2000; Perkins et al., 2002). Normally, the RAG post-cleavage complex prevents V(D)J DSBs from being repaired through alternative NHEJ, an error-prone mechanism for joining DSBs in mammalian cells (Corneo et al., 2007). Using certain RAG mutants that allow destabilization of the post-cleavage complex and alternative NHEJ, NBS1, and likely the MRN complex, is shown to regulate repair

pathway choice by enhancing the stability of DNA end complexes and participate in alternative NHEJ of coding ends (Deriano et al., 2009). Thus, I reasoned that the Abelson inducible V(D)J recombination system would allow me to uncover novel H2AX functions.

Based on the model of γ H2AX nucleating foci formation in response to general DSBs (Bonner et al., 2008), Chapter II of my thesis focuses on testing the hypothesis that one specific function of γ H2AX is to serve as an anchor for the assembly of multiple protein-protein/protein-DNA interactions involving MDC1, MRN and 53BP1, among others, around chromosomal V(D) breaks. These complexes would prevent irreversible dissociation and subsequent mis-repair of broken V, D, and J segments. Thus, by inducing V(D)J recombination in $H2ax^{-/-}$ Abelson cells, I speculate there might be accumulation of un-repaired DSB ends that have escaped from the post-synaptic complex, and they are capable of participating in illegitimate end joining either in G1 or subsequent cell cycles. Indeed, H2AX has been shown to prevent AID-dependent DNA breaks from progressing into chromosome breaks/translocations in cells undergoing CSR, where H2AX and ATM are required for long-range switch region synapsis (Franco et al., 2006; Ramiro et al., 2006). However, it is equally possible that no V(D)J end joining defects would be observed within G1-arrested $H2ax^{-/-}$ Abelson cells, either due to high affinity of RAG proteins to DNA ends evidenced at least *in vitro*, or the rapid kinetics of NHEJ as soon as breaks are induced, or a combination of both. If this is the case, H2AX-deficiency might need to be coupled with continued cell cycle progression in order to erroneously process RAG-initiated G1 breaks. To this end, $H2ax^{-/-}$ and $H2ax^{-/-}p53^{-/-}$

Abelson cells are released from G1-arrest, allow RAG2 degradation upon S-phase entry, and monitor fates of RAG-generated DSBs (Figure 4). Since in the context of rapid NHEJ the level of RAG-initiated breaks persisting into S-phase might be below detection even in the absence of p53-mediated checkpoint activation, I've also generated and utilized *Artemis*^{-/-}*H2ax*^{-/-} and *Artemis*^{-/-}*H2ax*^{-/-}*p53*^{-/-} Abelson cells, where NHEJ kinetics of coding ends is nearly down to zero due to inability to open hairpins. In these NHEJ/p53-deficient cells, H2AX deficiency might severely compromise positional stability of persistent broken DNA ends even in G1 phase, and after G1/S transition, lead to enhanced chromosome breaks/translocations involving ends that are permanently separated from their legitimate partners. Thus, when *Artemis*^{-/-}*H2ax*^{-/-} and *Artemis*^{-/-}*H2ax*^{-/-}*p53*^{-/-} Abelson cells are released from cell cycle arrest, H2AX deficiency may lead to more un-repaired V(D)J DSBs being replicated to form chromosome breaks or translocations (Figure 4).

Previous comparative genomic hybridization analysis of NHEJ/p53-deficient mice pro-B cell tumors show that the majority of these tumors carry a mono-allelic deletion of a region spanning the *H2ax* gene on chromosome 9, suggesting *H2ax* haploinsufficiency may have contributed to genomic instability and tumor development in NHEJ/p53 mice (Bassing et al., 2003). *Artemis*^{-/-}*p53*^{-/-} mice can develop thymic lymphomas with clonal TCR α/δ locus translocations (Rooney et al., 2004a), and provide a model to test the roles of H2AX during V(D)J recombination in vivo and in subsequent lymphomagenesis. To characterize the tumor phenotype of *Artemis*^{-/-}*p53*^{-/-} and *Artemis*^{-/-}*H2ax*^{-/-}*p53*^{-/-} mice is the focus of Chapter III of my thesis.

Extensive studies summarized above have placed H2AX, ATM and MRN into highly cooperative yet non-overlapping regulatory networks during DDR. ATM and MRN clearly have H2AX-independent functions, including roles in cell cycle checkpoints and p53-mediated apoptosis, the impairment of ATM or MRN components results in unique phenotypes associated with each disorder. On the other hand, H2AX is downstream of other kinases such as DNA-PKcs and ATR, and is shown to be critical for HR. The organization of H2AX and ATM genes in a syntenic group across species suggests their functional interactions could be particularly relevant in tumor suppression. The human H2AX gene (*H2AFX*) maps 11 Mb telomeric of *ATM* on Chr. 11 at 11q23, which frequently exhibits LOH or deletion spanning both gene loci in a number of human cancers, including immature T cell and mature B cell lymphomas (Stilgenbauer et al., 1996, 1999). By comparing G1-arrest *H2ax*^{-/-}, *Atm*^{-/-} and *H2ax*^{-/-}*Atm*^{-/-} Abelsons cells undergoing V(D)J recombination, I can test the hypothesis that H2AX and ATM occupy distinct chromatin regions around break sites to promote DNA ends stability. Moreover, haploinsufficient H2AX expression dramatically predisposes mice to genomic instability and cancer in a p53-deficient background (Bassing et al., 2003). In this context, it will be of particular interest to determine whether loss of one or both H2AX genes modifies the ATM-deficient phenotype in mice. In Chapter IV of my thesis, I present some preliminary results examining whether there are functional interplays between H2AX and ATM in V(D)J recombination, lymphocyte development and transformation.

DNA Damage Signals and Mono-allelic V(D)J Recombination

In the absence of any regulatory control mechanisms, both alleles of each antigen receptor locus in diploid human and mouse lymphocytes would be available for V(D)J recombination. However, most B and T cells express a unique antigen receptor encoded by V-to-(D)J rearrangements of only one of the two alleles for each individual TCR/Ig gene (Cedar and Bergman, 2008). The functional exclusion of the non-expressed alleles, also known as allelic exclusion, is observed at the TCR β locus in T cells and the IgH, IgL κ and IgL λ light chain loci in B cells. Despite extensive efforts, the precise mechanisms of how allelic exclusion is initiated and maintained remain largely unknown, partly due to asynchronous V(D)J recombination in populations of cells in vivo.

Allelic exclusion can be achieved at multiple levels, such as locus accessibility, DNA rearrangement, differential expression and cellular selection. For example, both IgH and TCR β loci exhibit allelic exclusion at the V-to-DJ step but not at the D-J step. First, due to the imprecise nature of V(D)J end joining and 2/3 of the time each joining is out of frame, it is suggested that the chances of both alleles undergoing productive V-to-DJ recombination simultaneously are small, assuming the choice of which allele to rearrange is stochastic. Second, once a productive rearrangement on one allele occurs, the pre-BCR/TCR can send a feedback signal to suppress further V-to-DJ recombination on the remaining allele. The pre-BCR/TCR signaling also drives proliferation and differentiation until the IgL or TCR α rearrangements, during which further IgH or TCR β rearrangements need to be suppressed. This suppression could be achieved in a number of ways, which are not mutually exclusive: down-regulation of the recombination machinery, changes in V chromatin structure that limit RAG1/2 access, decontraction of

chromatin between V and (D)J segments, and association of alleles with nuclear periphery or pericentromeric heterochromatic regions (Cedar and Bergman, 2008). In contrast to the stochastic model for the initiation of allelic exclusion, it has been suggested at least for *Igκ*, the two alleles are differentially marked as early and late replicating alleles. This regulated or deterministic model argues that in pre-B cells the early replicating allele becomes more transcriptionally accessible through DNA demethylation and thus is predisposed to rearrange first. However, this model still cannot explain why D-to-J recombination occurs on both TCRβ and IgH alleles. Since both TCRβ alleles are accessible by RAGs (Carpenter et al., 2009) and germ line transcription occurs bi-allelically (Jia et al., 2007), allelic exclusion must be initiated through other mechanisms.

Although V(D)J recombination is widely recognized as a physiological DNA damage response, surprisingly, the possibility of DNA damage signals in coordinating bi-allelic V(D)J recombination has never been explored. This lack of interest presumably comes from the observation that not all antigen receptor loci exhibit allelic exclusion, and for those that do, for example, IgH and TCRβ, D-J rearrangements can happen on both alleles in the same cell, as evidenced by Southern blot analysis of mature T cell hybridomas. However, it was never shown that the bi-allelic D-J rearrangements take place simultaneously. Thus it remains possible that DNA damage signals emanating from one allele can repress simultaneous break induction on the other allele. Intuitively, this intra-nucleus suppressive signal would work faster than the feedback signal following productive rearrangement on one allele.

In Chapter V of my thesis, I attempt to uncover roles of the DDR machinery in allelic exclusion. In *Artemis*^{-/-} Abelson cells un-repaired Igκ locus DNA ends accumulate, and mono-allelic recombination is not violated. On the contrary, both Igκ alleles undergo rearrangement in a substantial portion of *Artemis*^{-/-}*Atm*^{-/-} cells. DSBs generated on both alleles can persist and separate in G1 phase nuclei, and form chromosome breaks and/or translocations upon cell cycle re-entry. These data are consistent with the notion that ATM-mediated DNA damage signals emanating from one rearranging Igκ allele can prevent initiation of V(D)J recombination on the second allele, to provide a time window to test whether the first VJκ rearrangement is functional.

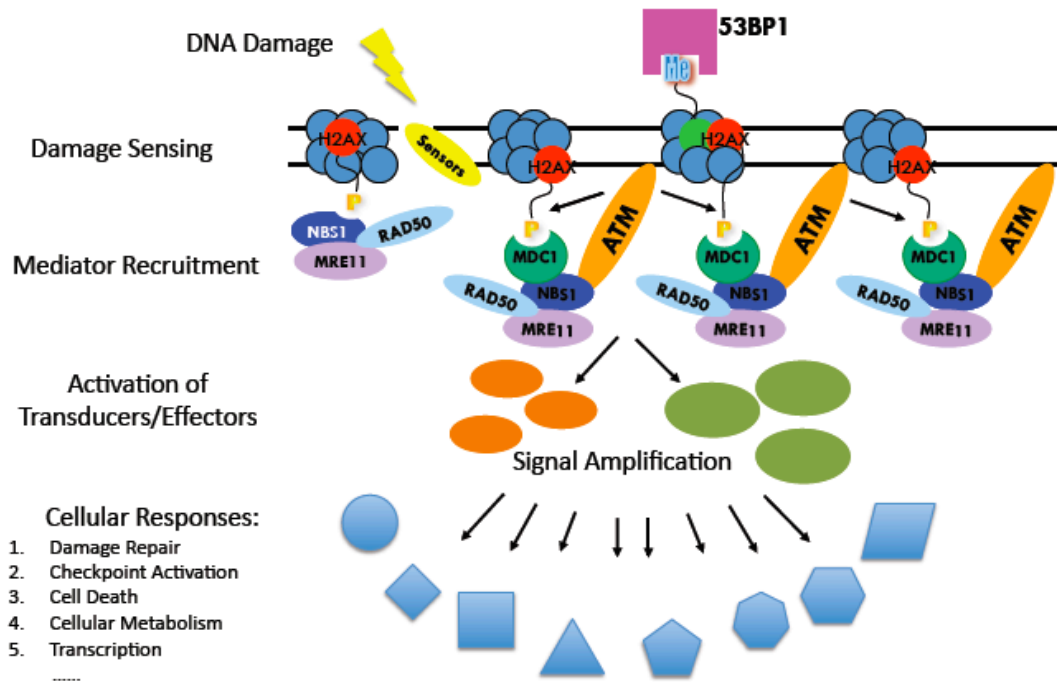


Figure 1. Model for signal propagation and amplification in DDR. Presence of DNA lesions are detected by sensors, and H2AX can be rapidly phosphorylated by kinases such as ATM. Recruitment of mediators through γ H2AX and/or chromatin conformation changes around the breaks can potentiate ATM activation, which leads to more H2AX phosphorylation. DDR signals are relayed and amplified through activation of transducer/effector proteins, which can impact a wide variety of cellular processes.

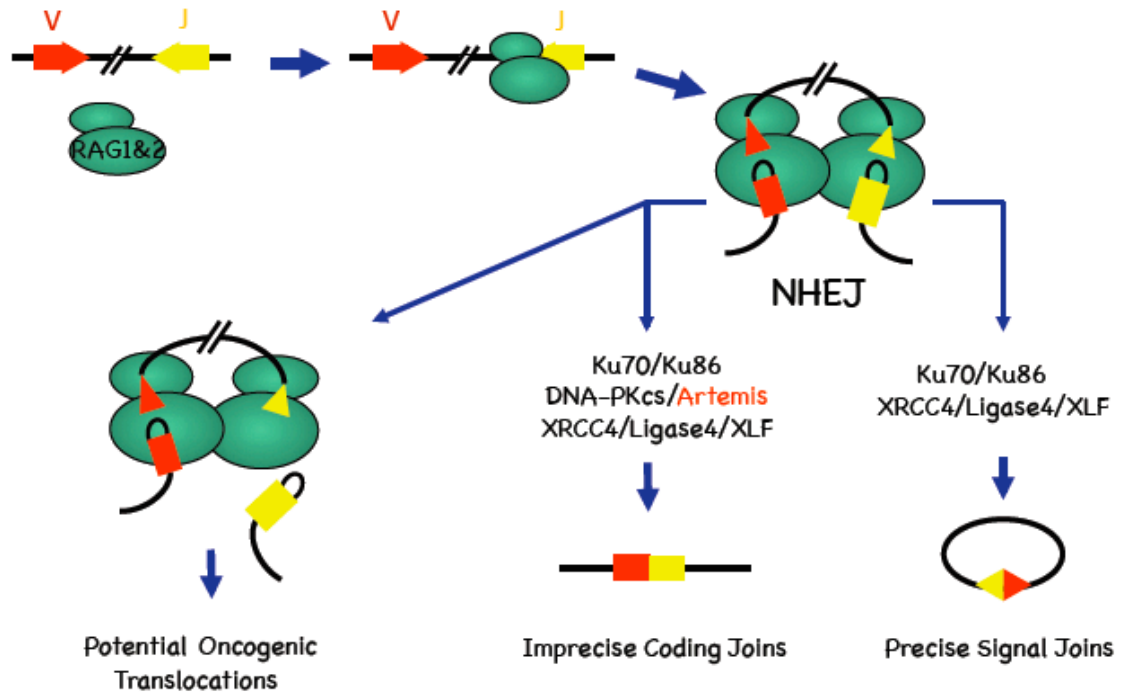
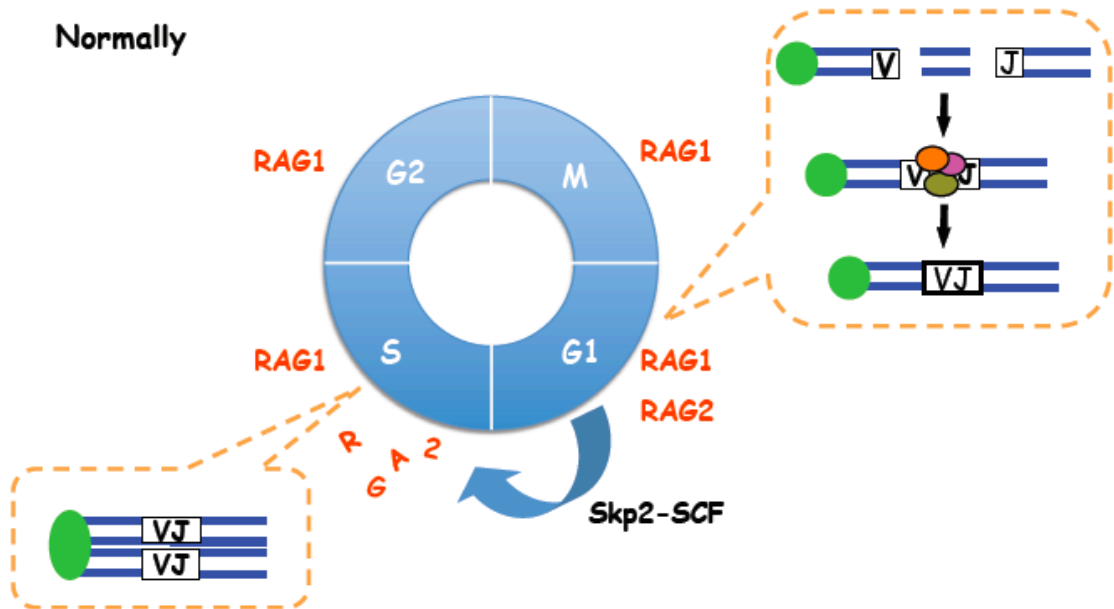


Figure 2. Model for the chromosomal V(D)J recombination reaction. RAG1/2

(green) binds to the RSSs (triangles) of the two segments that are to be joined, in this case a V and a J, and brings the two segments into a synaptic complex, generating two types of DNA DSBs. The blunt signal ends are re-joined through NHEJ with minimal processing to form an extra-chromosomal circle. The hairpin coding ends need to be opened by DNA-PKcs/Artemis, before they are joined through NHEJ. The required core NHEJ factors for coding join and signal join formation are listed. Distabilization of the post-synaptic complex may allow escape of the DNA ends, which can participate in potentially oncogenic translocations.

Normally



Defective Repair and Checkpoint

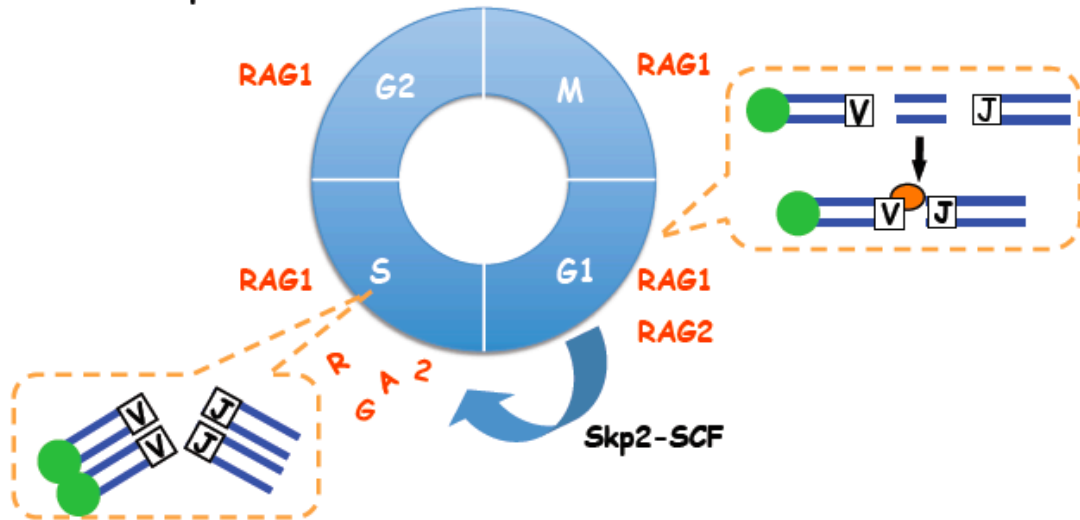


Figure 3. Defective repair of DSB intermediates in V(D)J recombination can lead to chromosome breaks/translocations. Normally, RAG1/2-mediated breaks are induced in G1 since RAG2 is targeted for proteasome-mediated degradation upon G1/S transition. Most V(D)J breaks are repaired before S phase entry, and un-repaired breaks can activate the G1/S checkpoint to arrest cell cycle progression. Low percentages of wild type lymphocytes can occasionally enter S phase with un-repaired V(D)J breaks. However, when the NHEJ repair pathway is defective, more un-repaired V(D)J DSB intermediates may accumulate in G1, and with concurrent defects in checkpoint activation, these DNA breaks can persist into S/G2 phases where they can be replicated to form chromosome breaks, or joined to other breaks in the genome to form translocations. Since some DDR factors (such as ATM and MRN) may have roles both in DNA repair and in checkpoint activation, mutations or deficiencies in these factors can result in elevated levels of genomic alterations.

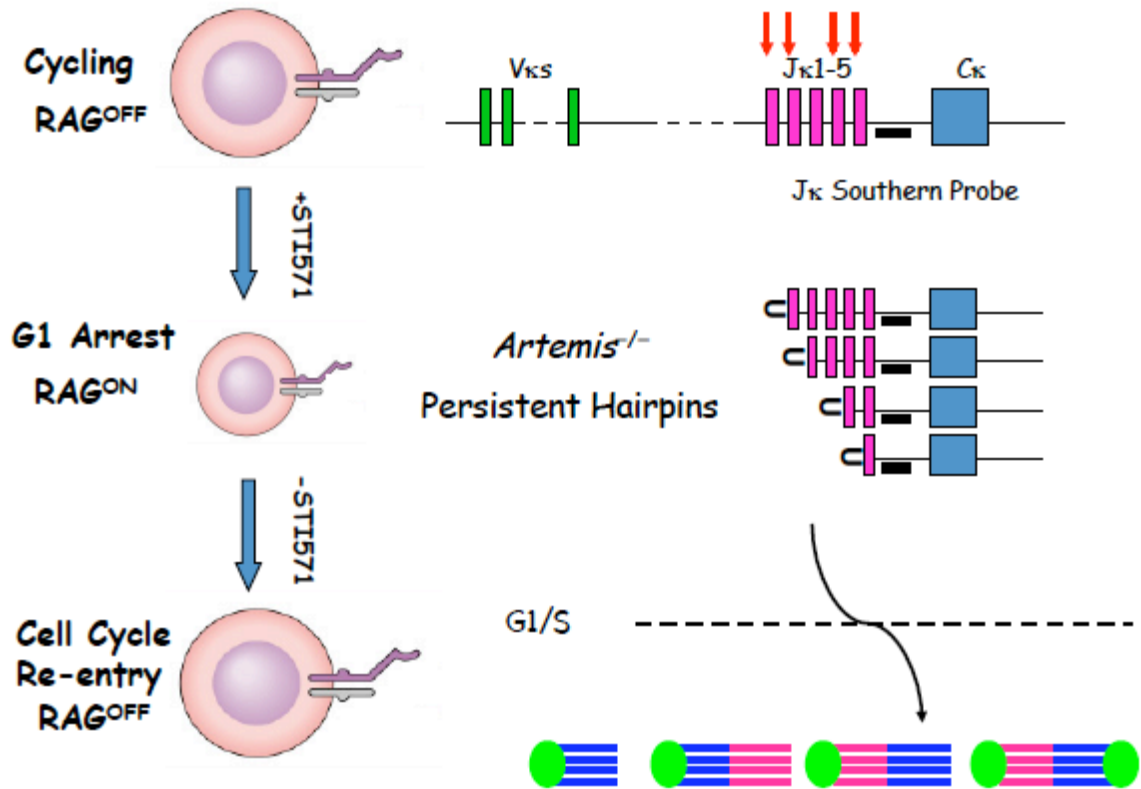


Figure 4. Inducible V(D)J recombination in the Abelson cell lines. STI571 treatment of v-abl transformed B cells leads to G1 cell cycle arrest and upregulation of RAG1/2 expression. RAG can introduce breaks at the endogenous Igκ locus (red arrows) and chromosomally integrated recombination substrates (not shown). *Artemis*^{-/-} Abelson cells are used as an example to show that DSB intermediates can be monitored by Southern blot. After break induction, STI571 can be withdrawn to allow cell cycle re-entry. DSBs induced during G1 arrest can progress into chromosome breaks and/or translocations.

Chapter II

Histone H2AX Stabilizes Broken DNA Strands to Suppress Chromosome Breaks and Translocations in V(D)J Recombination

Part of this chapter has been published in:

© Yin et al., 2009. *J. Exp. Med.* doi:10.1084/jem.20091320

With permission from the Rockefeller University Press

ABSTRACT

The H2AX core histone variant is phosphorylated in chromatin around DSB and functions through unknown mechanisms to suppress antigen receptor locus translocations during V(D)J recombination. Formation of chromosomal coding joins and suppression of translocations involve the ATM and DNA-PKcs serine/threonine kinases, each of which phosphorylates H2AX along cleaved antigen receptor loci. Using Abelson transformed pre-B cell lines, I now demonstrate that H2AX is not required for coding join formation within chromosomal V(D)J recombination substrates. Yet, I show that H2AX is phosphorylated along cleaved Ig κ DNA strands and prevents their separation in G1 phase cells and their progression into chromosome breaks and translocations following cellular proliferation. I also show that H2AX prevents chromosome breaks emanating from unrepaired RAG endonuclease generated TCR α/δ locus coding ends in primary thymocytes. My data indicate that histone H2AX suppresses translocations during V(D)J recombination by creating chromatin modifications that stabilize disrupted antigen receptor locus DNA strands to prevent their irreversible dissociation. I propose that such H2AX dependent mechanisms could function at additional chromosomal locations to facilitate the joining of DNA ends generated by other types of DSBs.

INTRODUCTION

The rapid phosphorylation of histone H2A proteins in chromatin for large distances around DSBs is a conserved feature of the cellular DNA damage response. In mammalian cells, the H2AX histone variant comprises 2-25% of the H2A pool and is non-uniformly incorporated into chromatin (Rogakou et al., 1998; Bewersdorf et al., 2006). Upon DSB induction, the ATM, DNA-PKcs, and ATR protein kinases phosphorylate H2AX on a conserved carboxyl terminal serine residue to form γ H2AX around DNA breakage sites (Rogakou et al., 1999; Paull et al., 2000; Burma et al., 2001; Ward and Chen, 2001; Stiff et al., 2004). Generation of γ H2AX creates binding sites for repair and checkpoint proteins, some of which catalyze other covalent modifications of γ H2AX to generate binding sites for additional repair and checkpoint proteins, all of which assemble into complexes in chromatin surrounding DNA breaks (Downs et al., 2007; Bonner et al., 2008). *H2ax*^{-/-} cells exhibit increased sensitivity to agents that cause DSBs, elevated levels of spontaneous and DSB-induced genomic instability, and defective repair of chromosomal DSBs (Bassing et al., 2002b; Celeste et al., 2002; Xie et al., 2004; Franco et al., 2006). Although *H2ax*^{-/-} cells display apparent normal activation of p53-dependent cell cycle checkpoints and apoptotic responses (Bassing et al., 2002b; Celeste et al., 2002), *H2ax*^{-/-} cells are defective in the G2/M checkpoint following induction of only a few DSBs (Fernandez-Capetillo et al., 2002). The phenotypes of *H2ax*^{-/-} cells suggest that the ability of γ H2AX to retain repair and checkpoint proteins around DSBs may promote accessibility of DNA ends, stabilize disrupted DNA strands, and/or amplify checkpoint signals (Bassing and Alt, 2004; Stucki and Jackson, 2006; Bonner et al., 2008; Kinner et al., 2008).

The health and survival of humans and mice depends upon the ability of their adaptive immune systems to generate lymphocytes with receptors capable of recognizing and eliminating large varieties of pathogens. In developing lymphocytes, Ig and TCR variable region exons are assembled from germline variable (V), diversity (D) and joining (J) gene segments by the lymphoid-specific RAG1/RAG2 endonuclease and the ubiquitously-expressed NHEJ DSB repair factors (Bassing et al., 2002a). The RAG proteins catalyze the coupled cleavage of DNA strands between a pair of gene segments and their flanking RSSs to generate covalently sealed coding ends (CEs) and blunt signal ends (SEs) (Fugmann et al., 2000). RAG mediated cleavage occurs only in G1 phase due to cell cycle phase restricted expression of RAG2 (Lee and Desiderio, 1999). The DNA-PKcs/Artemis endonuclease opens CEs (Ma et al., 2002), which are then processed by nucleases and polymerases (Nick McElhinny and Ramsden, 2004); core NHEJ factors join together CEs and SEs to form coding joins (CJs) and signal joins (SJs) respectively (Bassing et al., 2002a). RAG1/RAG2 can hold CEs and SEs within stable synaptic complexes (Agrawal and Schatz, 1997; Lee et al., 2004), however ATM, and likely the MRN complex, maintains chromosomal CEs in proximity to facilitate end-joining in G1 phase cells (Bredemeyer et al., 2006; Deriano et al., 2009; Helmink et al., 2009). The large combination of V(D)J joining events and the imprecision in CJ formation cooperate to generate a diverse repertoire of antigen receptor specificities.

Despite its benefits, V(D)J recombination poses substantial threats to the viability and genomic integrity of lymphocytes and lymphoma predisposition in host organisms.

DNA-PKcs-deficient mice lack mature lymphocytes due to inability to repair RAG generated DSBs, but only occasionally develop lymphoma (Bosma et al., 1983; Gao et al., 1998; Taccioli et al., 1998). However, DNA-PKcs/p53-deficient mice rapidly succumb to pro-B lymphomas with RAG-dependent IgH/c-myc translocations (Vanasse et al., 1999; Gladdy et al., 2003), demonstrating that p53 protects organisms from oncogenic translocations during V(D)J recombination. RAG generated DSBs activate ATM (Perkins et al., 2002; Bredemeyer et al., 2008), which is required for both coding join formation and p53 activation (Perkins et al., 2002; Bredemeyer et al., 2006). Consequently, *Atm*^{-/-} mice exhibit impaired lymphocyte development, increased frequencies of antigen receptor locus translocations in non-malignant lymphocytes, and marked predisposition to thymic lymphomas with RAG dependent TCR α/δ translocations (Barlow et al., 1996; Elson et al., 1996; Xu et al., 1996; Borghesani et al., 2000; Liyanage et al., 2000; Petiniot et al., 2000, 2002; Callén et al., 2007; Matei et al., 2007; Vacchio et al., 2007). The observation that RAG dependent γ H2AX foci co-localized with TCR α/δ loci suggested that H2AX may coordinate DSB repair, signaling, and surveillance during V(D)J recombination (Chen et al., 2000). Consistent with this notion, $\alpha\beta$ T cells of *H2ax*^{-/-} mice contain elevated frequencies of TCR α/δ translocations and *H2ax*^{-/-}*p53*^{-/-} mice develop pro-B lymphomas with RAG dependent IgH/c-myc translocations (Celeste et al., 2002, 2003b; Bassing et al., 2003, 2008). ATM and DNA-PKcs generate γ H2AX along RAG cleaved DNA strands (Savić et al., 2009). However, *H2ax*^{-/-} mice do not exhibit impaired or blocked lymphocyte development, as observed in mice deficient for ATM or DNA-PKcs, respectively, suggesting that H2AX is not required for the processing and/or joining of chromosomal coding ends. Yet, H2AX

prevents the progression of IgH locus DNA breaks into chromosome breaks and translocations during CSR (Franco et al., 2006; Ramiro et al., 2006), consistent with the notion that H2AX does function in chromosomal end-joining (Reina-San-Martin et al., 2003; Bassing and Alt, 2004). Consequently, the mechanisms by which H2AX suppresses antigen receptor locus translocations during V(D)J recombination remain unknown.

Based upon the disparate phenotypes of *Atm*^{-/-} and *H2ax*^{-/-} mice, I hypothesized that formation of γ H2AX for long distances along RAG cleaved antigen receptor loci promotes chromatin changes that hold together broken DNA strands (Bassing and Alt, 2004). I proposed that this stabilization of disrupted DNA strands would not be required for coding join formation in the G1 phase of developing lymphocytes, but that this H2AX dependent function would be important for preventing the irreversible dissociation of un-repaired coding ends persisting into S phase (Bassing and Alt, 2004). Quantitative analysis of DNA end-joining during V(D)J recombination of endogenous loci in developing lymphocytes is difficult due to asynchronous induction of RAG DSBs at multiple genomic locations in cycling cells and expansion of lymphocytes in which functional coding joins have been assembled. Consequently, I utilized a cell line based system that enables the controlled induction of RAG DSBs at single defined chromosomal locations in G1 arrested cells.

RESULTS

H2AX deficient cells exhibit normal coding join formation within chromosomal

substrates

Although H2AX is not required for coding join formation in extra-chromosomal substrates (Bassing et al., 2002b), the phosphorylation of H2AX could function downstream of ATM to facilitate chromosomal coding join formation. To investigate potential H2AX function in chromosomal end-joining during V(D)J recombination, I generated multiple independently derived abl pre-B cell lines from two different *H2ax*^{F/F} mice containing "floxed" *H2ax* loci on both alleles. *H2ax*^{F/F} cells express normal amounts of H2AX and exhibit phenotypes indistinguishable from wild-type cells (Bassing et al., 2002b). Treatment of abl pre-B cells with STI571, an inhibitor of the abl kinase, causes G1 arrest, induction of RAG expression, and robust rearrangement of endogenous Igκ loci and V(D)J recombination substrates (Muljo and Schlissel, 2003; Bredemeyer et al., 2006).

To evaluate potential H2AX function in chromosomal end-joining during V(D)J recombination by inversion, I first transduced *H2ax*^{+/+} and *H2ax*^{-/-} Abelson cells with the pMX-INV retroviral substrate and used human CD4 as a marker for sorting out populations of cells with pMX-INV integrated into the genome. V(D)J recombination of the chromosomally-integrated pMX-INV substrate results in formation of a CJ and an SJ within the same chromosome, placing the inverted GFP sequence in the sense orientation. Illegitimate V(D)J recombination, however, either joins one SE and one CE to form a hybrid join (HJ) and deletes the intervening GFP sequence, or leaves the CE un-repaired (Figure 5A). The induction and repair of RAG generated DSBs within integrated pMX-INV substrates can then be monitored by GFP⁺ cells. Treatment of populations of *H2ax*^{-/-}

:*INV* cells with STI571 for up to 96 hours induced robust recombination, as indicated by a high percentage of GFP⁺ cells (data not shown); however, neither the degree nor kinetics of successful recombination was significantly different between *H2ax*^{-/-}:*INV* and *H2ax*^{+/+}:*INV* cells (data not shown). In addition, Southern blot analysis can distinguish between un-rearranged (UR) substrates, cleaved but not repaired (CE) substrates, cleaved and repaired coding join (CJ), signal join (SJ) and hybrid join (HJ) substrates (Figure 5A). Thus, I conducted Southern blot of populations of *H2ax*^{-/-}:*INV* and *H2ax*^{+/+}:*INV* cells treated with STI571 for increasing amounts of time. Again, recombination by inversion was robust in both *H2ax*^{-/-}:*INV* and *H2ax*^{+/+}:*INV* cells as indicated by the formation of CJ substrates, but no defects of recombination efficiency or kinetics were observed in *H2ax*^{-/-}:*INV* cells (Figure 5B). Consistent with this, neither HJs nor un-repaired CEs were detected at any appreciable level in the absence of H2AX (Figure 5B). These data demonstrate that, unlike deficiency in ATM, Artemis or DNA-PKcs (Bredemeyer et al., 2006), H2AX deficiency does not lead to an observable accumulation of CEs or HJs during V(D)J recombination of pMX-*INV* within G1 phase cells. However, since sorted cells include clones with integrants of various copy numbers and at heterogenous genomic locations, defects of RAG-induced DSB repair at individual substrate may be masked by analysis of this mixed population. Indeed, DSBs in different chromatin compartments may differentially require certain factors for efficient repair (Goodarzi et al., 2008). Different genetic backgrounds and clonal variations between the parental *H2ax*^{+/+} and *H2ax*^{-/-} mice and cells may also have interfered with my analysis.

Most V(D)J recombination reactions occur by deleting the intervening sequences

between the two coding segments. To more rigorously test whether this form of V(D)J recombination requires H2AX, I transduced $H2ax^{F/F}$ abl pre-B cell lines with the pMX-DEL^{CJ} retroviral recombination substrate and used limiting dilution to isolate independent $H2ax^{F/F}$ clones with single pMX-DEL^{CJ} substrates integrated into their genome ($H2ax^{F/F}:DEL^{CJ}$ cells). V(D)J recombination of the chromosomally-integrated pMX-DEL^{CJ} retroviral substrate results in formation of a coding join within the chromosome and generation of a signal join on an extrachromosomal circle (Figure 6A). I next incubated individual $H2ax^{F/F}:DEL^{CJ}$ lines with TAT-Cre protein to delete the "floxed" $H2ax$ alleles and again used limiting dilution to recover $H2ax^{F/F}:DEL^{CJ}$ and $H2ax^{\Delta/\Delta}:DEL^{CJ}$ clones with pMX-DEL^{CJ} substrates integrated at identical genomic locations. The genotypes of these clones were confirmed by both PCR and Southern blot analyses that distinguish between the $H2ax^F$ and $H2ax^{\Delta}$ alleles (data not shown).

To evaluate potential H2AX function in chromosomal end-joining during V(D)J recombination by deletion, I sought to monitor the repair of RAG generated CE within identical pMX-DEL^{CJ} integrants in two different $H2ax^{F/F}:DEL^{CJ}$ and $H2ax^{\Delta/\Delta}:DEL^{CJ}$ clones of the same passage. The induction and repair of RAG generated DSBs within integrated pMX-DEL^{CJ} substrates can be monitored by Southern blot analysis that distinguishes between un-cleaved (GL) substrates, cleaved but not repaired (CE) substrates, and cleaved and repaired (CJ) substrates (Figure 6A). Thus, I conducted Southern blotting of identical pMX-DEL^{CJ} integrants in two $H2ax^{F/F}:DEL^{CJ}$ and $H2ax^{\Delta/\Delta}:DEL^{CJ}$ clones treated with STI571 for increasing amounts of time. As a control for the accumulation of un-repaired chromosomal CEs, I also conducted Southern blot

analysis of *Artemis*^{-/-}:*DEL*^{CJ} clones. At 48 hours STI571 treatment, I observed loss of the pMX-DEL^{CJ} GL fragment and appearance of the pMX-DEL^{CJ} CJ fragment to similar extents in the two *H2ax*^{F/F}:*DEL*^{CJ} and *H2ax*^{Δ/Δ}:*DEL*^{CJ} clones assayed (Figure 6B). In contrast, I detected loss of the pMX-DEL^{CJ} GL fragment and appearance of the pMX-DEL^{CJ} CE fragment at 24 hours STI571 treatment in *Artemis*^{-/-}:*DEL*^{CJ} cells (Figure 6B). At each time-point assayed between 48-96 hours STI571 treatment, I observed similar increasing loss of the pMX-DEL^{CJ} GL fragment and appearance of the pMX-DEL^{CJ} CJ fragment in *H2ax*^{F/F}:*DEL*^{CJ} and *H2ax*^{Δ/Δ}:*DEL*^{CJ} cells (Figure 6B), but increasing loss of the pMX-DEL^{CJ} GL fragment and appearance of the pMX-DEL^{CJ} CE fragment in *Artemis*^{-/-}:*DEL*^{CJ} cells (Figure 6B). Notably, despite conducting Southern analysis on twice as much genomic DNA for *H2ax*^{F/F}:*DEL*^{CJ} and *H2ax*^{Δ/Δ}:*DEL*^{CJ} cells than for *Artemis*^{-/-}:*DEL*^{CJ} cells, I was unable to detect the pMX-DEL^{CJ} CE fragment in *H2ax*^{Δ/Δ}:*DEL*^{CJ} cells. These data again demonstrate that H2AX deficiency does not lead to an observable accumulation of un-repaired coding ends during V(D)J recombination of chromosomal substrates within G1 phase cells.

Since lymphomas with RAG dependent antigen receptor locus translocations arise at a higher frequency in *H2ax*^{-/-}*p53*^{-/-} mice than in *H2ax*^{-/-} mice (Bassing et al., 2003; Celeste et al., 2003b), I considered the possibility that p53 deficiency might reveal a role of H2AX in formation of chromosomal coding joins in G1 phase cells. To investigate this issue, I generated two independently derived *abl* pre-B cell lines from different *H2ax*^{F/F} mice also containing "floxed" *p53* exons on both alleles. I used the same approach as above to generate *H2ax*^{F/F}*p53*^{F/F}:*DEL*^{CJ} and *H2ax*^{Δ/Δ}*p53*^{Δ/Δ}:*DEL*^{CJ} clones of the same

passage with pMX-DEL^{CJ} substrates integrated at identical genomic locations. Southern blot analysis of identical pMX-DEL^{CJ} integrants in two different *H2ax^{F/F}p53^{F/F}:DEL^{CJ}* and *H2ax^{Δ/Δ}p53^{Δ/Δ}:DEL^{CJ}* clones treated with STI571 for increasing amounts of time revealed similar increasing loss of the pMX-DEL^{CJ} GL fragment and appearance of the pMX-DEL^{CJ} CJ fragment in the two *H2ax^{F/F}p53^{F/F}:DEL^{CJ}* and *H2ax^{Δ/Δ}p53^{Δ/Δ}:DEL^{CJ}* cells (Figure 6C). Again, despite conducting Southern analysis on twice as much genomic DNA for *H2ax^{F/F}p53^{F/F}:DEL^{CJ}* and *H2ax^{Δ/Δ}p53^{Δ/Δ}:DEL^{CJ}* cells than for *Artemis^{-/-}:DEL^{CJ}* cells, I did not observe detectable levels of the pMX-DEL^{CJ} CE fragment in *H2ax^{Δ/Δ}p53^{Δ/Δ}:DEL^{CJ}* cells (Figure 6C). These data further support the notion that H2AX is not required for end-joining of chromosomal coding ends in G1 phase lymphocytes.

Since RAG dependent formation of γH2AX occurs at Jκ segments and over adjacent sequences telomeric to the Igκ locus (Savić et al., 2009), I also considered that H2AX might be required for resolution of Jκ CEs. The mouse Igκ locus resides on chromosome 6 and is composed of 140 Vκs spanning 3 Mb and four functional Jκs spanning 2 kb and residing 60 kb from the Vκs. Igκ locus V(D)J recombination occurs through the coupled cleavage and subsequent joining of a Vκ and Jκ segment. Due to the small size of the Jκ cluster, Southern blot analysis with a 3' Jκ probe can be used to monitor and quantify the induction of RAG generated Igκ locus DSBs (Figure 7A, 7B). Thus, I next conducted Southern blotting of *H2ax^{-/-}* pre-B cells either un-treated or treated with STI571 for 72 hours. As a control for the accumulation of un-repaired Jκ CEs, I also conducted Southern blot analysis of previously described *Artemis^{-/-}* cells

(Helmink et al., 2009). I observed decreased intensity of the J κ GL band in both *H2ax*^{-/-} and *Artemis*^{-/-} cells treated with STI571, and appearance of bands corresponding to J κ CEs in STI571-treated *Artemis*^{-/-} cells, but not in STI571-treated *H2ax*^{-/-} cells (Figure 7B). These data indicate that H2AX deficiency does not result in the detectable accumulation of un-repaired Ig κ coding ends in G1 phase cells. Consequently, I conclude that H2AX function is not required for chromosomal end-joining during V(D)J recombination in G1 phase lymphocytes.

H2AX dependent chromatin changes prevent separation of RAG cleaved Ig κ DNA strands in G1 phase cells

I first sought to define the entire γ H2AX chromatin domain formed along Ig κ loci during V(D)J recombination in G1 phase cells. For this purpose, I conducted chromatin immunoprecipitation (ChIP) to measure γ H2AX densities in nucleosomes on DNA strands located within and adjacent to Ig κ loci in *Artemis*^{-/-} pre-B cells, either un-treated or treated with STI571 for 96 hours to ensure complete RAG mediated cleavage. I used *Artemis*^{-/-} cells rather than wild-type cells since the accumulation of un-repaired coding ends enhances ability to detect γ H2AX along RAG cleaved antigen receptor loci (Savić et al., 2009). Using ChIP, I detected significant increases in γ H2AX densities within Ig κ and for ~500 kb on both sides of Ig κ in STI571-treated *Artemis*^{-/-} pre-B cells (Figure 7C). The numbers of V κ and J κ DSBs within the experimental population of cells must be equal because V(D)J recombination proceeds through coupled cleavage. Because the Ig κ locus contains a cluster of 140 V κ segments spanning 2 Mb and a cluster of four

functional J κ segments spanning 1.8 kb, the chromosomal density of V κ cluster DSBs should be less than the chromosomal density of J κ cluster DSBs within my experimental population of cells. Thus, the simplest explanation for the observed γ H2AX pattern across the Ig κ locus is that it reflects the density of DSBs induced at the assayed genomic locations. However, these observations are also consistent with the notion that different features of local chromatin environment among the V κ segments and downstream of the J κ segments may influence γ H2AX dynamics. Regardless, my data demonstrate that a γ H2AX chromatin domain forms along chromosomal DNA strands containing RAG-cleaved Ig κ loci for distances extending at least 500 kb from Ig κ coding ends.

To test my hypothesis that H2AX mediated chromatin changes function to hold together broken DNA strands, I sought to monitor the positional stability of RAG cleaved Ig κ loci in G1 phase cells. I used two-dimensional two-color DNA fluorescent *in situ* hybridization (2D-2C-FISH) with a 5' V κ BAC (RP24-243E11) and a 3' C κ BAC (RP23-341D5) probe to monitor the positional stability of RAG cleaved Ig κ locus DNA strands in STI571-treated *Artemis*^{-/-}*p53*^{-/-} and *Artemis*^{-/-}*Atm*^{-/-} abl pre-B cells (Hewitt et al., 2009). These 5' V κ and 3' C κ probes hybridize to genomic sequences located near the ends of γ H2AX domain that forms along RAG cleaved Ig κ loci within STI571 treated pre-B cells (Figure 7C). 2D-FISH cannot distinguish between signals that appear on top of each other that are really separate, and therefore likely underestimates the numbers of cells with un-stabilized Ig κ locus DNA ends. However, since this should be equal across

cells of different genotypes, conclusions about different genotypes relative to each other are still possible with 2D-2C-FISH.

I first conducted 2D-2C-FISH using these 5' V κ and 3' C κ probes on G1 interphase nuclei prepared from three independent *Rag2*^{-/-} abl pre-B cells treated with STI571 for 96 hours (Figure 8A). I measured the distances between 5' V κ (red) and 3' C κ (green) signals on both alleles in ~200 nuclei of each cell line assayed, designated the shorter distance from "Allele 1" and the longer distance from "Allele 2", and plotted these values onto scatter plots. I observed overlapping or coincident probe hybridization signals (<1 μ m apart) on both alleles in greater than 95% of nuclei and non-coincident signals on one allele in less than 4% of nuclei (Figure 8B). Using three independent *Artemis*^{-/-} cell lines, I observed overlapping or coincident probe signals on both alleles in ~80% of nuclei and non-coincident probe signals on a single allele in ~20% of nuclei (Figure 8B). With three independent *Artemis*^{-/-}*H2ax*^{-/-} cell lines, I observed overlapping or coincident probe signals on both alleles in ~60% of nuclei and non-coincident probe signals on a single allele in ~40% of nuclei (Figure 8B). Although similar levels of un-repaired Ig κ locus CEs accumulated in all *Artemis*^{-/-} and *Artemis*^{-/-}*H2ax*^{-/-} cells assayed, I also normalized the percentage of nuclei with non-coincident probe hybridization signals to the extent of Ig κ locus cleavage (Figure 8C, Figure 9). These data show that RAG cleaved Ig κ locus DNA strands physically separate in a significantly higher percentage of *Artemis*^{-/-}*H2ax*^{-/-} cells than in *Artemis*^{-/-} cells. Similar results were obtained using a larger distance (>1.5 μ m) to score non-coincident hybridization (Figure 8C). Consequently, I conclude that

γ H2AX mediated chromatin changes suppress physical separation of RAG cleaved antigen receptor loci in G1 phase cells to prevent their irreversible disassociation or aberrant joining.

H2AX prevents transition of RAG cleaved DNA strands into chromosome breaks and translocations during cellular proliferation

Molecular characterization of IgH/c-myc translocations in $H2ax^{-/-}p53^{-/-}$ pro-B lymphomas revealed that these lesions occurred following the replication of chromosomes containing un-repaired RAG initiated IgH locus DNA breaks (Bassing et al., 2003; Celeste et al., 2003b). Thus, I hypothesized that γ H2AX formation along RAG cleaved antigen receptor loci promotes chromatin changes that hold together broken DNA strands to prevent un-repaired coding ends from transitioning into chromosome breaks and translocations during S phase (Bassing and Alt, 2004). To test my hypothesis, I sought to quantify the frequency of Igk chromosome breaks and translocations in $H2ax^{-/-}$, $Artemis^{-/-}$, and $Artemis^{-/-}H2ax^{-/-}$ abl pre-B cell lines treated with STI571 and then released back into cell cycle by STI571 removal. For this purpose, I used whole chromosome painting (WCP) for Chr. 6 (red) and conducted FISH with the 5' V κ and 3' C κ BACs (green) on metaphase spreads prepared from untreated cells or cells that had been treated with STI571 and then released back into cell cycle (Figure 10A). I found chromosome 6 chromosome breaks or translocations in less than 1% of metaphases prepared from untreated $H2ax^{-/-}$, $Artemis^{-/-}$, or $Artemis^{-/-}H2ax^{-/-}$ cells of three different cell lines for each genotype (Figure 10A, 10B). These data indicate that structural abnormalities of chromosome 6 are not frequent occurrences in abl pre-B cells with

deficiencies in H2AX and/or Artemis. I also detected chromosome 6 abnormalities in less than 1% of metaphases prepared from *H2ax*^{-/-} or *Artemis*^{-/-} cells treated and then released from STI571 (Figure 10A, 10B). However, I observed chromosome 6 breaks or translocations involving Igκ in 4-5% of metaphases prepared from *Artemis*^{-/-}*H2ax*^{-/-} cells treated and then released from STI571 (Figure 10A, 10B). Southern blot analysis of STI571-treated cells before removal of the STI571 revealed similar levels of unrepaired Igκ locus DSBs in all cells (data not shown). These data suggest that unrepaired Igκ locus coding ends progress into chromosome breaks and translocations at a significantly higher frequency in *Artemis*^{-/-}*H2ax*^{-/-} cells than in *Artemis*^{-/-} or *H2ax*^{-/-} cells after STI571 treatment and release. I also found chromosome 6 breaks and translocations involving Igκ in a significantly higher percentage of STI571-treated and released *Artemis*^{-/-}*H2ax*^{-/-} *p53*^{-/-} abl pre-B cells, as compared with *H2ax*^{-/-}*p53*^{-/-} and *Artemis*^{-/-}*p53*^{-/-} abl pre-B cells (data not shown). Although these data are consistent with a role of H2AX in promoting chromatin changes that hold together un-repaired coding ends persisting into S phase, potential effects of mutations in cell cycle checkpoints that arise during v-abl mediated immortalization more frequently or profoundly in *H2ax*^{-/-} cells than in *H2ax*^{+/+} cells could contribute to this observation.

H2AX prevents chromosome breaks emanating from un-repaired TCRα/δ locus coding ends

I next sought to test the hypothesis that H2AX prevents un-repaired coding ends from transitioning into chromosome breaks and translocations during continued cell cycle progression using primary lymphocytes. This approach also enables assessment of this

potential H2AX function during a physiologic cell cycle, rather than during recovery from the prolonged G1 arrest associated with STI571 treatment and release. Although a small fraction of un-repaired coding ends persists into S phase in normal primary thymocytes (Pedraza-Alva et al., 2006), I decided to dramatically increase the percentage of cells with un-repaired coding ends for analyses by using *Artemis*^{-/-} thymocytes. Because *Artemis*^{-/-} cells with un-repaired coding ends are eliminated by p53-mediated apoptosis (Rooney et al., 2004a), I also needed to use p53-deficiency allow thymocytes with un-repaired coding ends to survive and proliferate. I first generated germline *H2ax*^{-/-} *p53*^{-/-}, *Artemis*^{-/-} *p53*^{-/-}, and *H2ax*^{-/-} *Artemis*^{-/-} *p53*^{-/-} mice to test my hypothesis; unfortunately *H2ax*^{-/-} *Artemis*^{-/-} *p53*^{-/-} mice rapidly succumbed to multiple malignancies preventing analysis of un-repaired coding ends in non-malignant thymocytes. I reasoned that the specific deletion of *H2ax* and/or *p53* in *Artemis*^{-/-} thymocytes should prevent early onset of lymphomas and provide the requisite *in vivo* experimental system. Transgenic mice expressing Cre under control of the proximal *Lck* promoter (*Lck*-Cre mice) direct excision of target genes such as "floxed" p53 (*p53*^{F/F}) in thymocytes prior to the initiation of V(D)J recombination (Orban et al., 1992; Lee et al., 2001). Thus, I generated *Lck-CreArtemis*^{-/-} *p53*^{F/F} (*LAP*), *Lck-CreH2ax*^{F/F} *p53*^{F/F} (*LHP*) and *Lck-CreArtemis*^{-/-} *H2ax*^{F/F} *p53*^{F/F} (*LAHP*) mice. All mice were created heterozygous for *Lck-Cre* to avoid potential complications associated with transgene integration site. The low cellularity of *LAP* and *LAHP* thymocytes posed an insurmountable obstacle for quantitative cytogenetic analyses, thus I prepared metaphase spreads from c-kit⁻ CD25⁺CD4⁻CD8⁻ thymocytes, in which normal TCR rearrangements occur, from cultured bone marrow of *LHP*, *LAP*, and *LAHP* mice on OP9-DL1 stromal cells (Schmitt

and Zúñiga-Pflücker, 2002). Occasionally the OP9 feeder cells gave rise to metaphases that were scattered among lymphocyte metaphases; I demonstrated that the OP9 feeder cell metaphases can be easily separated from those of lymphocytes based on distinct features, such as four copies of Chr. 6 and four copies of Chr. 14, as shown by spectral karyotyping (SKY) and WCP/FISH (Figure 11).

In mouse thymocytes, V(D)J recombination occurs at TCR α/δ loci on chromosome 14, TCR β loci on chromosome 6, TCR γ loci on chromosome 13, and to a limited extent IgH loci on chromosome 12. TCR γ translocations are rarely observed in human and mouse $\alpha\beta$ T cells and T lineage lymphomas. Thus, to assay for potential chromosome breaks and translocations initiating from un-repaired RAG generated coding ends, I hybridized whole chromosome 14, 6, and 12 paints and conducted FISH with BAC probes that hybridize to genomic sequences 5' or 3' of TCR α/δ , TCR β , or IgH loci on metaphase spreads prepared from *LHP*, *LAP* and *LAHP* thymocytes (Figure 12A). For this purpose, I prepared metaphase spreads from independent thymocyte cultures from two different three to five week old mice of each genotype. I analyzed 200 or greater numbers of metaphases for each chromosome paint and FISH probe set on each culture. Chromosome breaks or translocations involving antigen receptor loci were scored when the 5' and 3' FISH probe signals were non-coincident (Figure 12A). Through this approach, I did not find any chromosome 12 or IgH locus breaks or translocations in metaphases prepared from *LAHP*, *LHP*, or *LAP* thymocytes (Figure 12A). However, I observed a modest increase in the frequency of chromosome 6 breaks and translocations

involving TCR β loci in metaphases prepared from *LAHP* thymocytes, as compared to in metaphases prepared from *LHP* or *LAP* thymocytes (Figure 12A, 12B). These findings indicate that structural abnormalities of chromosome 6 and 12 are not frequent occurrences in primary thymocytes deficient in H2AX and/or Artemis, but suggest that H2AX may suppress TCR β translocations. Notably, I observed a substantial increase in the frequency of chromosome 14 abnormalities involving TCR α/δ loci in metaphases prepared from *LAHP* thymocytes, as compared to those prepared from *LHP* or *LAP* thymocytes (Figure 12A, 12B). All chromosome 14 abnormalities in *LAHP* cells were replicated TCR α/δ chromosome breaks and, among the metaphases with these lesions, ~90% contained replicated breaks on a single copy of chromosome 14 (Figure 12C). Although I cannot exclude the possibility that these TCR α/δ chromosome abnormalities represent rare events in a few DN thymocytes that preferentially expand, my data still support a role of H2AX in preventing accumulation of such cells. Based upon these data, I conclude that H2AX mediated chromatin changes along RAG cleaved antigen receptor loci prevent un-repaired coding ends from transitioning into chromosome breaks during continued cell cycle progression.

DISCUSSION

The mechanisms by which H2AX suppresses translocations during V(D)J recombination have remained enigmatic since the findings that a significant percentage of $H2ax^{-/-}$ $\alpha\beta$ T cells contain TCR α/δ locus translocations and $H2ax^{-/-}p53^{-/-}$ mice develop pro-B lymphomas with RAG initiated IgH/c-myc translocations (Bassing et al., 2003; Celeste et al., 2003b). I have demonstrated here that H2AX is not required for the joining of chromosomal coding ends during V(D)J recombination in G1 phase lymphocytes. In this context, I have shown that H2AX deficiency in *abl* pre-B cells does not lead to accumulation of un-repaired coding ends during the rearrangement of chromosomal substrates, as previously observed in *abl* pre-B cells deficient for ATM or DNA-PKcs (Bredemeyer et al., 2006). These data are consistent with the observations that lymphocyte development in $H2ax^{-/-}$ mice is not blocked or impaired at stages in which antigen receptor variable region genes are assembled, as is the case in $DNA-PKcs^{-/-}$ and $Atm^{-/-}$ mice (Bosma et al., 1983; Barlow et al., 1996; Elson et al., 1996; Xu et al., 1996; Gao et al., 1998; Taccioli et al., 1998; Borghesani et al., 2000; Matei et al., 2007; Vacchio et al., 2007). Consequently, I conclude that γ H2AX formation is not critical for ability of DNA-PKcs and ATM to process and join chromosomal coding ends during variable region gene assembly in G1 phase cells. Although generation of γ H2AX has been proposed to facilitate DSB repair kinetics by promoting accessibility of broken DNA ends and recruiting repair factors (Rogakou et al., 1998), I did not observe a difference in the kinetics of chromosomal coding join formation between $H2ax^{+/+}$ and $H2ax^{-/-}$ *abl* pre-B cells. However, potential accessibility and recruitment functions of γ H2AX might not be evident during V(D)J recombination since initiation of RAG

generated DSBs requires prior opening of chromosomal substrates and the RAG proteins may recruit end-joining factors (Agrawal and Schatz, 1997; Bassing et al., 2002a; Lee et al., 2004; Raval et al., 2008). Thus, I conclude that impaired coding join formation in G1 phase cells is not the predominant mechanism through which translocations arise during V(D)J recombination in H2AX deficient lymphocytes.

Despite no obvious requirement for H2AX in coding join formation, the data that IgH/c-myc translocations arise by identical mechanisms in *H2ax*^{-/-}*p53*^{-/-} mice and NHEJ/p53-deficient mice suggested that H2AX serves critical functions during end-joining in G1 phase cells. One advantage of STI571-treated abl pre-B cells is that molecular events associated with V(D)J recombination can be studied in G1 arrested cells; NHEJ-deficient abl pre-B cells offer additional advantages by enabling analysis of particular DSB intermediates and amplification of DNA damage responses. Through the use of *Artemis*^{-/-} and *Artemis*^{-/-}*H2ax*^{-/-} abl pre-B cells, I have demonstrated here that H2AX-mediated chromatin changes suppress the physical separation of RAG cleaved Igk locus strands in G1 phase cells. This could be due to the γ H2AX mediated anchoring of proteins (such as 53BP1 or cohesins) that hold broken DNA ends together (Bassing and Alt, 2004), limit flexibility of DNA strands (Difilippantonio et al., 2008; Dimitrova et al., 2008), and/or promote interactions of chromatin with components of the nuclear matrix (Rogakou et al., 1998). Based upon the impaired joining and progression of IgH locus DNA breaks into chromosome breaks and translocations during class switch recombination in *H2ax*^{-/-} B lymphocytes (Reina-San-Martin et al., 2003; Franco et al., 2006; Ramiro et al., 2006), H2AX has been concluded to function in NHEJ by promoting

synapsis of DNA ends. Yet, considering that class switch recombination occurs in rapidly proliferating cells (Chaudhuri et al., 2007), these phenotypes could be attributable to H2AX mediated activation of p53-independent cell cycle checkpoints. Thus to my knowledge, the data presented here that H2AX suppresses separation of RAG cleaved DNA strands in G1 arrested cells is the first direct evidence that H2AX exhibits synaptic functions during NHEJ.

Since RAG1/RAG2 can hold CEs and SEs within stable synaptic complexes *in vitro* (Agrawal and Schatz, 1997; Lee et al., 2004) and ATM maintains chromosomal CEs in proximity (Bredemeyer et al., 2006), my finding that Igk locus strands with un-repaired CEs separated in *Artemis*^{-/-} cells was unexpected. In this context, ATM alone is not sufficient to prevent disassociation of CEs that are held much less tightly than SEs in the RAG post-cleavage complex. However, this observation is in accord with live cell imaging experiments demonstrating mobility of DNA ends at DSBs generated in Ku80-deficient cells (Soutoglou et al., 2007). My data could reflect baseline mobility of un-repaired Igk locus DSBs or indicate a role of Artemis in maintaining RAG generated DNA ends within synaptic complexes, either directly or indirectly through Ku70/Ku80, DNA-PKcs, and/or other end-binding factors. My finding that H2AX suppresses the physical separation of broken Igk locus strands appears in contrast with experiments demonstrating a role of Ku80, but not H2AX, in promoting immobility of DSBs (Soutoglou et al., 2007). Upon DSB induction, more unrepaired DNA ends should accumulate in *Ku80*^{-/-} cells as compared with *H2ax*^{-/-} cells as a result of the differential functions of these proteins in end joining. In my study, I used Artemis deficiency to

compare the positional stability of disrupted chromosomal DNA strands between *H2ax*^{+/+} and *H2ax*^{-/-} cells that have accumulated equivalent levels of unrepaired DSBs. Thus, I believe that the disparate conclusions regarding the role of H2AX in maintaining broken chromosomal DNA ends in proximity is the result of a greater level of unrepaired DNA ends that can physically separate in cells deficient for Ku80 versus H2AX.

Although V(D)J recombination occurs in G1 phase cells, some fraction of developing lymphocytes with un-repaired CEs progress into S phase (Pedraza-Alva et al., 2006). I have shown here that H2AX prevents accumulation of chromosome breaks from RAG initiated antigen receptor locus DNA breaks that are not repaired prior to DNA replication. In this context, I have demonstrated that H2AX deficiency in Artemis/p53-deficient thymocytes leads to a substantial increase in the percentage of cells with replicated TCR α/δ chromosome breaks. Replication through hairpin sealed CEs should lead to either dicentric or ring chromosomes in metaphase cells. The absence of such chromosome abnormalities in metaphases prepared from *LAP* or *LAHP* thymocytes suggests that TCR α/δ CEs persisting into S phase are opened prior to DNA replication. Detection of replicated TCR α/δ chromosome breaks in *LAHP*, but not *LAP*, metaphases indicates that H2AX holds together DNA strands with un-repaired TCR α/δ CEs to facilitate end-joining and/or activates the G2/M checkpoint to prevent mitosis. ATM similarly prevents the continued proliferation of lymphocytes with un-repaired RAG generated coding ends (Callén et al., 2007). Thus, I conclude that ATM-mediated H2AX-dependent chromatin changes along RAG cleaved antigen receptor loci prevent un-

repaired coding ends from transitioning into chromosome breaks during continued cell cycle progression.

The data presented in this chapter further contribute to understanding the mechanisms by which chromosomal DSBs are repaired through NHEJ in G1 phase mammalian cells (Figure 13). My findings that H2AX, but not ATM or the MRN complex (Bredemeyer et al., 2006; Helmink et al., 2009), is dispensable for end-joining of chromosomal CEs in G1 phase cells is consistent with the lower frequency of inter-locus V(D)J recombination events and the milder lymphopenia of *H2ax*^{-/-} mice, as compared to *Atm*^{-/-}, *Nbs1*^{m/m} and *Mre11*^{ATLD/ATLD} mice (Kang et al., 2002; Theunissen et al., 2003). ATM (Bredemeyer et al., 2006), and likely MRN (Deriano et al., 2009; Helmink et al., 2009), facilitates end-joining by maintaining chromosomal CEs within RAG post-cleavage synaptic complexes, which engage the proximal ends of cleaved DNA strands. My observations that γ H2AX densities are low near J κ CEs, but elevated over sequences extending at least 500 kb on both sides of Ig κ CEs, indicates that γ H2AX formation stabilizes broken DNA strands at locations distal to breakage sites (Bassing and Alt, 2004). During V(D)J recombination, this ATM dependent formation of γ H2AX along RAG cleaved DNA strands (Savić et al., 2009) is dispensable for end-joining of chromosomal CEs in G1 phase cells due to cooperation between the DNA end synaptic functions of RAG1/RAG2 and ATM/MRN. In contrast, the ATM dependent generation of γ H2AX along DNA strands would be more critical for the NHEJ mediated repair of DSBs generated by genotoxic insults such as IR or nucleases lacking DNA end synaptic functions such as those that initiate IgH locus CSR (Figure 13).

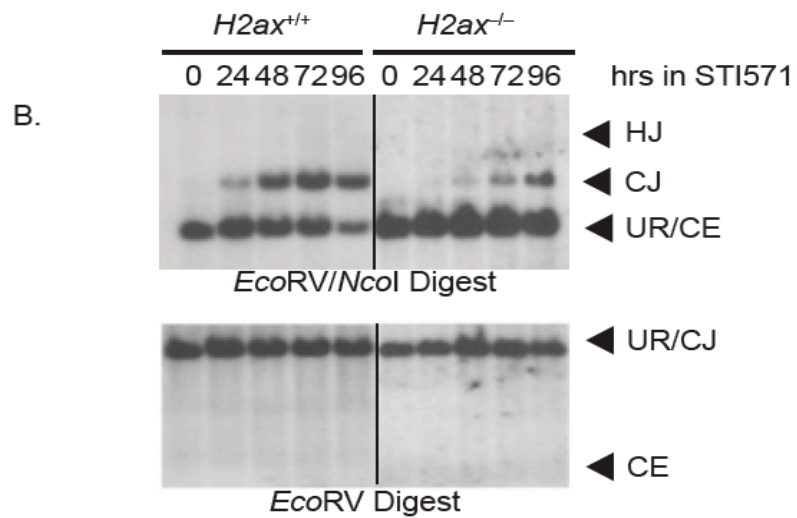
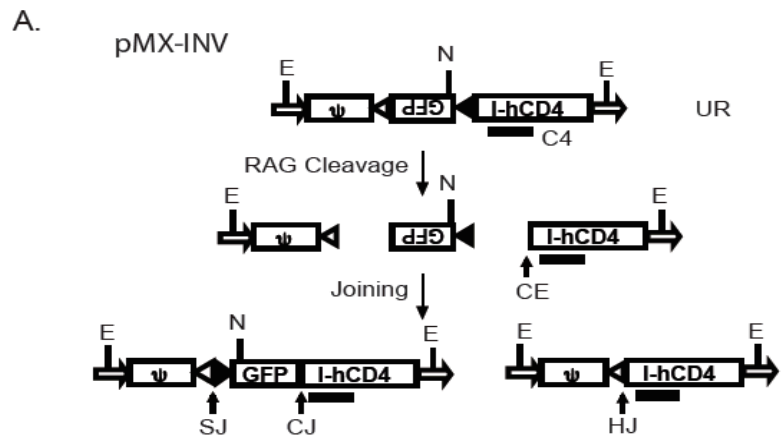


Figure 5. H2AX is not required for normal resolution of V(D)J recombination

intermediates of chromosomally integrated pMX-INV in G1-arrested *abl* cells. A)

The non-rearranged (NR), coding joined (CJ) and hybrid joined (HJ) configurations, and the 3' coding end (CE) generated by Rag cleavage of the pMX-INV retroviral recombination substrate are shown, with the IRES-human CD4 cDNA (I-hCD4), the GFP cDNA and the recombination signals (triangles). Also indicated are the relative positions of the *EcoRV* (E) and *NcoI* (N) restriction sites. The relative position of the C4 probe used for Southern blot analysis and sizes of different DNA fragments after *EcoRV/NcoI* digestion is also shown. **B)** Coding joint and 3' coding end formation in *H2ax*^{+/+} and *H2ax*^{-/-} cells transfected with the pMX-DEL^{CJ} recombination substrate was monitored by Southern blot on cells treated with STI571 for the indicated time (hrs). Fragments of the correct size for pMX-INV NR, CJ, HJ, and CE are indicated, along with the restriction enzyme used for digestion.

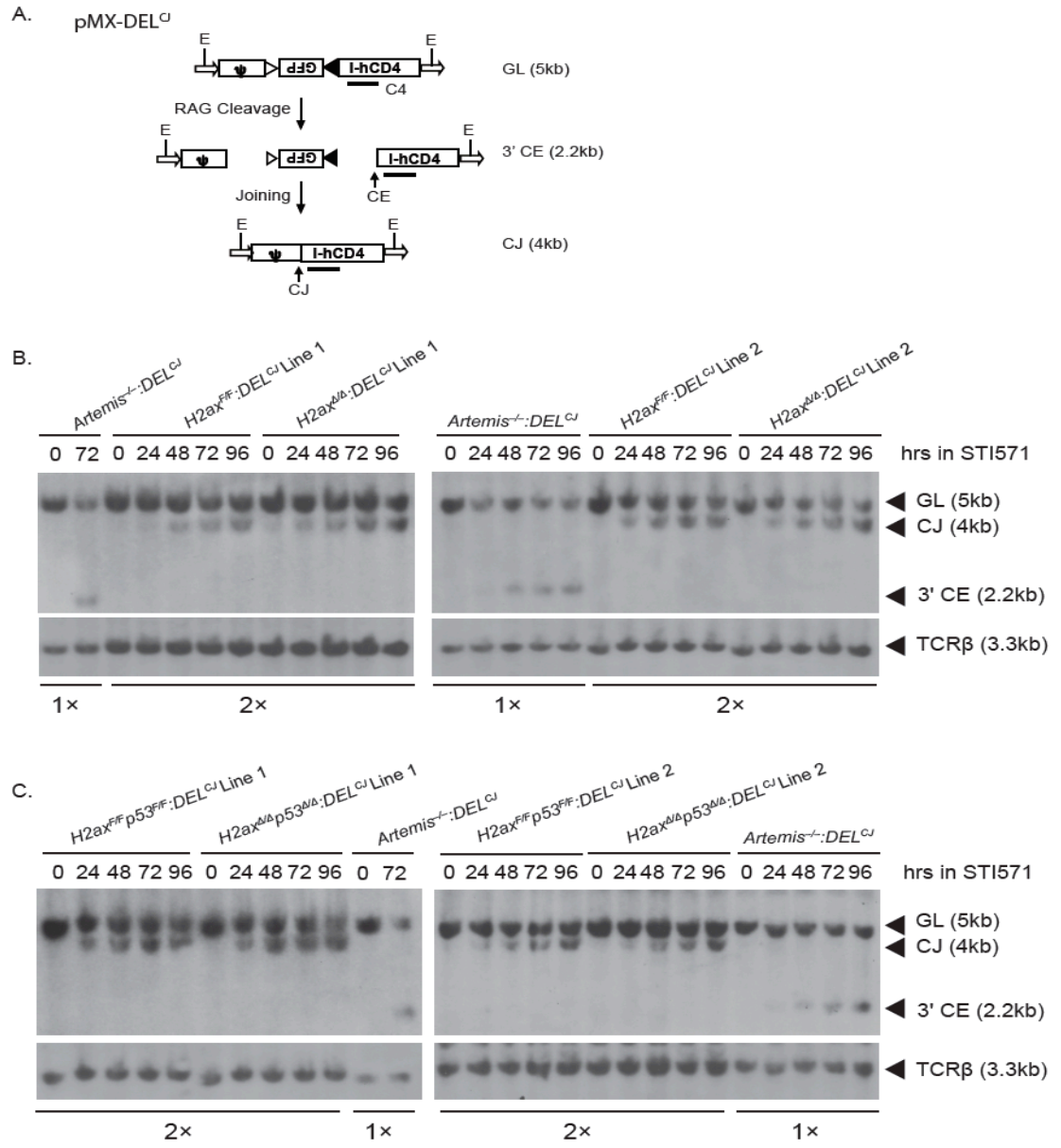
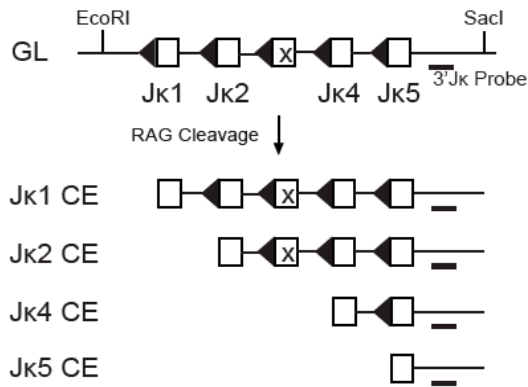
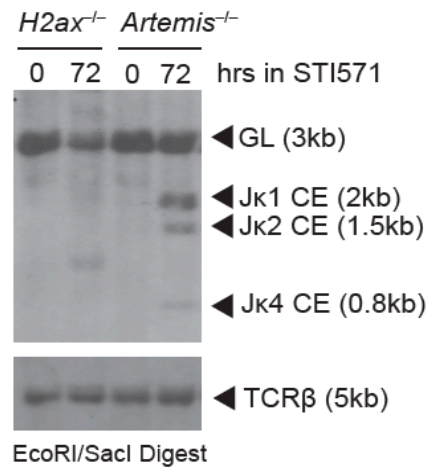


Figure 6. H2AX deficient cells exhibit normal coding join formation within chromosomal substrates. **A)** Shown are schematic diagrams of the pMX-DEL^{CJ} V(D)J recombination substrate in the un-cleaved (GL), cleaved but not repaired (CE), and cleaved and repaired (CJ) configurations. The recombination signal sequences are represented by triangles. Arrows represent the LTR sequences. Indicated are the relative positions of the EcoRV sites (E) and C4 probe used for Southern blot analysis and the sizes of the C4-hybridizing EcoRV fragments in pMX-DEL^{CJ} substrates of the GL, CE, and CJ configuration. **B-C)** Southern blot analysis of recombination products generated in cells of two different **B)** *H2ax*^{F/F}:*DEL*^{CJ} and *H2ax*^{Δ/Δ}:*DEL*^{CJ} abl pre-B cell lines or **C)** *H2ax*^{F/F}*p53*^{F/F}:*DEL*^{CJ} and *H2ax*^{Δ/Δ}*p53*^{Δ/Δ}:*DEL*^{CJ} abl pre-B cell lines treated with STI571 for the indicated times. EcoRV-digested genomic DNA was hybridized with the C4 probe. The bands corresponding to pMX-DEL^{CJ} substrates of the GL, CE, and CJ configurations are indicated. Blots were stripped and then probed with a TCRβ probe as a control for DNA content. *Artemis*^{-/-}:*DEL*^{CJ} abl pre-B cell lines were used as a positive control for detection of pMX-DEL^{CJ} CEs, with half as much genomic DNA loaded to increase the sensitivity of detection for pMX-DEL^{CJ} CEs in experimental cells. These data are representative of experiments performed more than three independent times.

A.



B.



C.

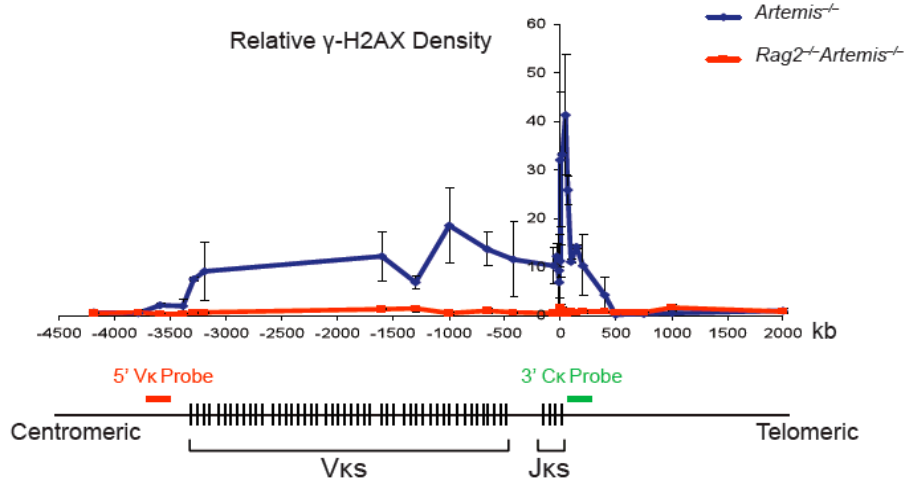


Figure 7. No accumulation of J κ coding ends in the absence of H2AX

phosphorylation along RAG cleaved Ig κ DNA strands. A) Shown are schematic

diagrams of the J κ cluster of the Ig κ locus in the un-cleaved (GL) and cleaved but not repaired (CE) configurations. Open boxes represent the J κ segments and triangles their recombination signal sequences. Indicated are the relative positions of the EcoRI and SacI sites and 3'J κ probe used for Southern blot analysis. **B)** Southern blot analysis of

recombination products generated in *H2ax*^{-/-} and *Artemis*^{-/-} abl pre-B cell lines, either untreated or treated with STI571 for 72 hours. EcoRI/SacI-digested genomic DNA was hybridized with the 3'J κ probe. The bands corresponding to J κ loci of the GL and CE configurations are indicated. The STI571 treated *H2ax*^{-/-} cells harbor a band that likely

represents a predominant V κ J κ rearrangement. Blots were stripped and then probed with a TCR β probe as a control for DNA content. These data are representative of experiments performed more than ten independent times. **C)** Schematic diagram of the mouse Ig κ

locus and graphical representation of γ H2AX densities as determined by ChIP at locations along DNA strands within and adjacent to Ig κ in *Artemis*^{-/-} abl pre-B cells treated with STI571 for 96 hours. The 0 kb value of the X axis corresponds to the 3' end

of the J κ 5 coding segment. Red and green lines indicate the approximate genomic

locations to which the 5' V κ (RP24-243E11) and 3' C κ (RP23-341D5) BACs hybridize.

The lengths of these lines are not drawn to scale. These data are representative of

experiments performed more than twenty independent times.

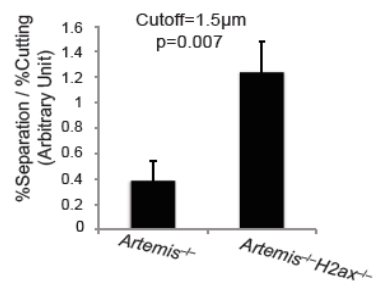
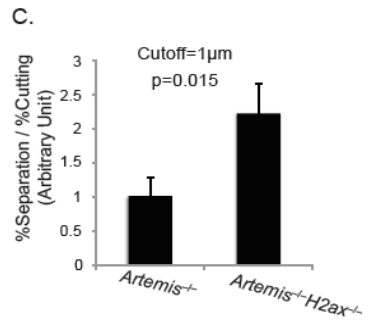
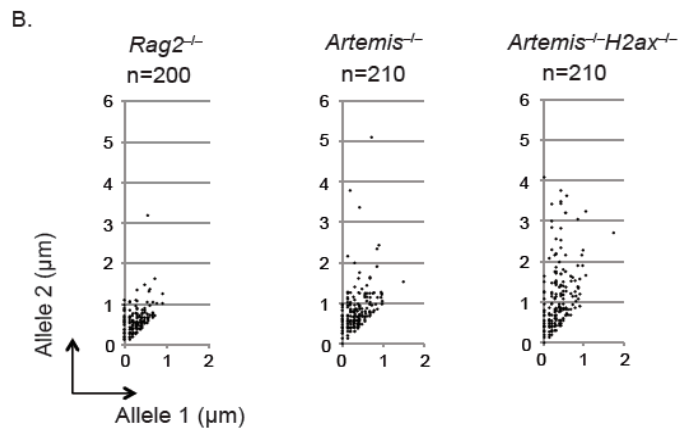
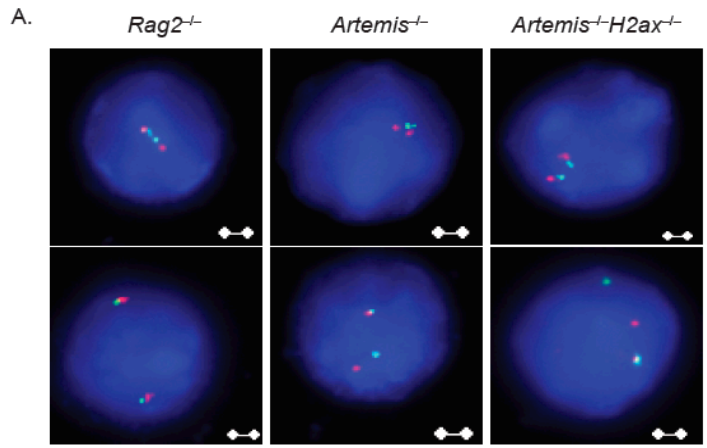


Figure 8. H2AX suppresses separation of RAG cleaved Igκ locus DNA strands. A)

Shown are representative fluorescent light microscopy images of 2C-FISH analysis conducted on G1 phase nuclei of *abl* pre-B cells treated with STI571 for 96 hours. Nuclei were hybridized with the 5' Vκ (red) and 3' Cκ (green) BAC and stained with DAPI to visualize DNA. The representative *Rag2*^{-/-} image shows a nucleus with coincident probe hybridization signals on both Igκ alleles; the top nucleus contains paired Igκ alleles and the bottom un-paired Igκ alleles. The representative *Artemis*^{-/-} and *Artemis*^{-/-}*H2ax*^{-/-} images each shows nuclei with coincident probe signals on both Igκ alleles and paired Igκ alleles (top images); or non-coincident probe signals on one Igκ allele, overlapping probe hybridization on the other Igκ allele, and un-paired Igκ alleles (bottom images). Bars, ~3μm. **B)** Shown are representative scatter plots depicting the distances between red and green signals on Allele 1 (shorter distance) and Allele 2 (longer distance) in G1 phase nuclei of *abl* pre-B cells treated with STI571 for 96 hours. The numbers (n) of nuclei assayed to generate the representative data are indicated. These data are representative of experiments performed three independent times for each genotype. **C)** Shown are bar graphs depicting in arbitrary units the nuclei with separated RAG cleaved Igκ DNA strands normalized to the extent of cutting in three experiments conducted on cells of independent *Artemis*^{-/-}, and *Artemis*^{-/-}*H2ax*^{-/-} *abl* pre-B cells treated with STI571 for 96 hours. The graphs use either 1μm (left) or 1.5μm (right) as the cutoff for distinction between coincident or overlapping versus non-coincident probe hybridization signals. Three independent experiments were conducted for each genotype.

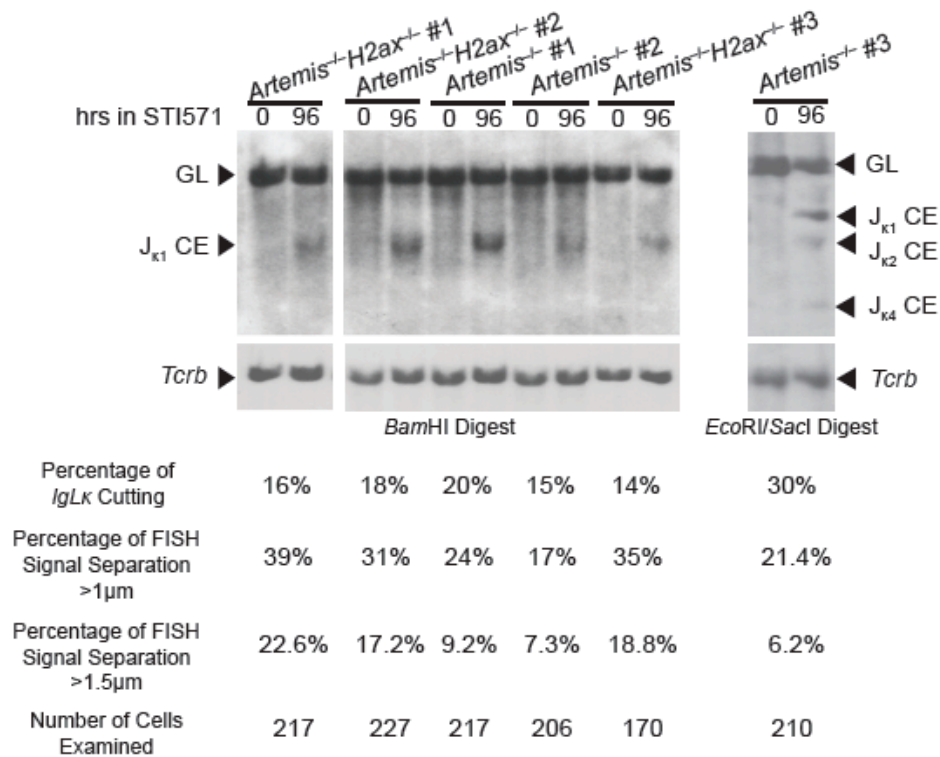
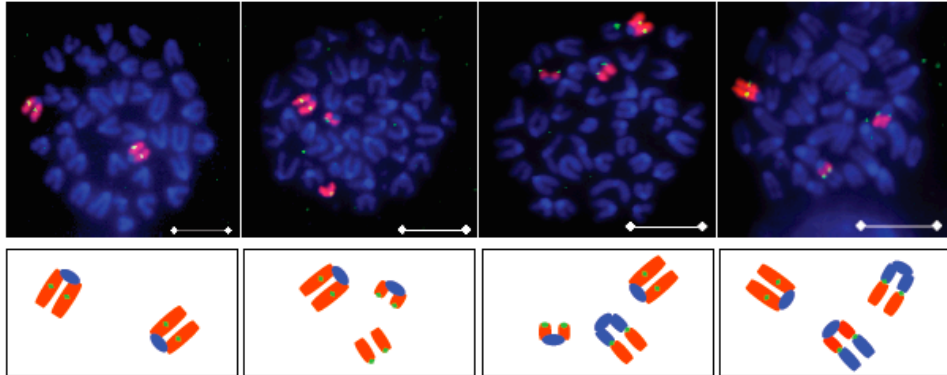


Figure 9. Quantification of *Igk* cutting following STI571 induction of the three *Artemis*^{-/-} and three *Artemis*^{-/-}*H2ax*^{-/-} cell lines used in 2D-2C-FISH. Southern blot analysis of recombination products generated in *Artemis*^{-/-} and *Artemis*^{-/-}*H2ax*^{-/-} *abl* pre-B cell lines, either untreated or treated with STI571 for 96 hours. BamHI- or EcoRI/SacI-digested genomic DNA was hybridized with the 3'*Jk* probe. The bands corresponding to *Jk* loci of the GL and CE configurations are indicated. Blots were stripped and then probed with a TCRβ probe as a control for DNA content. The percentages of *Igk* cutting, the percentages of FISH signal separation and the numbers of cells examined are listed for each cell line. 2D-2C-FISH for the BamHI-digested samples were conducted blind, while that for the EcoRI/SacI-digested sample was not.

A.

Chr. 6 / 3' Igk and 5' Igk BACs / DAPI



B.

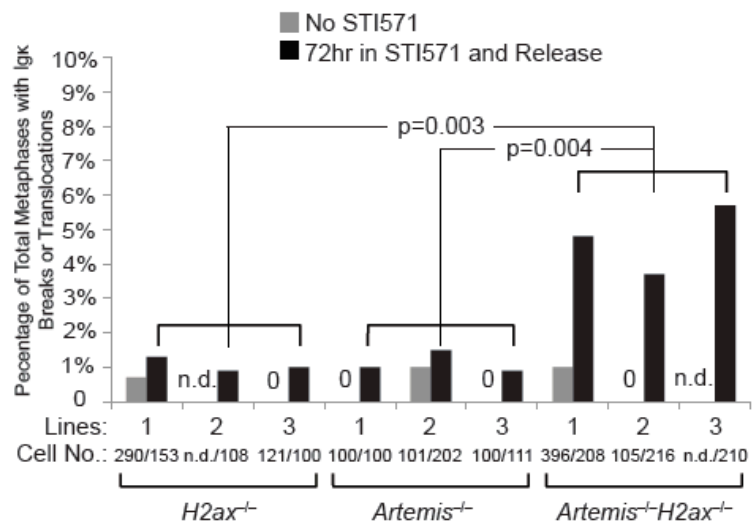
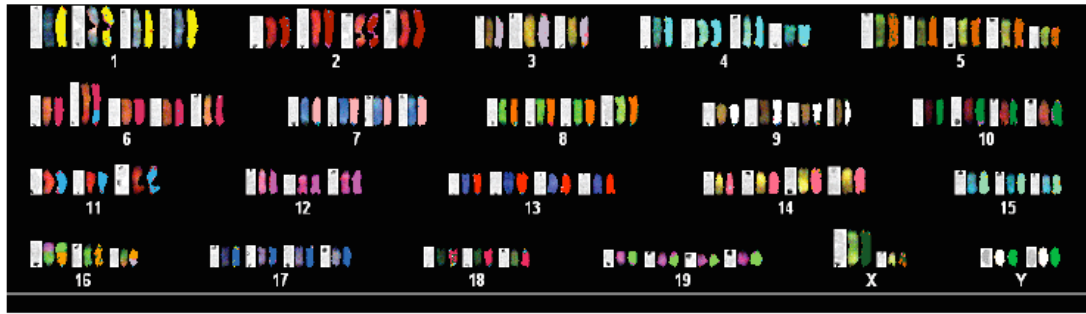


Figure 10. H2AX prevents transition of RAG cleaved Igκ DNA strands into chromosome breaks and translocations during cellular proliferation. **A)** Shown are representative fluorescent light microscopy images of whole chromosome (Chr.) 6 paints (red) and FISH analysis using the 5' Vκ and 3' Cκ BACs (both green) and DAPI (blue) to visualize DNA on metaphases prepared from STI571-treated and released *Artemis*^{-/-} *H2ax*^{-/-} abl pre-B cells. Below each image is a schematic representation of the observed Chr. 6 configurations. Bars, ~1μm. **B)** Shown is a bar graph with quantification of RAG initiated Igκ chromosome breaks or translocations in metaphases prepared from cells of three independent *H2ax*^{-/-}, *Artemis*^{-/-}, and *Artemis*^{-/-}*H2ax*^{-/-} pre-B cell lines released from STI571 treatment. Metaphases prepared from cells of the same lines without STI571 treatment were assayed for Igκ chromosome breaks or translocations to control for potential spontaneous rearrangement and genomic instability accumulated during cell culture. The data represent the percentage of total metaphases analyzed that contained Igκ chromosome abnormalities. The numbers of metaphases assayed are indicated. The values of 0 mean that no Igκ abnormalities were observed, while n.d. means not determined. The *p* values for comparison between cells of the indicated different genotypes are shown. These data were obtained from three independent experiments.

A.



B.

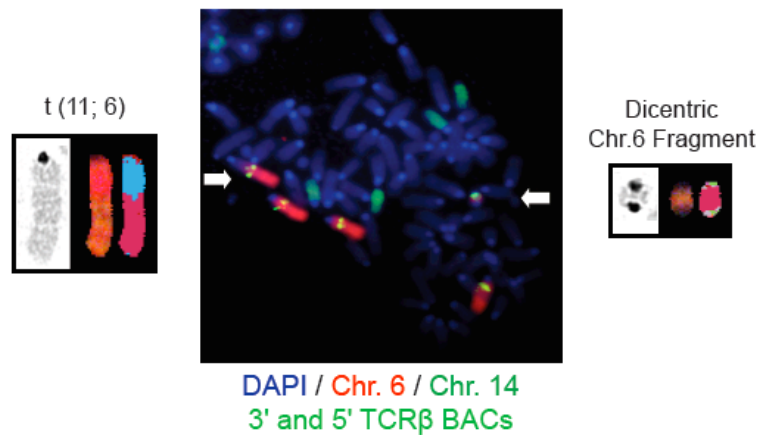


Figure 11. OP9-DL1 feeder cell metaphases can be separated from lymphocyte spreads. A) Representative SKY of the OP9-DL1 feeder cell line, note that the clonal translocations and aneuploidy (multiple copies of certain chromosomes, totally chromosome number >40) make it easy to separate them from metaphase spreads of primary lymphocytes. **B)** WCP/FISH (Chr. 6, red; TCR β FISH, green; Chr. 14, green) image of the OP9-DL1 feeder cell line. Note there are 4 copies of Chr. 6, one of which engages in a t(11;6) translocation, and one dicentric Chr. 6 fragment. There are also 4 copies of full length Chr. 14.

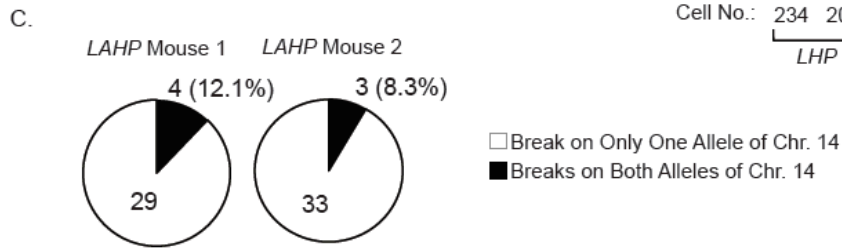
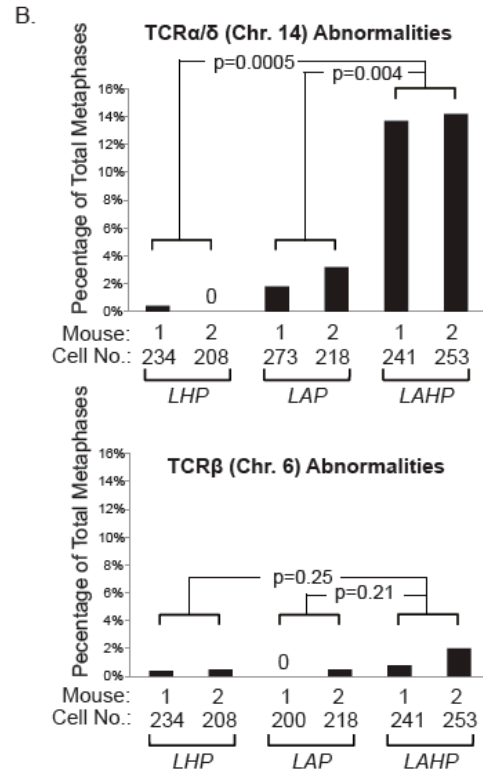
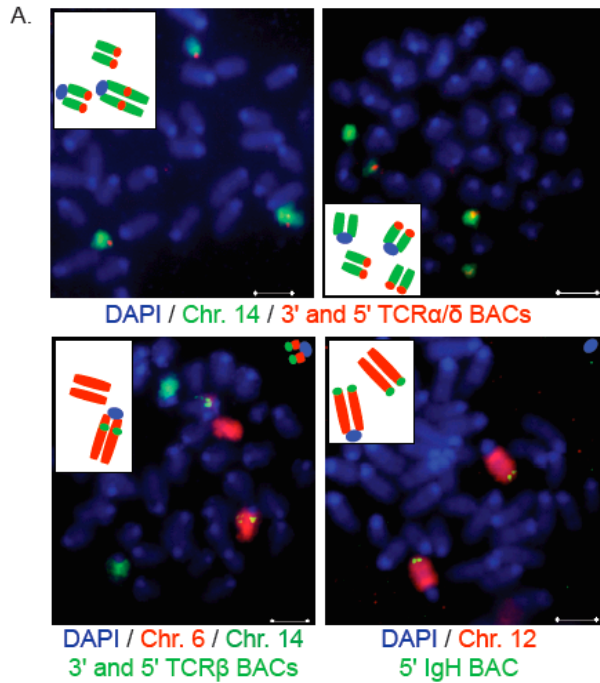


Figure 12. H2AX prevents chromosome breaks emanating from un-repaired TCR α / δ locus coding ends in primary thymocytes. **A)** Shown are representative fluorescent light microscopy images of whole chromosome paints and FISH analysis of antigen receptor loci on metaphases prepared from *LAHP* primary thymocytes. The inserts contain schematics depicting the chromosome abnormalities within each metaphase. Shown in the top images is Chr. 14 paints (green) and FISH with 5' V α and 3' C α BACs (both red) and DAPI (blue) to visualize DNA. Shown in the bottom left image is Chr. 6 paint (red) and FISH with 5' V β and 3' C β BACs (both green) and DAPI (blue) to visualize DNA. Shown in the bottom right image is Chr. 12 paint (red) and FISH with a 5' V H BAC (green) and DAPI (blue) to visualize DNA. Bars, $\sim 2\mu\text{m}$. **B)** Shown are bar graphs with quantification of chromosome abnormalities involving TCR α / δ loci (left) or TCR β loci (right) in metaphases prepared from primary thymocytes of two independent *LHP*, *LAP*, and *LAHP* mice. The numbers of metaphases assayed to generate the data are indicated. The values of 0 mean that no TCR abnormalities were observed. These data were obtained from experiments performed two independent times. **C)** Shown are pie charts depicting the percentages of *LAHP* cells with TCR α / δ chromosome breaks that contain these abnormalities on either one (white) or both (black) allelic copies of Chr. 14.

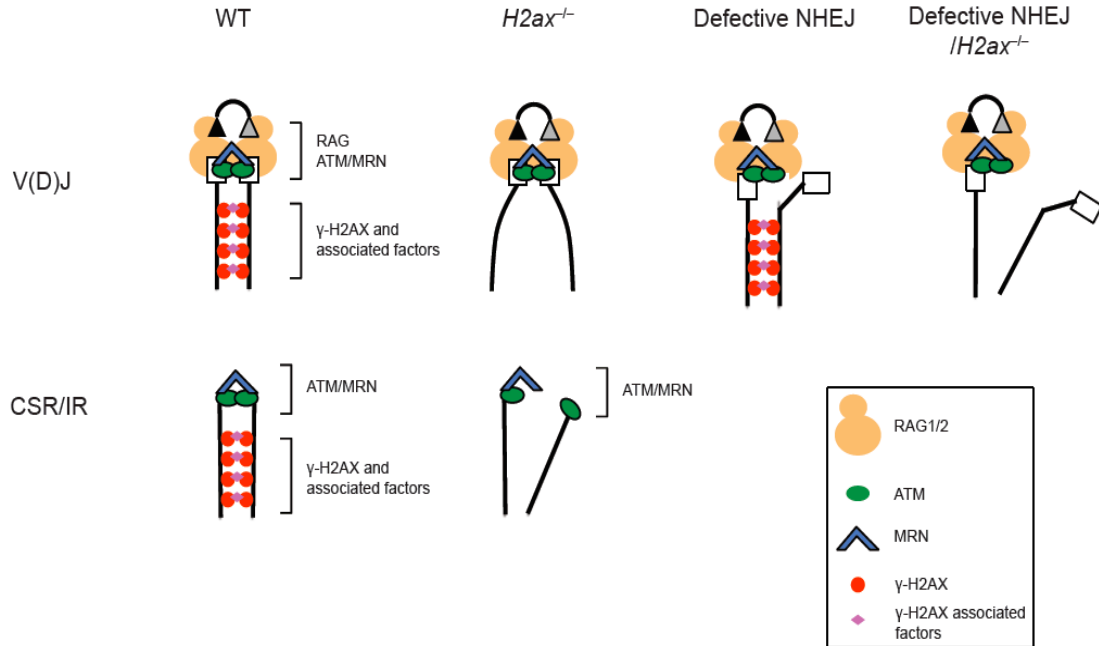


Figure 13. Models of H2AX function during end-joining repair of chromosomal DSBs. Schematic diagrams depicting the potential positional stability of broken chromosomal DNA strands during V(D)J recombination, CSR, or general DSB repair in G1 phase wild-type and H2AX-deficient cells. Boxes and triangle represent RAG-generated coding and signal ends, respectively. H2AX-mediated stabilization of broken DNA strands would be dispensable for end-joining during V(D)J recombination due to DNA end stabilization by ATM/MRN and RAG post-cleavage synaptic complexes. However, this H2AX function would be important for end-joining during CSR and general DSB repair.

Chapter III

Cellular Context Dependent Effects of *H2ax* and *p53* Deletion upon the Development of Thymic Lymphomas

ABSTRACT

Histone H2AX and Artemis each cooperate with p53 to suppress lymphomas harboring clonal translocations. Germline *H2ax*^{-/-}*p53*^{-/-} mice succumb to TCRβ⁻ thymic lymphomas with genomic lesions characteristic of human T-cell acute lymphoblastic leukemia (T-ALL). Here, I demonstrate that mice with somatic inactivation of *H2ax* and *p53* in thymocytes succumb at later ages to TCRβ⁻ or TCRβ⁺ thymic lymphomas containing a similar pattern of translocations as *H2ax*^{-/-}*p53*^{-/-} tumors. Germline *Artemis*^{-/-}*p53*^{-/-} mice succumb to lymphomas with antigen receptor locus translocations, while germline *Artemis*^{-/-}*H2ax*^{-/-}*p53*^{-/-} mice die at earlier ages from multiple malignancies. I show here that *Artemis*^{-/-} mice with *p53* deletion in thymocytes succumb to TCRβ⁻ thymic lymphomas containing clonal *Tcrα/δ* translocations, other clonal translocations, or aneuploidy. Strikingly, *Artemis*^{-/-} mice with combined *H2ax* and *p53* deletion in thymocytes exhibit a lower rate of mortality from TCRβ⁻ thymic lymphomas, which harbor significantly elevated levels of chromosome fragments and detached centromeres. My data reveal that the cellular origin of *H2ax* and *p53* loss impacts the rate of mortality from and developmental stage of thymic lymphomas, and also indicate that ARTEMIS inhibition might provide more specific and less toxic therapies for T-ALL and other cancers with loss of H2AX and p53 function.

INTRODUCTION

The accumulation of genomic instability can result in genetic changes that prevent cell death, enable self-renewal, and drive uncontrolled proliferation of somatic cells. Such transforming lesions include inter-chromosomal translocations, intra-chromosomal deletions, and gene amplifications that arise from the aberrant repair of DNA double strand breaks (DSBs). Inactivating mutations in genes encoding DSB repair/response proteins frequently lead to increased genomic instability in cells and cancer predisposition in mice and humans (Hakem, 2008). Thus, investigating pathological consequences of defects in DSB repair/response mechanisms is important for understanding etiologies of human cancers. Combined defects in DSB repair/response factors can result in substantially elevated levels of genomic instability and prevent sustained cellular proliferation (Gladdy et al., 2006). Targeted inhibition of particular DNA repair/response factors can inhibit the growth of transformed cells with deficiencies in complementary mechanisms, while not affecting normal cells (Bryant et al., 2005; Farmer et al., 2005). Consequently, elucidating functional cooperation between DSB repair/response factors is important for development of more specific and less toxic cancer therapies, and identification of candidate patients. Since *TP53* is inactivated in ~50% of human malignancies (Hollstein et al., 1991), investigating potential physiologic interactions between DSB repair/response factors on *TP53*-deficient backgrounds is paramount.

T-ALL is an aggressive cancer caused by the accumulation of genetic changes that block differentiation of thymocytes and drive their transformation (Armstrong and Look,

2005; Grabher et al., 2006; Pui et al., 2008). Thymocytes mature through differentiation programs that involve cellular proliferation and RAG mediated recombination of TCR genes (von Boehmer, 2004). Early thymocyte progenitors seed the thymus and differentiate into CD4⁻CD8⁻ double-negative (DN) thymocytes that progress through four successive stages: c-kit⁺CD25⁻ DNI cells, c-kit⁺CD25⁺ DNII cells, c-kit⁻CD25⁺ DNIII cells, and c-kit⁻CD25⁻ DNIV cells (Allman et al., 2003; Bhandoola et al., 2007; Godfrey et al., 1993). Assembly of in-frame TCR γ and TCR δ genes in DNII/III cells leads to $\gamma\delta$ TCRs that promote survival and signal differentiation into $\gamma\delta$ T cells without cellular proliferation (Raulet et al., 1991). In contrast, assembly of in-frame TCR β genes in DNIII cells generates TCR β chains that associate with pre-T α chains to form pre-TCRs, which promote survival, drive proliferation, and signal differentiation into CD4⁺CD8⁺ double-positive (DP) thymocytes (von Boehmer, 2004). Assembly of functional TCR α genes in β -selected DP cells leads to $\alpha\beta$ TCRs that promote survival and signal differentiation into CD4⁺ or CD8⁺ single-positive (SP) thymocytes, which emigrate to the periphery as mature CD4⁺ or CD8⁺ $\alpha\beta$ T cells (von Boehmer, 2004). T-ALL tumors frequently harbor translocations, deletions, and amplifications that arise from the aberrant repair of RAG-generated and/or spontaneous DSBs (Armstrong and Look, 2005; Grabher et al., 2006; Pui et al., 2008). These genomic lesions cause genetic changes that block differentiation at the DN, DP, or SP stages, prevent apoptosis, enable self-renewal, and drive uncontrolled proliferation of TCR β ⁻ or TCR β ⁺ cells (Armstrong and Look, 2005; Grabher et al., 2006; Pui et al., 2008).

Current T-ALL treatments consist of chemotherapy with multiple genotoxic agents, which lead to survival rates of ~80% in pediatric patients, but less than 30% in adults (Linker et al., 2002; Pui and Evans, 2006; Silverman et al., 2001). Development of novel treatment strategies clearly is important for T-ALL patients with recurrent or non-responding malignancies. In addition, considering that adult survivors of pediatric cancers treated with genotoxic agents are predisposed to chronic health conditions (Oeffinger et al., 2006), more specific and less toxic therapies are desirable for all T-ALL patients. Molecular profiling of T-ALL cell lines and primary malignancies has revealed four major tumor subtypes (Ferrando et al., 2002). Although somatic changes associated with T-ALL have been identified, the pathogenesis of these tumors remains undetermined (Pui et al., 2008). This lack of knowledge and the paucity of physiologically comparable animal models provide obstacles for the development of more effective and less toxic T-ALL treatment strategies (Armstrong and Look, 2005; Grabher et al., 2006; Pui et al., 2008).

One T-ALL subtype involves TCR β^+ cells with activating *NOTCH1* mutations, *H2AFX* deletions, and inactivation of the p53 pathway (Armstrong and Look, 2005; Ferrando et al., 2002). *H2AFX* encodes the H2AX histone that functions in DSB repair/responses (Downs et al., 2007). *H2ax*^{-/-} cells accumulate genomic instability (Celeste et al., 2002; Bassing et al., 2002b), but *H2ax*^{-/-} mice only exhibit a slightly increased cancer predisposition (Celeste et al., 2003b; Bassing et al., 2003). In contrast, *H2ax*^{-/-} *p53*^{-/-} mice rapidly succumb to aggressive TCR β^- thymic lymphomas with chromosome translocations that occasionally involve *Tcr α / δ* loci, chromosome deletions,

amplifications, and activating *Notch1* mutations (Bassing et al., 2003; Celeste et al., 2003b). The accumulation of genomic instability in H2AX/p53-deficient cells occurs through aberrant repair of RAG-generated or spontaneous DSBs and leads to genetic changes that block thymocyte differentiation and drive transformation of TCR β ⁻ cells (Bassing et al., 2008). Although *H2ax*^{-/-}*p53*^{-/-} thymic lymphomas harbor genomic lesions characteristic of T-ALL, the tumors that arise in germline H2AX/p53-deficient mice are TCR β ⁻, while the malignancies that develop in humans with somatic inactivation of *H2AFX* and *TP53* predominantly express TCR β (Ferrando et al., 2002). This phenotypic difference suggests that loss of H2AX and p53 functions in cells during embryogenesis or prior to lineage commitment may influence the developmental stage (pre versus post β -selection) at which thymocyte malignancies arise.

ARTEMIS is an endonuclease required for the repair of DSBs that require end-processing, such as coding ends generated by RAG cleavage (Moshous et al., 2001; Ma et al., 2002). Despite increased genomic instability of *Artemis*^{-/-} cells (Rooney et al., 2002), *Artemis*^{-/-} mice are not tumor prone (Rooney et al., 2003). However, *Artemis*^{-/-}*p53*^{-/-} mice succumb to pro-B lymphomas with *IgH* translocations and occasionally thymic lymphomas with *Tcr α / δ* translocations (Rooney et al., 2004a). Germline *Artemis*^{-/-}*H2ax*^{-/-}*p53*^{-/-} mice die shortly after birth from multiple malignancies, while *Artemis*^{-/-} mice with conditional deletion of both *H2ax* and *p53* in thymocytes survive tumor-free into adulthood (Yin et al., 2009), revealing that the developmental timing of *H2ax* and *p53* inactivation influences the rate of cancer mortality in *Artemis*^{-/-} mice. Non-malignant *Artemis*^{-/-} thymocytes with combined *H2ax* and *p53* deletion contain an increased

frequency of *Tcr α / δ* chromosome breaks and translocations, as compared to *Artemis*^{-/-} thymocytes with *p53* deletion and *Artemis*^{+/+} thymocytes with *H2ax/p53* deletion (Yin et al., 2009). Collectively, these data suggest that somatic inactivation of *H2ax* and *Artemis* in *p53*-deficient thymocytes may increase spontaneous genomic instability to levels that decrease tumor predisposition and mortality. Based on these results, targeted inhibition of ARTEMIS function might provide more specific and less toxic therapies for T-ALL and other human cancers with loss of H2AX and *p53* function.

RESULTS

Somatic inactivation of *H2ax* and *p53* in thymocytes predisposes mice to clonal TCR β ⁺ thymic lymphomas

To evaluate whether germline and somatic loss of H2AX and *p53* functions have different effects upon the rate of mortality from thymic lymphomas and/or the developmental stage at which these malignancies arise, I sought to characterize the cancer predisposition of mice with conditional deletion of *H2ax* and *p53* in lineage-committed thymocytes. I previously bred together *Lck-Cre* mice, "floxed" *H2ax* mice, and "floxed" *p53* mice to establish *Lck-CreH2ax*^{F/F}*p53*^{F/F} (*LHP*) mice (Yin et al., 2009). In addition to my previous cytogenetic analysis of *LHP* thymocytes generated *ex vivo* (Yin et al., 2009), I have also characterized thymocyte development and quantified *H2ax* and *p53* deletion in T lineage cells of *LHP* mice. I conducted flow cytometric analysis of $\alpha\beta$ T cell development in 4-6 week old *LHP* mice and normal control *H2ax*^{F/F}*p53*^{F/F} (*HP*) mice. Similar to previous analysis of *H2ax*^{-/-}*p53*^{-/-} mice (Bassing et al., 2003), I found that *LHP* mice contain normal populations of DNI, DNII, DNIII, DNIV, DP, and

SP thymocytes (Figure 14A). I next performed Southern blot analysis on genomic DNA isolated from *LHP* thymocytes using restriction enzyme digests and probes that distinguish between un-deleted "floxed" and Cre-deleted alleles. I found near complete Cre-mediated deletions of *H2ax* and *p53* alleles in thymocytes isolated from three different 4-6 week old *LHP* mice (Figure 14B). The un-deleted "floxed" *H2ax* and *p53* alleles could represent contaminating thymic epithelial cells, DN thymocytes in which Cre has not yet been expressed, and/or thymocytes that have developed in the absence of *H2ax* and *p53* deletion. I favor one or both of the former two possibilities since H2AX was not detectable by Western blot analysis of proteins isolated from *LHP* total thymocytes (Figure 14C).

To determine the effect of *H2ax* and *p53* deletion in thymocytes on tumor predisposition, I generated and characterized a cohort of 34 *LHP* mice. These mice survived tumor-free between 64-269 days with a median age of mortality at 143 days, which is significantly longer than the lifespan of *H2ax*^{-/-}*p53*^{-/-} mice (Figure 14D) (Bassing et al., 2003; Celeste et al., 2003b). All 34 *LHP* mice developed thymic lymphomas without obvious dissemination to peripheral lymphoid organs during necropsy (Table 1). *LHP* cohort mice did not develop other malignancies or display any other obvious phenotypes. FACS analysis of 28 *LHP* tumors revealed that 14 were TCRβ⁺, nine were TCRβ⁻, and five contained a mixture of TCRβ⁺ and TCRβ⁻ cells (Figure 14E, Table 1), demonstrating that most *LHP* tumors arose from the transformation of TCRβ-selected thymocytes, rather than TCRβ⁻ cells as in *H2ax*^{-/-}*p53*^{-/-} thymic lymphomas (Bassing et al., 2003; Celeste et al., 2003b). Some *LHP* lymphomas

were comprised of CD4⁻CD8⁻, CD4⁺CD8⁺, or CD4⁻CD8⁺ cells, while others contained mixed populations of CD4⁻CD8⁻, CD4⁺CD8⁺, CD4⁻CD8⁺, and/or CD4⁺CD8⁺ cells (Figure 14E, Table 1). This pattern of CD4 and CD8 cell surface expression is similar to that observed on *H2ax*^{-/-}*p53*^{-/-} thymic lymphomas (Bassing et al., 2003; Celeste et al., 2003b). Thus, as compared to mice with germline *H2ax/p53* deletion, mice with somatic inactivation of *H2ax* and *p53* in lineage-committed thymocytes exhibit a lower rate of mortality from thymic lymphomas and generally succumb to tumors of a later developmental stage.

Since *LHP* thymic lymphomas often exhibited mixed populations of cells as assessed by TCR β , CD4, and CD8 expression, I conducted Southern blot analysis to determine whether these tumors arose from transformation of one or more thymocyte. The *Tcr β* locus consists of 35 *V β* segments and two *D β -J β* clusters (*D β 1-J β 1* and *D β 2-J β 2*) (Figure 14F). To characterize *Tcr β* rearrangements, I conducted Southern blot analysis of *Hind*III-digested genomic DNA with a 3'*J β 1* probe and a 3'*J β 2* probe (Figure 14F). I found that 22 of 25 *LHP* tumors analyzed contained two rearranged *Tcr β* alleles and therefore arose through the clonal expansion of a single thymocyte (Figure 14F). The remaining three *LHP* thymic lymphomas (#461, #527, and #667) harbored three *Tcr β* alleles, revealing these tumors either developed from the expansion of two distinct cells or continued to rearrange *Tcr β* gene segments after transformation of a single thymocyte. Collectively, my data indicate that *LHP* malignancies predominantly develop from the clonal expansion of a single thymocyte with subsequent changes leading to

heterogeneous cell surface expression of TCR β , CD4, and/or CD8.

Somatic inactivation of *H2ax* and *p53* suppress lymphoma by preventing spontaneous genomic instability in lineage-committed cells

To evaluate whether lymphomas caused by conditional deletion of *H2ax* and *p53* in lineage-committed thymocytes exhibit genomic instability, I conducted SKY on metaphases prepared from *LHP* tumor cells. *LHP* tumor #111 contained clonal and non-clonal translocations (Figure 15A, arrows), chromosome fragments/detached centromeres (Figure 15A, circles) and chromosome gains or losses (Figure 15A, karyotype table). I analyzed in total five *LHP* thymic lymphomas by SKY and found that all contained at least one clonal translocation, none of which was observed in more than one tumor (Figure 15B; Table 2). All *LHP* thymic lymphomas analyzed by SKY also contained five or more non-clonal translocations, with three tumors harboring 15 or more (Table 2). In addition, all five *LHP* tumors exhibited clonal whole chromosome gains or losses (Table 2). *LHP* thymic lymphoma (#67) contained a t(14;15) translocation along with normal copies of chromosomes 14 and 15 in approximately 50% of metaphases (Figure 15B; Table 2). One published *H2ax*^{-/-}*p53*^{-/-} thymic lymphoma contained a clonal t(14;15) translocation involving *Tcr α / δ* and *c-myc* (Celeste et al., 2003b). I conducted fluorescence *in situ* hybridization (FISH) using *Tcr α / δ* or *c-myc* probes combined with chromosome 14 or 15 specific paints on metaphases from *LHP* tumor #67 and found that the t(14;15) translocation juxtaposed *Tcr α / δ* and *c-myc* (Figure 15C). These cytogenetic data demonstrate that *LHP* thymic lymphomas develop in association with clonal translocations that arise predominantly from the aberrant repair of spontaneous DSBs and

occasionally from V(D)J recombination errors. This pattern of genomic instability is similar to that observed in *H2ax*^{-/-}*p53*^{-/-} thymic lymphomas (Bassing et al., 2003; Celeste et al., 2003b).

Combined inactivation of *H2ax* and *Artemis* in *p53*-deficient thymocytes reduces the rate of mortality of mice from thymic lymphoma

As a means to investigate whether ARTEMIS inhibition might provide an effective therapy for human cancers with *H2AFX* and *TP53* inactivation, I evaluated whether inactivation of *H2ax* and *Artemis* in *p53*-deficient thymocytes would reduce rate of mortality of mice from thymic lymphoma as compared to inactivation of *H2ax* or *Artemis* alone in *p53*-deficient thymocytes. I previously established *Lck-CreArtemis*^{-/-}*p53*^{F/F} (*LAP*) and *Lck-CreArtemis*^{-/-}*H2ax*^{F/F}*p53*^{F/F} (*LAHP*) (Yin et al., 2009). In addition to my previous cytogenetic analysis of *LAP* and *LAHP* thymocytes generated *ex vivo* (Yin et al., 2009), I also characterized thymocyte development and quantified *p53* and/or *H2ax* deletion. I conducted flow cytometric analysis of $\alpha\beta$ T cell development and Southern blot analysis of thymocytes from 4-6 week old *LAP* and *LAHP* mice. As expected, due to inability of *Artemis*^{-/-} cells to assemble functional *Tcr β* chains (Rooney et al., 2002), I found that *LAP* and *LAHP* mice each contain a block in thymocyte development at the DNIII stage (Figure 16A). I also found that the majority of *H2ax* and/or *p53* alleles were deleted in total thymocytes isolated from three different 4-6 week old *LAHP* and *LAP* mice (Figure 16B). The lower extent of *H2ax* and *p53* deletion in *LAP* and *LAHP* thymocytes, as compared to *LHP* thymocytes, likely reflects a greater percentage of thymic epithelial cells and DN thymocytes with germline "floxed" alleles in the total

thymocyte population due to lack of TCR β -mediated expansion in *Artemis*^{-/-} thymuses. Importantly, the significant deletion of *H2ax* in *LAHP* thymocytes and the comparable deletion of *p53* between *LAP* and *LAHP* thymocytes enables us to evaluate whether combined inactivation of *H2ax*, *Artemis*, and *p53* in thymocytes reduces the rate of mortality of mice to lymphoma, as compared to inactivation of *Artemis* and *p53* or *H2ax* and *p53* in thymocytes.

To determine the effect of combined *Artemis* and *H2ax* inactivation in *p53*-deficient thymocytes on tumor mortality, I generated and characterized parallel cohorts of 38 *LAP* mice and 35 *LAHP* mice for one year. These cohorts were generated and aged at the same time as the *LHP* cohort described above. Of the 24 *LAP* cohort mice that died from tumors, 23 (96%) succumbed to thymic lymphomas and one to a sarcoma (Table 3). All 16 *LAHP* cohort mice that died from tumors succumbed to thymic lymphomas, three of which spread into peripheral lymphatic tissues (Table 4). The remaining 14 *LAP* mice and 19 *LAHP* mice developed prolapsed rectums, succumbed to opportunistic infection, or appeared sick and were subject to euthanasia (Table 3, Table 4). No visual evidence of lymphoma was evident in any of these mice upon necropsy. *LAP* cohort mice survived tumor-free between 105-285 days with a 50% survival time of 185 days (Figure 16C). The tumor-free survival of *LAP* mice was significantly longer than that of *LHP* mice (Log-rank test $p = 0.0062$). *LAHP* mice survived tumor-free between 112 days and one year of age, with a 50% survival time of 262 days (Figure 16C). The tumor-free survival of *LAHP* mice was significantly longer than that of both *LAP* (Log-rank test $p = 0.0017$) and *LHP* mice (Log-rank test $p < 0.0001$). These data demonstrate that *Artemis*^{-/-} mice

with somatic inactivation of *H2ax* and *p53* in lineage-committed thymocytes exhibit significantly lower rate of mortality from thymic lymphomas, as compared to *Artemis*^{-/-} mice with *p53* deletion in thymocytes and *Artemis*^{+/+} mice with combined *H2ax* and *p53* deletion in thymocytes.

I also determined the developmental stage and clonality of *LAP* and *LAHP* thymic lymphomas. The 16 *LAP* and 13 *LAHP* tumors analyzed were all TCRβ⁻ and comprised of CD4⁻CD8⁻, CD4⁺CD8⁺, CD4⁻CD8⁺, and/or CD4⁺CD8⁻ cells (Figure 16D, Table 3). Almost all *LAP* and *LAHP* thymic lymphomas contained two rearranged *Tcrβ* alleles and therefore arose through the clonal expansion of a single thymocyte (Figure 16E). Thus, *LAP* and *LAHP* tumors each mainly develop from the transformation of a single TCRβ⁻ thymocyte with subsequent genetic or epigenetic changes leading to heterogeneous CD4 and/or CD8 expression.

***LAP* and *LAHP* thymic lymphomas harbor different patterns of genomic instability**

Germline *Artemis*^{-/-}*p53*^{-/-} mice occasionally develop thymic lymphomas with clonal *Tcrα/δ* translocations (Rooney et al., 2004a), while *p53*^{-/-} mice reproducibly succumb to thymic lymphomas lacking clonal translocations (Liao et al., 1998). To evaluate whether *Artemis*^{-/-} mice with somatic deletion of *p53* in thymocytes develop tumors harboring translocations, I conducted SKY on metaphases prepared from seven *LAP* thymic lymphomas. SKY revealed that five *LAP* tumors (#34, #51, #91, #144, and #734) contained one or more one clonal translocation and whole chromosome gains/losses (Figure 17A, Table 5). *LAP* tumors #51 and #144 gave rise to metaphases

with two distinct patterns of clonal translocations. The *LAP* tumor #51 translocation pattern is consistent with transformation of a single thymocyte involving a t(13;15) translocation and accumulation of additional translocations in daughter cells derived from the parental clone. The *LAP* tumor #144 pattern is consistent with the clonal expansion of two distinct thymocytes, one containing a t(11;14) translocation and a chromosome 15 short arm fusion (SAF) and the other a chromosome 5 SAF. Southern blot analyses of *LAP* tumors #51 and #144 showing three and two *Tcrβ* alleles, respectively, support this notion (Figure 17E). In addition to clonal translocations, *LAP* tumors #34 and #144 also contained short arm fusions (Figure 17A, Table 5). All seven *LAP* tumors also harbored either clonal whole chromosome gains and losses or aneuploidy involving numerous chromosomes (Figure 17A, Table 5). Notably, *LAP* tumors #246 and #688 exhibited aneuploidy but lacked clonal chromosomal aberrations (Figure 17A, Table 5). These SKY data demonstrate that inactivation of *p53* in lineage-committed *Artemis*^{-/-} thymocytes leads to thymic lymphomas that harbor clonal translocations and/or aneuploidy.

Three of the analyzed *LAP* thymic lymphomas (#34, #51, and #144) contained clonal translocations involving chromosome 14 on which *Tcrα/δ* resides. *LAP* tumor #34 contained clonal reciprocal t(14;6) and t(6;14) translocations, one t(14;4) translocation, and one t(12;14) translocation (Figure 17A, Table 5). *LAP* tumor #51 contained clonal t(19;14;19) and t(7;14) translocations and multiple other chromosome 14 derivatives or fragments (Figure 17A, Table 5). *LAP* tumor #144 contained a clonal t(11;14) translocation and a chromosome 14 fragment with centromere (Figure 17A, Table 5). To

determine whether these translocations involved *Tcr α / δ* loci, I conducted FISH using *Tcr α / δ* probes combined with chromosome 14 specific paints. These analyses indicated that the t(11;14) translocation of tumor *LAP* tumor #144, the t(7;14) translocations of tumor *LAP* tumor #51, and the reciprocal t(14;6) and t(6:14) translocations, t(12;14) and t(14;4) of *LAP* tumor #34 each involved *Tcr α / δ* loci (Figure 17B). Since the *Tcr β* locus resides on chromosome 6, I also conducted FISH using *Tcr β* probes combined with chromosome 6 specific paints on *LAP* tumor #34. This analysis revealed that the clonal reciprocal t(14;6) and t(6:14) translocations also involve one allelic copy of the *Tcr β* locus and formed through fusion of *Tcr α / δ* and *Tcr β* DNA breaks (Figure 17B). These FISH data demonstrate that *LAP* tumors frequently harbor clonal translocations that arise through the aberrant repair of RAG-generated *Tcr α / δ* locus DSBs.

H2AX prevents *Tcr α / δ* DNA breaks from progressing into chromosome breaks and translocations in non-malignant *Artemis/p53*-deficient thymocytes (Yin et al., 2009). To evaluate whether combined inactivation of *H2ax* and *p53* in *Artemis*^{-/-} thymocytes leads to a corresponding increased frequency of *Tcr α / δ* translocations in transformed cells, I conducted SKY on metaphases prepared from seven *LAHP* thymic lymphomas. All *LAHP* tumors contained one or more one clonal translocation (Figure 17C, Table 6); however, clonal chromosome 14 translocations were observed in only one *LAHP* tumor (#300). This tumor contained clonal reciprocal t(14;6) and t(6;14) translocations, one t(14;1) translocation, and one t(11;14) translocation (Figure 17C, Table 6), consistent with a reciprocal translocation involving *Tcr α / δ* and *Tcr β* loci and non-reciprocal *Tcr α / δ*

translocations. Six of the seven *LAHP* thymic lymphomas analyzed also harbored whole chromosome gains and losses like *LAP* and *LHP* tumors, but none lacked clonal translocations or contained short arm fusions (Table 6) as were observed in *LAP* thymic lymphomas (Table 5). These data demonstrate that inactivation of *H2ax* and *p53* in lineage-committed *Artemis*^{-/-} thymocytes leads to tumors harboring a different pattern of genomic instability than inactivation of *p53* in lineage-committed *Artemis*^{-/-} thymocytes. Strikingly, despite the seven-fold greater frequency of chromosome breaks involving *Tcrα/δ* loci in non-malignant *LAHP* thymocytes as compared to *LAP* cells (Yin et al., 2009), *LAHP* thymic lymphomas develop in association with clonal translocations that arise predominantly from spontaneous DNA breakage and only occasionally from aberrant *Tcrα/δ* rearrangements.

***LAHP* thymic lymphomas contain substantially elevated levels of chromosome fragments and detached centromeres as compared to *LAP* and *LHP* tumors**

To evaluate whether the reduced rate of mortality from thymic lymphomas of *LAHP* mice as compared to *LAP* and *LHP* mice could be attributed to increased genomic instability, I conducted extensive SKY analysis of *LHP*, *LAP*, and *LAHP* tumors to identify and quantify all non-clonal chromosomal abnormalities. I found that all five *LHP* tumors contained non-reciprocal and reciprocal translocations, chromosome fragments, and detached centromeres (Table 2). The five *LAP* thymic lymphomas with clonal translocations also contained among them non-clonal abnormalities including reciprocal and non-reciprocal translocations, chromosome fragments, detached centromeres, dicentric chromosome translocations, elongated chromosomes, and short arm fusions

(Table 5). All *LAHP* thymic lymphomas analyzed contained among them non-reciprocal and reciprocal translocations, chromosome fragments, detached centromeres, dicentric chromosome translocations, and elongated chromosomes (Figure 18A, Table 6). The average number of non-clonal translocations per metaphase was similar between *LHP* and *LAHP* tumors and higher in *LHP* and *LAHP* tumors than in *LAP* tumors (Figure 18B), consistent with ability of H2AX to stabilize broken DNA strands and prevent chromosome breaks from progressing into translocations (Franco et al., 2006; Ramiro et al., 2006; Yin et al., 2009). In contrast, the average number of chromosome fragments and detached centromeres per metaphase was higher in *LAHP* tumors as compared to *LAP* and *LHP* tumors (Figure 18C), revealing that H2AX and Artemis cooperate to prevent spontaneous DNA breaks from progressing into chromosome breaks. Based upon these data, I conclude that the higher levels of spontaneous genomic instability in *LAHP* cells as compared to *LAP* or *LHP* cells, contributes to the slower rate of mortality of *LAHP* mice from thymic lymphoma as compared to *LAP* and *LHP* mice.

DISCUSSION

In this chapter, I have characterized *LHP* mice with *H2ax/p53* deletion in lineage-committed thymocytes to evaluate the effect that somatic inactivation of *H2ax* and *p53* has upon tumor predisposition and phenotype. These mice invariably succumbed to thymic lymphomas demonstrating that cooperation of H2AX and p53 in lineage-committed thymocytes is essential for inhibiting transformation. Yet, *LHP* mice died from thymocyte malignancies at a later median age than germline *H2ax^{-/-}p53^{-/-}* mice (143 days versus 79 days), indicating that cooperation of H2AX and p53 during embryogenesis and/or in cells prior to lineage-commitment contributes to the suppression of thymocyte malignancies in adult mice. Most *LHP* thymic lymphomas expressed cell surface TCR β chains, whereas almost all *H2ax^{-/-}p53^{-/-}* tumors are TCR β ⁻ (Bassing et al., 2003; Celeste et al., 2003b), revealing that somatic inactivation of *H2ax* and *p53* predisposes mice to thymocyte malignancies of a later developmental stage than germline *H2ax/p53* deletion. Notably, *LHP* mice succumb to a similar spectrum of TCR β ⁻ and TCR β ⁺ tumors as human T-ALL patients with somatic inactivation of *H2AFX* and *TP53*, thereby providing a more physiologic T-ALL model than *H2ax^{-/-}p53^{-/-}* mice. All *LHP* thymic lymphomas harbored clonal translocations not involving T-cell receptor loci, though one tumor contained a *Tcr α / δ :c-myc* translocation in approximately 50% of cells. This pattern of genomic instability indicates that cooperation of H2AX and p53 in lineage-committed thymocytes is essential for preventing translocations that arise from the aberrant repair of spontaneous and programmed DNA breakage. Spontaneous DSBs could be induced by intrinsic factors such as DNA replication errors in proliferating DNII, DNIV, and ISP cells or reactive oxygen species generated by cellular metabolism

in thymocytes of any developmental stage. The resultant translocations likely cause genetic changes that block differentiation of thymocytes and drive their transformation.

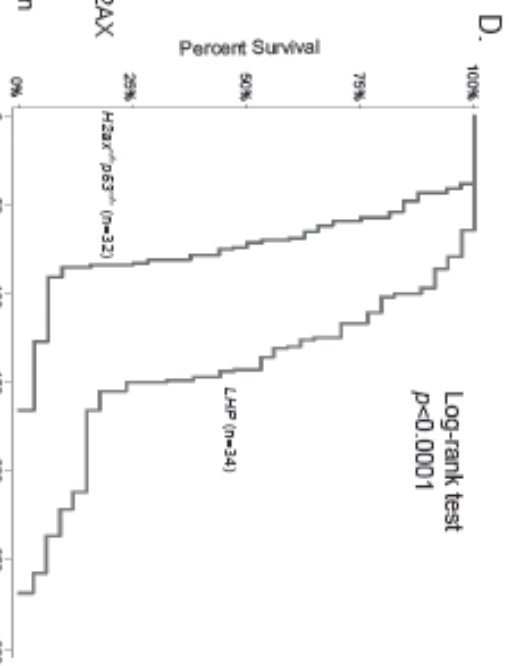
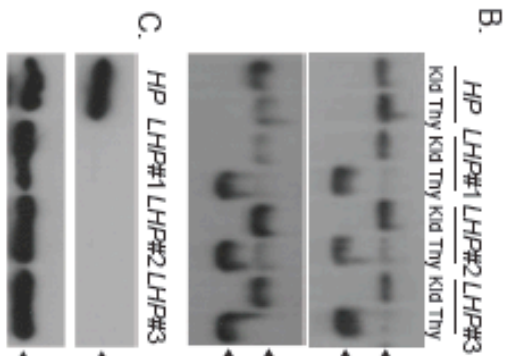
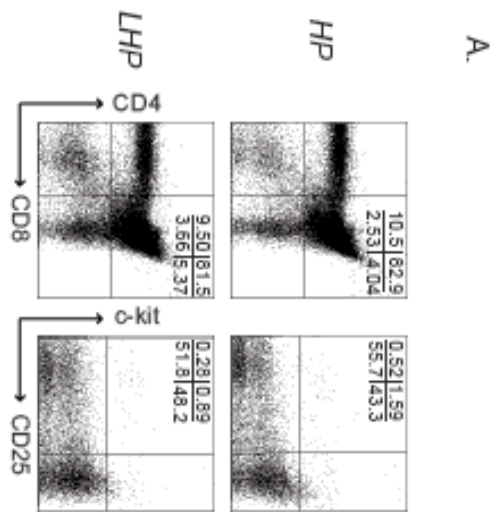
In parallel, I characterized *LAP* and *LAHP* mice with *p53* or *H2ax/p53* deletion in lineage-committed *Artemis*^{-/-} thymocytes to evaluate the effect that combined inactivation of *H2ax* and *Artemis* in p53-deficient cells has upon tumor predisposition and phenotype. *LAHP* mice exhibited a significantly reduced rate of mortality from spontaneous thymocyte malignancies as compared to *LAP* and *LHP* mice. In theory, a smaller thymocyte pool for transformation and/or lack of DN-to-DP expansion and differentiation for the accumulation or activation of oncogenic translocations could influence the slower rate of mortality from thymic lymphoma of *LAHP* versus *LHP* mice. However, the slower rate of mortality from thymocyte malignancies of *LAHP* mice as compared to *LAP* mice must be due to cell-intrinsic effects of *H2ax* deletion. Loss of H2AX functions may provide additional selection pressures that limit tumor initiation and/or affect transformed thymocytes in a manner that inhibits tumor progression. *LAP* tumors harbored clonal translocations that arose from the aberrant repair of DNA breakage, or whole chromosome gains/losses most likely generated from chromosome segregation errors during mitosis. In contrast, all *LAHP* thymic lymphomas contained clonal translocations and exhibited higher levels of random chromosome fragments and detached centromeres than *LAP* and *LHP* tumors. These data demonstrate that H2AX and Artemis cooperate to suppress chromosome lesions arising from spontaneous DNA breakage in p53-deficient thymocytes, with the elevated levels of genomic instability reducing the rate of mortality from thymic lymphomas.

How does combined inactivation of H2AX and Artemis in p53-deficient cells lead to substantially elevated levels of spontaneous genomic instability? H2AX is subject to biochemical modifications in chromatin around DSBs, which creates binding sites for DNA repair/response factors (Kinner et al., 2008). Assembly of these proteins into complexes around DNA breakage sites may stabilize broken DNA strands, promote accessibility of DNA ends, and amplify intracellular signaling pathways to activate the G2/M checkpoint (Bassing and Alt, 2004; Kinner et al., 2008; Rogakou et al., 1998; Stucki and Jackson, 2006; Yin et al., 2009). Artemis functions in the repair of spontaneous and radiation-induced DSBs (Moshous et al., 2001; Rooney et al., 2003), likely those with damaged nucleotides at DNA ends that need to be removed prior to end-joining or homology-mediated repair (Beucher et al., 2009; Ma et al., 2002). Artemis also is required for normal maintenance of the G2/M checkpoint (Zhang et al., 2004). I previously demonstrated that H2AX stabilizes broken DNA strands that require Artemis-dependent end-processing prior to repair in G1 phase cells and prevents these DNA ends from physically separating and progressing into chromosome breaks and translocations during cell cycle progression (Yin et al., 2009). Such H2AX-mediated structural functions also could maintain disrupted DNA strands adjacent to their undamaged sister chromatids in late S and G2 phases of the cell cycle and thereby suppress translocations and intra-chromosomal deletions (Bassing and Alt, 2004; Unal et al., 2004). Artemis endonuclease activity is required for end-resection and homology-mediated repair of a subset of DSBs induced in G2 phase cells (Beucher et al., 2009). Thus, it seems likely that the elevated levels of spontaneous chromosome breaks and detached centromeres in

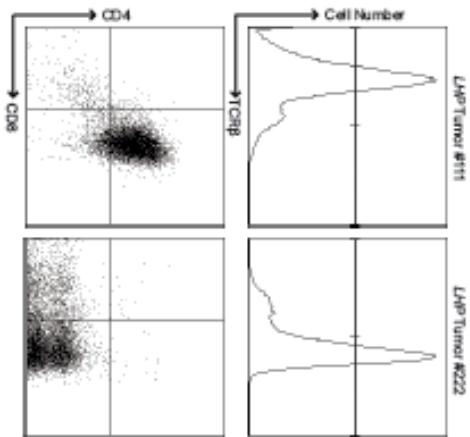
p53-deficient cells with combined inactivation of *H2ax* and *Artemis* is due to an increased frequency in the physical separation of DNA ends that require end-processing, coupled with an inability to activate and maintain the G2/M checkpoint in cells with such persistent lesions.

My observations that combined inactivation of H2AX and Artemis in p53-deficient thymocytes reduces the incidence and rate of mortality from thymic lymphomas identifies Artemis as a potential therapeutic target for T-ALL, and possibly other malignancies with inactivation of *H2AFX* and *TP53*. The availability and accessibility of *in vitro* and cell-line based assays for Artemis endonuclease function (Bredemeyer, 2008; Ma et al., 2002; Moshous et al., 2001; Rooney et al., 2003; Rooney et al., 2002) should enable identification of potential lead compound inhibitors through the screening of available small molecule libraries. In addition, ongoing analyses of the metallo- β -lactamase family of proteins (Dominski, 2007), in which Artemis is a member, should facilitate subsequent rationale-based drug design to improve efficacy and selectivity of candidate drugs. Inactivating mutations of *ARTEMIS* cause radiation sensitive severe combined immunodeficiency (RS-SCID) that leads to early death from opportunistic infections (Moshous et al., 2001). *Artemis* mutation causes a similar phenotype in mice, however *Artemis*^{-/-} mice housed under pathogen-free conditions exhibit no other obvious phenotypes including increased predisposition to cancer (Rooney et al., 2002). Accordingly, systemic administration of Artemis inhibitors should not affect the proliferation of normal cells throughout the body. Moreover, since the carboxy-terminus of Artemis is dispensable for V(D)J recombination but required for sensing/repair of

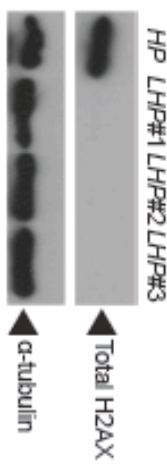
radiation-induced DSBs (Poinsignon et al., 2004), it is conceivable that an inhibitor of Artemis functions in general DSB responses but not V(D)J recombination could be developed. The functional interaction of H2AX with known human tumor suppressors, such as the ATM and BRCA1 proteins (Kinner et al., 2008), suggests that ARTEMIS inhibitors could be effective for the treatment of human malignancies in addition to those with *H2AFX* and *TP53* inactivation.



E.



C.



F.

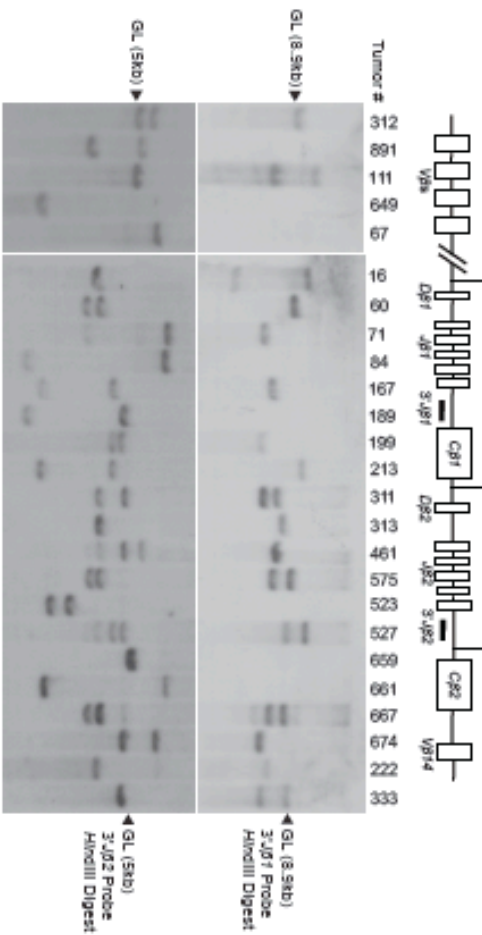


Figure 14. Mice with somatic inactivation of *H2ax* and *p53* in thymocytes succumb to clonal thymic lymphomas. **A)** *LHP* mice exhibit normal thymocyte development. Shown are representative anti-CD4 and anti-CD8 flow cytometric analysis of total *LHP* and *HP* thymocytes, and anti-c-kit and anti-CD25 flow cytometric analysis of lineage-negative *LHP* and *HP* thymocytes. The percentage of cells within each quadrant is indicated. **B)** *H2ax* and *p53* are deleted in *LHP* thymocytes. Southern blot analyses of *H2ax* and *p53* status in genomic DNA isolated from thymocytes (Thy) or kidneys (Kid) of *LHP* or *HP* mice. Bands corresponding to the floxed (F) and deleted (Δ) alleles are indicated. **C)** H2AX expression is lost in *LHP* thymocytes. Western blot analysis of H2AX and α -tubulin protein levels in total thymocytes of *LHP* and *HP* mice. **D)** *LHP* mice succumb to thymic lymphomas. Kaplan-Meier curves showing the percentage of tumor-free survival of *LHP* and *H2ax*^{-/-}*p53*^{-/-} mice. The *H2ax*^{-/-}*p53*^{-/-} cohort was characterized previously (Bassing et al., 2008). Log-rank test $p < 0.0001$. **E)** *LHP* mice develop TCR β ⁻ and TCR β ⁺ thymic lymphomas. Shown are anti-TCR β and anti-CD4 and anti-CD8 flow cytometric analyses of *LHP* tumor #111 and #222. The gates used to determine TCR β , CD4, and CD8 status of tumors are depicted. **F)** *LHP* tumors arise from the clonal expansion of single thymocytes. Shown is a schematic diagram of the *Tcr β* locus with gene segments represented by open boxes, the locations of the 3'*J β 1* and 3'*J β 2* probes indicated by black bars, the *Hind*III sites indicated by arrows, and the sizes of the *Hind*III fragments depicted. Southern blot analyses of *Tcr β* rearrangements in *Hind*III-digested genomic DNA isolated from *LHP* thymic lymphomas. The locations of bands corresponding to un-rearranged germline (GL) *J β 1* and *J β 2* segments are indicated.

Table 1: Characterization of *LHP* Cohort Mice

Mouse	Age at Death (Days)	Cause of Death	FACS Analysis	
			TCR β Stain	CD4/CD8 Stain
71	64	Thymic Lymphoma	TCR β^+	CD4 $^+$ CD8 $^+$
523	79	Thymic Lymphoma	TCR β^-	CD4 $^-$ CD8 $^+$
312	86	Thymic Lymphoma	TCR β^+	CD4 $^+$ CD8 $^+$, CD4 $^+$ CD8 $^-$
168	97	Thymic Lymphoma	n.d.	n.d.
173	100	Thymic Lymphoma	n.d.	n.d.
169	100	Thymic Lymphoma	TCR β^-	CD4 $^-$ CD8 $^+$, CD4 $^-$ CD8 $^-$
891	102	Thymic Lymphoma	TCR β^+	CD4 $^+$ CD8 $^-$, CD4 $^+$ CD8 $^+$
313	111	Thymic Lymphoma	TCR β^-	CD4 $^-$ CD8 $^+$
84	117	Thymic Lymphoma	TCR β^+	CD4 $^+$ CD8 $^+$, CD4 $^+$ CD8 $^-$, CD4 $^-$ CD8 $^-$
16	117	Thymic Lymphoma	TCR β^-	CD4 $^+$ CD8 $^+$, CD4 $^+$ CD8 $^-$, CD4 $^-$ CD8 $^+$, CD4 $^-$ CD8 $^-$
213	125	Thymic Lymphoma	TCR β^+	CD4 $^-$ CD8 $^+$
203	125	Thymic Lymphoma	n.d.	n.d.
167	126	Thymic Lymphoma	TCR β^+	CD4 $^+$ CD8 $^+$
520	130	Thymic Lymphoma	TCR β^+	CD4 $^-$ CD8 $^+$, CD4 $^-$ CD8 $^-$
111	131	Thymic Lymphoma	TCR β^-	CD4 $^+$ CD8 $^+$
311	136	Thymic Lymphoma	TCR β^- , TCR β^+	CD4 $^-$ CD8 $^+$
661	143	Thymic Lymphoma	TCR β^+	CD4 $^-$ CD8 $^-$
667	143	Thymic Lymphoma	TCR β^+ , TCR β^-	CD4 $^-$ CD8 $^-$, CD4 $^-$ CD8 $^+$
649	144	Thymic Lymphoma	TCR β^+	CD4 $^-$ CD8 $^-$, CD4 $^+$ CD8 $^-$, CD4 $^-$ CD8 $^+$
199	147	Thymic Lymphoma	TCR β^-	CD4 $^+$ CD8 $^+$
461	147	Thymic Lymphoma	TCR β^-	CD4 $^-$ CD8 $^+$
333	149	Thymic Lymphoma	TCR β^+	CD4 $^+$ CD8 $^+$, CD4 $^-$ CD8 $^-$
67	149	Thymic Lymphoma	TCR β^+ , TCR β^-	CD4 $^+$ CD8 $^+$
648	150	Thymic Lymphoma	TCR β^+	CD4 $^-$ CD8 $^-$
647	150	Thymic Lymphoma	TCR β^-	CD4 $^-$ CD8 $^+$, CD4 $^-$ CD8 $^-$

316	150	Thymic Lymphoma	n.d.	n.d.
527	155	Thymic Lymphoma	TCR β ⁻ , TCR β ⁺	CD4 ⁻ CD8 ⁺
517	155	Thymic Lymphoma	TCR β ⁻	CD4 ⁺ CD8 ⁺
659	166	Thymic Lymphoma	TCR β ⁺	CD4 ⁻ CD8 ⁺ , CD4 ⁻ CD8 ⁻ , CD4 ⁺ CD8 ⁺
674	212	Thymic Lymphoma	TCR β ⁺ , TCR β ⁻	CD4 ⁺ CD8 ⁺ , CD4 ⁺ CD8 ⁻
530	222	Thymic Lymphoma	n.d.	n.d.
515	237	Thymic Lymphoma	TCR β ⁺	CD4 ⁺ CD8 ⁺
444	258	Thymic Lymphoma	n.d.	n.d.
222	269	Thymic Lymphoma	TCR β ⁺	CD4 ⁻ CD8 ⁺ , CD4 ⁻ CD8 ⁻

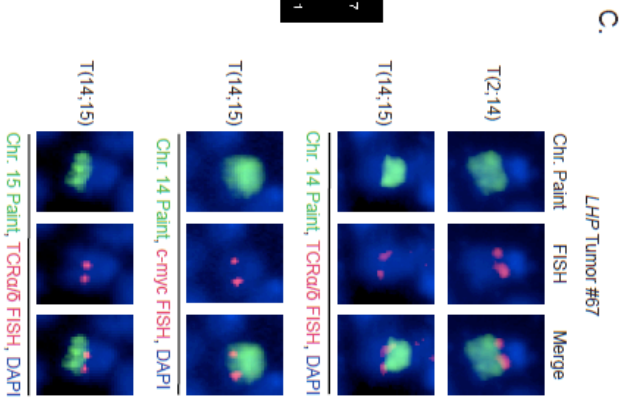
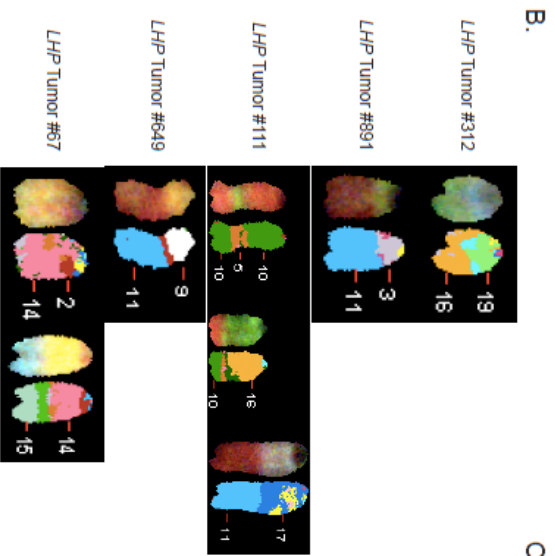
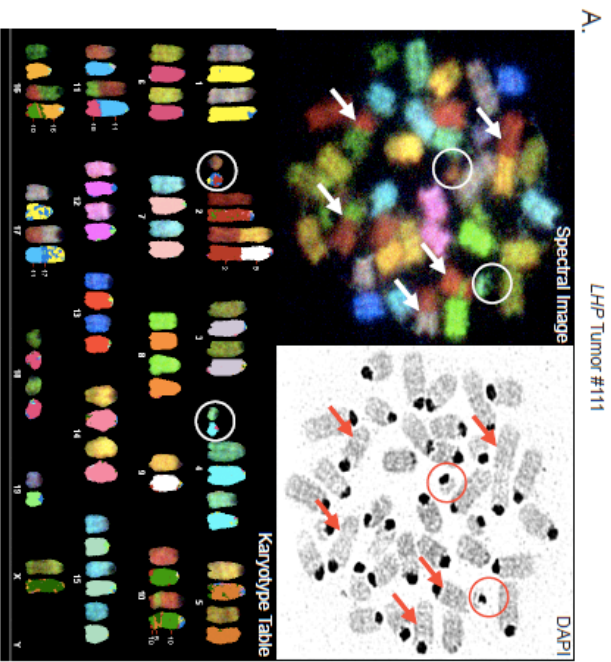


Figure 15. *LHP* thymic lymphomas harbor translocations that arise from spontaneous and programmed DNA breakage. **A)** *LHP* tumors exhibit clonal and non-clonal chromosome abnormalities. Shown are spectral and DAPI images of a representative metaphase spread prepared from *LHP* tumor #111 (top panels) and the karyotype table (bottom panel) of this metaphase. Arrows indicate clonal and non-clonal translocations. Circles indicate chromosome fragments. **B)** *LHP* thymic lymphomas harbor clonal translocations. Shown are spectral and computer classified images of the clonal translocations observed in each of the five *LHP* tumors (#312, #891, #111, #649, and #67) analyzed by SKY. The identities of the chromosomes participating these translocations are indicated. **C)** *LHP* thymic lymphoma #67 contains a *Tcr α / δ :c-myc* translocation. Shown are representative FISH and chromosome paint analyses of *LHP* tumor #67 for potential involvement of *Tcr α / δ* and *c-myc* loci in the clonal t(2;14) and t(14;15) translocations. Depicted in each set of panels are green paints specific for chromosome 14 or chromosome 15, the same metaphases with red *Tcr α / δ* or *c-myc* FISH probes, and merged images. Slides were counterstained with DAPI to visualize chromosomes.

Table 2: SKY Analysis of LHP Tumors

Tumor	Life Span	Clonal Translocations [Frequency]	Non-clonal Translocations [Frequency]	Chromosome Fragments and Other Abnormalities [Frequency]	Gain or Loss of Chromosome	Average Chromosome Number
312	86 Days	t(19;16) [21/21]	t(8;10) and t(10;8) [3/21]; t(15;2) [2/21]; t(15;6) [2/21]; t(4;5) [1/21]; t(16;X) [1/21]	Chr.2 fragment [17/21]; Dicentric Chr.2 [1/21]; Chr.6 fragment [2/21]; Chr.7 fragment [2/21]; Detached centromeres	+1; +2; +4; +5; +14; +15; -Y	47
891	102 Days	t(3;11) [12/26]	t(16;2) [3/26]; t(3;2) [3/26]; t(11;9) [2/26]; t(14;16) [2/26]; t(2;3) and t(3;2) [2/26]; t(2;3) [1/26]; t(4;9) [1/26]; t(13;16) [1/26]; t(17;4) [1/26]; t(11;10) [1/26]; t(18;11) [1/26]; t(13;8) [1/26]; t(2;10) and t(10;2) [1/26]; t(10;2) [1/26]; t(16;10) [1/26]; t(9;11) [1/26]	Chr.4 fragment [1/26]; Chr.8 fragment [1/26]; Chr.10 fragment [1/26]; Detached centromeres	+4; +5; +10; +14; +15	47
111	131 Days	t(10;5;10) [41/41]; t(16;10) [35/41]; t(17;11) [30/41]	t(1;2) [4/41]; t(15;6) [4/41]; t(11;18) [3/41]; t(16;11) [2/41]; t(9;2) [1/41]; t(4;18) and t(18;4) [1/41]; t(15;16) [1/41]; t(11;9) [1/41]; t(8;18) and t(18;8) [1/41]; t(16;3) [1/41]; t(15;13) [1/41]; t(11;6) [1/41]; t(10;12) [1/41]; t(13;7) [1/41]; t(10;16;10) [1/41]; t(15;19) [1/41]; t(16;2) [1/41]; t(X;3) and t(3;X) [1/41]; t(2;16;10) [1/41]; t(19;12) [1/41]	Chr.2 fragment [5/41]; Chr.3 fragment [1/41]; Chr.4 fragment [11/41]; Chr.6 fragment [3/41]; Chr.17 fragment [2/41]; Chr.14 with multiple centromere structures [2/41]; Detached centromere	+6; +15; -18; -19; -Y	39
649	144 Days	t(9;11) [21/25]	t(15;1) [1/25]; t(4;14) [1/25]; t(17;15) [1/25]; t(12;10) [1/25]; t(9;11;12) [1/25]	Big Chr.7 fragment without centromere [1/25]; Big Chr.1 fragment [1/25]	+8; -9; +15; -16; -Y	39
67	149 Days	t(14;15) [15/31]; t(2;14) [14/31]	t(10;14) [4/31]; t(12;2) [4/31]; t(14;11) [3/31]; t(18;2) [3/31]; t(19;16) [2/31]; t(14;4) [1/31]; t(14;16) [1/31]; t(15;14) and t(14;15) [1/31]; t(10;13) [1/31]; t(3;16) [1/31]; t(3;5) [1/31]; t(10;2) [1/31]; t(1;11) [1/31]; t(10;4) [1/31]	Chr.2 fragment [5/31]; Chr.9 fragment [6/31]; Chr.11 fragment [4/31]; Chr.12 fragment [4/31]; Chr.14 fragment [5/31]; Chr.4 SAF [2/31]; Chr.14 SAF [1/31]	+1; +2; +4; +5; +14; +15	48

Note: SAF=Short-arm fusions

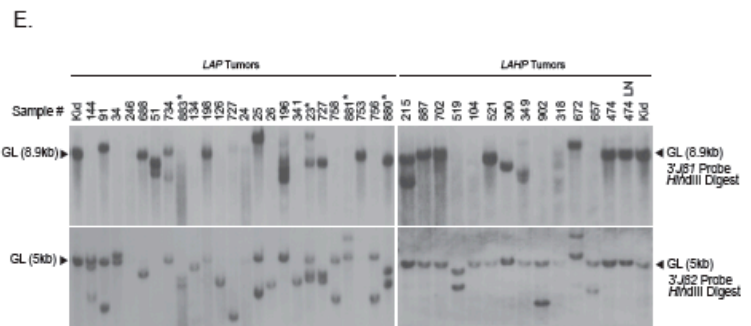
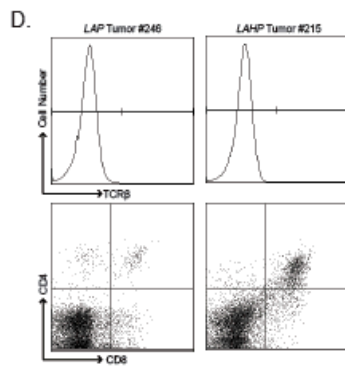
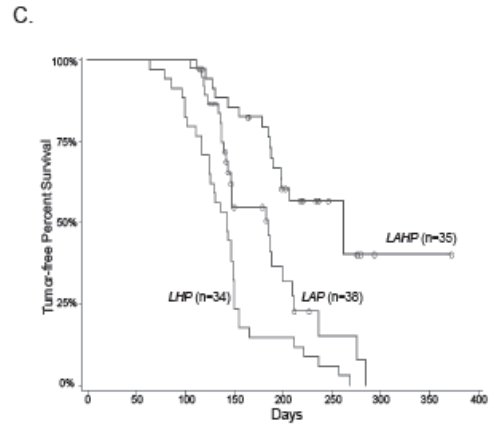
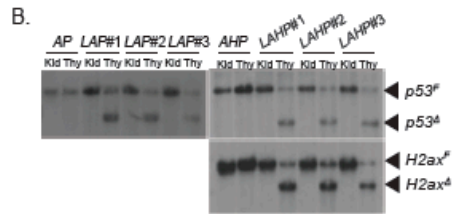
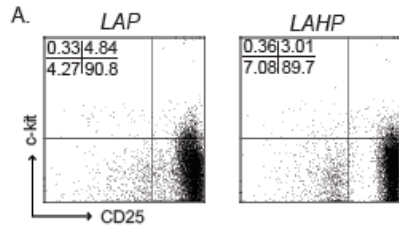


Figure 16. Combined inactivation of *H2ax* and *Artemis* in *p53*-deficient thymocytes reduces the rate of mortality of mice from thymic lymphoma. **A)** *LAP* and *LAHP* mice exhibit a block in thymocyte development. Shown is a representative anti-c-kit and anti-CD25 flow cytometric analysis of lineage-negative *LAP* and *LAHP* thymocytes. The percentage of cells within each quadrant is indicated. **B)** *p53* and *H2ax/p53* are deleted in *LAP* and *LAHP* thymocytes. Southern blot analyses of *p53* and *H2ax* status in genomic DNA isolated from thymocytes (Thy) or kidneys (Kid) of *LAP* or *LAHP* mice. Bands corresponding to the floxed (F) and deleted (Δ) alleles are indicated. **C)** *LAHP* mice exhibit a lower rate of mortality from thymic lymphomas than *LAP* and *LHP* mice. Kaplan-Meier curves showing the percentage of tumor-free survival of *LHP* (n=34), *LAP* (n=38), and *LAHP* (n=35) mice. A drop in the curve represents the sacrifice or death of an animal diagnosed at necropsy with thymic lymphomas (except for one *LAP* mouse, a sarcoma). Open circles represent the sacrifice or death of an animal due to prolapsed rectum, infections, or no apparent tumors at necropsy. Log-rank test $p(\text{LAHP vs LHP}) < 0.0001$, $p(\text{LAHP vs LAP}) = 0.0017$, $p(\text{LHP vs LAP}) = 0.0062$. **D)** *LAP* and *LAHP* mice only develop TCR β ⁻ thymic lymphomas. Shown are anti-TCR β and anti-CD4 and anti-CD8 flow cytometric analyses of *LAP* tumor #246 and *LAHP* tumor #215. The gates used to determine TCR β , CD4, and CD8 status of tumors are depicted. **E)** *LAP* and *LAHP* tumors arise from the clonal expansion of single thymocytes. Southern blot analyses of *Tcr β* rearrangements in *Hind*III-digested genomic DNA isolated from *LAP* and *LAHP* thymic lymphomas, as well as one *LAHP* tumor that spread into lymph nodes (#474 LN). Kidney (Kid) DNA from non-tumor mice was used as controls. Tumors marked with an asterisk (*) were of other genotypes (#880 and #883, *Lck-CreArtemis*^{+/-} *H2ax*^{+/F} *p53*^{F/F};

#23 and #881, *Lck-CreArtemis^{+/-}H2ax^{+/+}p53^{F/F}*). The locations of bands corresponding to un-rearranged germline (GL) *Jβ1* and *Jβ2* segments are indicated.

Table 3: Characterization of LAP Cohort Mice

Mouse	Age at Death (Days)	Cause of Death	FACS Analysis	
			TCR β Stain	CD4/CD8 Stain
170	105	Thymic Lymphoma	n.d.	n.d.
199	115	No Tumor	—	—
144	117	Thymic Lymphoma	TCR β ⁻	CD4 ⁻ CD8 ⁺
134	119	Thymic Lymphoma	TCR β ⁻	CD4 ⁻ CD8 ⁺
198	120	Thymic Lymphoma	TCR β ⁻	CD4 ⁻ CD8 ⁻ , CD4 ⁻ CD8 ⁺
146	123	Thymic Lymphoma	n.d.	n.d.
207	126	No Tumor	—	—
248	131	Prolapsed Rectum	—	—
251	131	Prolapsed Rectum	—	—
91	134	Thymic Lymphoma	TCR β ⁻	CD4 ⁻ CD8 ⁺ , CD4 ⁻ CD8 ⁻
127	136	Thymic Lymphoma	n.d.	n.d.
727	137	Thymic Lymphoma	TCR β ⁻	CD4 ⁺ CD8 ⁺ , CD4 ⁻ CD8 ⁻ , CD4 ⁻ CD8 ⁺
125	137	Sarcoma	—	—
34	140	Thymic Lymphoma	TCR β ⁻	CD4 ⁺ CD8 ⁺ , CD4 ⁻ CD8 ⁺ , CD4 ⁺ CD8 ⁻
20	141	Prolapsed Rectum	—	—
24	142	Thymic Lymphoma	n.d.	n.d.
21	142	No Tumor	—	—
739	144	No Tumor	—	—
753	144	Thymic Lymphoma	TCR β ⁻	CD4 ⁻ CD8 ⁻ , CD4 ⁻ CD8 ⁺
246	147	Thymic Lymphoma	TCR β ⁻	CD4 ⁻ CD8 ⁻
199	147	No Tumor	—	—
25	148	Thymic Lymphoma	TCR β ⁻	CD4 ⁻ CD8 ⁻ , CD4 ⁻ CD8 ⁺
126	148	Thymic Lymphoma	TCR β ⁻	CD4 ⁻ CD8 ⁺ , CD4 ⁻ CD8 ⁻
769	150	Infection	—	—
117	179	Infection	—	—
196	183	Thymic Lymphoma	TCR β ⁻	CD4 ⁻ CD8 ⁺
343	183	No Tumor	—	—
26	185	Thymic Lymphoma	TCR β ⁻	CD4 ⁻ CD8 ⁻
688	187	Thymic Lymphoma	TCR β ⁻	CD4 ⁻ CD8 ⁻ , CD4 ⁻ CD8 ⁺

17	189	Thymic Lymphoma	n.d.	n.d.
19	200	Thymic Lymphoma	n.d.	n.d.
51	210	Thymic Lymphoma	TCR β ⁻	CD4 ⁺ CD8 ⁺
341	211	Thymic Lymphoma	TCR β ⁻	CD4 ⁻ CD8 ⁺ , CD4 ⁻ CD8 ⁻
22	212	No Tumor	—	—
88	227	Prolapsed Rectum	—	—
698	237	Thymic Lymphoma	n.d.	n.d.
734	276	Thymic Lymphoma	TCR β ⁻	CD4 ⁻ CD8 ⁻
18	285	No Tumor	—	—

Note: n.d., not determined; —, not applicable.

Table 4: Characterization of LAHP Cohort Mice

Mouse	Age at Death (Days)	Cause of Death	FACS Analysis	
			TCR β Stain	CD4/CD8 Stain
215	112	Thymic Lymphoma; Enlarged Spleen and Lymph Nodes; Sarcoma	TCR β ⁻	CD4 ⁻ CD8 ⁻
785	117	Prolapsed Rectum	—	—
887	121	Thymic Lymphoma	TCR β ⁻	CD4 ⁻ CD8 ⁺
474	128	Thymic Lymphoma; Enlarged Spleen and Lymph Nodes	TCR β ⁻	CD4 ⁻ CD8 ⁻
672	131	Thymic Lymphoma	TCR β ⁻	CD4 ⁺ CD8 ⁺ , CD4 ⁻ CD8 ⁺
702	144	Thymic Lymphoma	TCR β ⁻	CD4 ⁻ CD8 ⁺
107	155	Thymic Lymphoma	n.d.	n.d.
301	164	Infection	—	—
384	165	Infection	—	—
318	179	Thymic Lymphoma	TCR β ⁻	CD4 ⁻ CD8 ⁻
519	185	Thymic Lymphoma	TCR β ⁻	CD4 ⁻ CD8 ⁻ , CD4 ⁻ CD8 ⁺
104	187	Thymic Lymphoma	TCR β ⁻	CD4 ⁻ CD8 ⁺ , CD4 ⁻ CD8 ⁻
705	188	Thymic Lymphoma; Enlarged Liver and Spleen	n.d.	n.d.
902	190	Thymic Lymphoma	TCR β ⁻	CD4 ⁺ CD8 ⁻ , CD4 ⁻ CD8 ⁺
706	198	Thymic Lymphoma	n.d.	n.d.
303	199	Prolapsed Rectum	—	—
300	199	Thymic Lymphoma	n.d.	n.d.
231	203	Prolapsed Rectum	—	—
559	203	No Tumor	—	—
521	207	Thymic Lymphoma	TCR β ⁻	CD4 ⁺ CD8 ⁺ , CD4 ⁻ CD8 ⁻
706	218	No Tumor	—	—
705	218	No Tumor	—	—
358	220	Prolapsed Rectum	—	—
664	221	No Tumor	—	—
111	234	Prolapsed Rectum	—	—
205	236	Prolapsed Rectum	—	—
355	237	No Tumor	—	—
492	247	No Tumor	—	—
352	262	Thymic Lymphoma	TCR β ⁻	CD4 ⁻ CD8 ⁻
349	262	Thymic Lymphoma	TCR β ⁻	CD4 ⁻ CD8 ⁺

117	276	Prolapsed Rectum	—	—
561	277	No Tumor	—	—
544	280	No Tumor	—	—
471	294	No Tumor	—	—
317	373	No Tumor	—	—
657	n.d.	Thymic Lymphoma	TCR β ⁻	CD4 ⁻ CD8 ⁺

Note: *LHP* #657 was not included in the Kaplan-Meier curve.

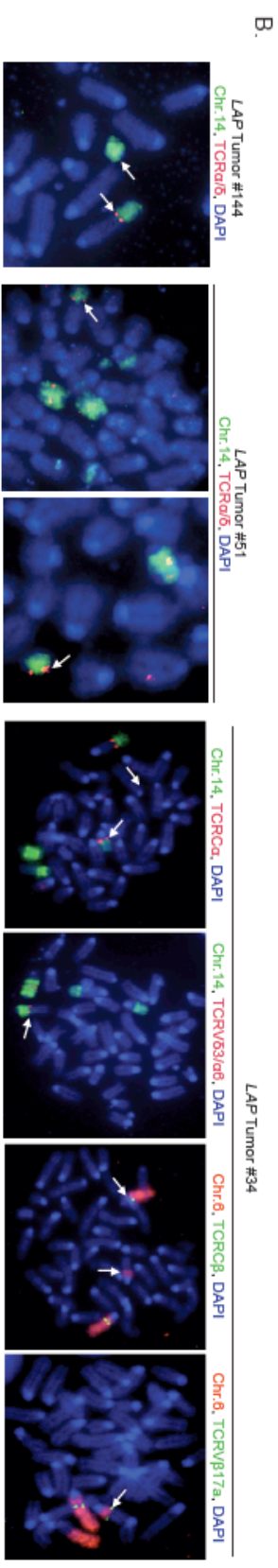
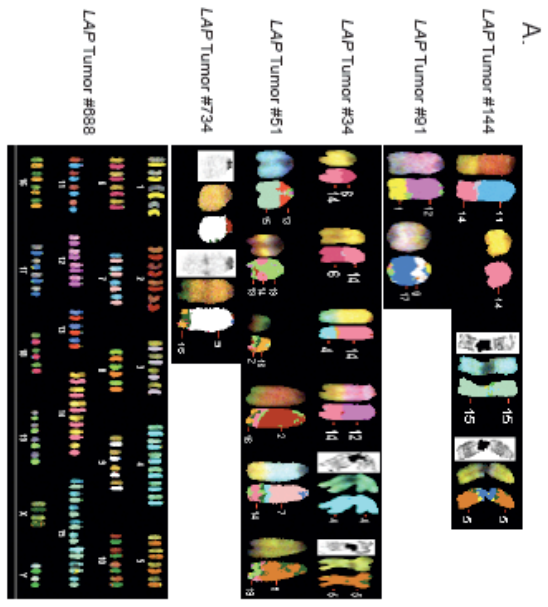


Figure 17. *LAP* and *LAHP* thymic lymphomas exhibit distinct patterns of genomic instability. **A)** *LAP* thymic lymphomas harbor clonal translocations. Shown are spectral and computer classified images of the clonal translocations observed in five of the *LAP* tumors (#144, #91, #34, #51, and #734) and the short arm fusions found in two of the *LAP* tumors (#144 and #34) by SKY. Also shown is the karyotype table of one metaphase from *LAP* tumor #688 demonstrating aneuploidy but no apparent translocations. The identities of the chromosomes participating these translocations or fusions are indicated. DAPI images are depicted for the chromosome fusions within *LAP* tumors #144 and #34 to reveal the structure of these chromosome lesions. DAPI images also are shown for the normal chromosome 9 and t(9;16) translocation in *LAP* tumor #734 to reveal a centromere-like structure on the chromosome 9 portion of the t(9;16) translocation. **B)** *LAP* thymic lymphomas contain clonal *Tcr α / δ* translocations. Shown are representative FISH and chromosome paint analyses of *LAP* tumors with clonal chromosome 14 translocations (#144, #51, and #34) to evaluate for potential involvement of *Tcr α / δ* loci (tumors #144, #51, and #34) and *Tcr β* loci (tumor #34). All images were counterstained with DAPI to visualize chromosomes. Arrows indicate translocation sites that involve *Tcr α / δ* or *Tcr β* loci. **C)** *LAHP* thymic lymphomas harbor clonal translocations. Shown are spectral and classified images of the clonal translocations observed in each of the seven *LHP* tumors (#215, #887, #702, #519, #104, #300, and #521) analyzed by SKY. The identities of the chromosomes participating these translocations are indicated. For tumor #215, a normal chromosome 6 and a normal chromosome 12 are shown to reveal the chromosome 6 fragment and the elongated chromosome 12.

Table 5: SKY Analysis of LAP Tumors

Tumor	Life Span	Clonal Translocations [Frequency]	Non-clonal Translocations [Frequency]	Chromosome Fragments and Other Abnormalities [Frequency]	Gain or Loss of Chromosome	Average Chromosome Number
144	117 Days	t(11;14) [15/59]; Chr.14 fragment [12/15]; Chr.15 SAF [15/59]	t(5;7) and t(7;5) [1/15]; t(19;16) [1/15]; t(12;16) [1/15]	Chr.12 SAF [1/15]; Chr.5 SAF [1/15]; Big Chr.12 [1/15]	+12; -13	40
		Chr.5 SAF [44/59]	t(9;3) [2/44]; t(3;19) [1/44]; t(1;7) [1/44]	Chr.12 SAF [17/44]; Chr.1 fragment [1/44]; Chr.7 fragment [4/44]; Chr.11 fragment [1/44]; Chr.12 fragment [1/44]; Big Chr.12 [5/44]; Chr.15 SAF [1/44]; Chr.12 and Chr.1 SAF [1/44]	None	40
91	134 Days	t(12;1) [11/13]; Dicentric Chr.9 [6/13]; Dicentric t(9;17) [6/13]	t(12;1;12;1) [2/13]	Chr.12 SAF [2/13]; Chr.9 fragment [1/13]; Chr.14 fragment [3/13]	+4; +5; +6; +10; +11; +14; +15; -X	45
34	140 Days	t(14;6) and t(6;14) [63/64]; t(12;14) [63/64]; t(14;4) [63/64]; Chr.4 SAF [55/64]; Chr.5 SAF [34/64]	t(4;5) [3/64]; t(9;11) [1/64]; t(2;3) [1/64]; t(X;6) [1/64]; t(11;10) [1/64]; t(10;16) [1/64]; t(6;3) [1/64]; t(13;2) [1/64]; t(4;1) [1/64]; t(11;6) [1/64]; t(11;14) [1/64]; t(12;4;12) [1/64]; t(4;10) [1/64]; t(3;8) [1/64]	Chr.4 fragment [3/64]; Chr.6 fragment [2/64]; Chr.10 fragment [1/64]; Chr.11 fragment [1/64]; Dicentric Chr.4 [1/64]; Dicentric Chr.16 [1/64]	-Y [26/64]; +Y [24/64]	40
246	147 Days	None	t(X;6) [1/36]	Chr.14 fragment [1/36]; Chr.9 with centromere structure on the long arm [7/36]	Aneuploidy	57
734	276 Days	t(9;16) with long arm centromere structure on Chr.9 [18/20]	t(14;2) [2/20]; t(5;15) [1/20]; t(17;1) [1/20]; t(17;2) [1/20]; t(17;19) [1/20]	Chr.1 fragment [2/20]; Chr.14 fragment [2/20]	Aneuploidy	47
688	187 Days	None	None	None	Aneuploidy	83
51	210 Days	t(19;14;19) [15/15]; t(13;15) [13/15]; t(2;16) [14/15]; t(7;14) [11/15]; t(5;19) [13/15]	t(16;2) [6/15]; t(5;1) [2/15]; t(16;1) [1/15]; t(2;17) [1/15]; t(17;13) [1/15]; t(14;19) [1/15]; t(2;6) [1/15]; t(11;17) and t(17;11) [1/15]; t(12;11) [1/15]; t(5;3) [1/15]; t(16;3) [1/15]; t(15;7) [1/15]; t(4;14) [1/15]; t(18;2) [1/15]	Chr.14 fragment [6/15]; Chr.X fragment [1/15]; Chr.1 fragment [1/15]; Chr.5 fragment [1/15]; Chr.7 fragment [1/15]; Big Chr.12 [1/15]	Aneuploidy	64
		t(13;15) [57/59]; t(8;11) [17/59]	t(12;13) [11/59]; t(7;16) [10/59]; t(14;16) [7/59]; t(19;4) [6/59]; t(4;15) [1/59]; t(6;11) [1/59]; t(17;13) [1/59]; t(12;4) [1/59]; t(3;10) and t(10;3) [1/59]; t(5;6) [1/59]	Chr.8 fragment [14/59]; Chr.5 fragment [5/59]; Big Chr.12 [1/59]; Big Chr.6 [1/59]; Chr.5 and Chr.13 SAF [2/59]	+5; +15; -13; +Y	40

Table 6: SKY Analysis of LAHP Tumors

Tumor	Life Span	Clonal Translocations [Frequency]	Non-clonal Translocations [Frequency]	Chromosome Fragments and Other Abnormalities [Frequency]	Gain or Loss of Chromosome	Average Chromosome Number
215	112 Days	t(12;5) [29/65]; t(12;X) [17/65]; Chr.6 fragment [44/65]; Big Chr.12 [26/65]; Broken Chr.9 fragment [22/65]	t(12;3) [6/65]; t(6;3) [5/65]; t(12;6) [3/65]; t(5;4) and t(4;5) [3/65]; t(12;19) [2/65]; t(11;15) [2/65]; t(14;3) [1/65]; t(17;16) [1/65]; t(12;2) [1/65]; t(5;7;5) [1/65]; t(6;9) [1/65]; t(14;X) [1/65]; t(5;6) and t(6;5) [1/65]; t(4;10) and t(10;4) [1/65]; t(5;13;5) [1/65]; t(11;6) [1/65]; t(3;6) [1/65]; Dicentric t(1;16) [1/65]	Big Chr.14 [2/65]; Dicentric Chr.13 [3/65]; Dicentric 9 [3/65]; Dicentric 6 [1/65]; Dicentric 14 [1/65]; Dicentric 16 [1/65]; Dicentric 18 [1/65]; Dicentric 19[1/65]; Chr.3 fragment [5/65]; Chr.2 fragment [4/65]; Chr.5 fragment [1/65]; Chr.19 fragment [1/65]; Chr.8 fragment [1/65]; Chr.X fragment [1/65]; Detached centromeres	+14; +15; +17; -X	44
887	121 Days	t(9;16) [28/35]; t(19;4) [19/35]	t(1;14) [2/35]; t(13;18) [1/35]; t(17;16) [1/35]; t(9;11) [1/35]; t(11;4) [1/35]; t(11;17) [1/35]; t(15;19) [1/35]; t(9;2) [1/35]; t(16;5) [1/35]; t(19;15) [1/35]; t(4;19) [1/35]	Big Chr.6 [1/35]; Chr. 6 fragments; Chr.14 fragments; Chr. X fragments; Detached centromeres	None	41
702	144 Days	t(9;19) [31/34]; Chr.9 with long arm centromere structure [26/34]; t(4;6) [14/34]	t(3;1) [1/34]; t(10;19) [1/34]; t(4;16) [1/34]; t(11;14) and t(14;11) [2/34]; t(6;4) [3/34]; t(6;4;6) without centromere [2/34]; t(18;6) [1/34]; t(16;11) [1/34]; t(8;15) and t(15;8) [1/34]	Dicentric Chr.14 [9/34]; Dicentric 9 [2/34]; Dicentric 10 [2/34]; Dicentric 12 [1/34]; Chr.3 fragment [1/34]; Chr.5 fragment [2/34]; Chr.6 fragment [14/34]; Chr.8 fragment [3/34]; Chr.9 fragment [2/34]; Chr.10 fragment [1/34]; Chr.14 fragment [3/34]; Chr.16 fragment [1/34]; Detached centromeres	+12; +14; +15; -13; -19	41
519	185 Days	t(17;4) [7/10]; Chr.9 with long arm centromere structure [9/10]	t(17;9) [3/10]; t(8;6) [2/10]; t(4;13) [2/10]; t(5;3) [1/10]; t(1;3) and t(3;1) [1/10]; t(9;2) [1/10]; t(4;15) [1/10]; t(2;Y) [1/10]; t(X;8) [1/10]; t(12;6) [1/10]; t(17;19) [1/10]; Dicentric t(14;15) [1/10]	Chr.10 with long arm centromere structure [1/10]; Chr.5 fragment [1/10]; Chr.6 fragment [1/10]; Chr.9 fragment [1/10]; Chr.10 fragment [2/10]; Chr.15 fragment [1/10]; Chr.X fragment [1/10]; Chr.Y fragment [1/10]; Detached centromeres	Aneuploidy	58
104	187 Days	t(17;3); t(7;4)	n.d.	n.d.	n.d.	n.d.
300	199 Days	t(7;10) and t(10;7) [42/42]; t(9;X) and t(X;9) [40/42]; Chr.2 with long arm centromere structure [42/42]; t(11;14) [38/42]; t(14;6) and t(6;14) [37/42]; t(14;1) [35/42]; t(5;7) [18/42]	t(2;16) [7/42]; t(14;6) [7/42]; t(9;11) and t(11;9) [4/42]; t(9;11) [2/42]; t(5;1) [2/42]; t(9;10) [1/42]; t(1;7) [1/42]; t(18;5) [1/42]; t(5;10) [1/42]; t(1;2) [1/42]; t(13;5) [1/42]; t(5;19) [1/42]; t(8;10) [1/42]; t(14;9) [1/42]; t(5;2) [1/42]; t(11;7) [1/42]; t(2;14) [1/42]; t(12;18) [1/42]; t(5;16) [1/42]; t(12;16) [1/42]; t(15;14) [1/42]; t(1;14;1) without centromere [1/42]; t(2;15) with centromere structure at the junction [1/42]; t(2;18) with centromere structure at the junction [1/42];	Dicentric Chr.6 [2/42]; Dicentric 14 [1/42]; Chr.1 fragment [1/42]; Chr.4 fragment [3/42]; Chr.6 fragment [5/42]; Chr.7 fragment [5/42]; Chr.8 fragment [1/42]; Chr.14 fragment [4/42]; Chr.18 fragment [2/42]; Detached centromere	Aneuploidy	58
521	207 Days	t(5;4) [22/32]; t(17;4) [9/32]	t(1;14) [1/32]; t(9;12) [1/32]; t(13;3) [1/32]; t(4;5) [1/32]; t(19;14) [1/32]; t(7;17) [1/32]; Dicentric (12;15) [1/32]	Chr.9 fragments; Chr.14 fragments; Detached centromeres	Aneuploidy	68

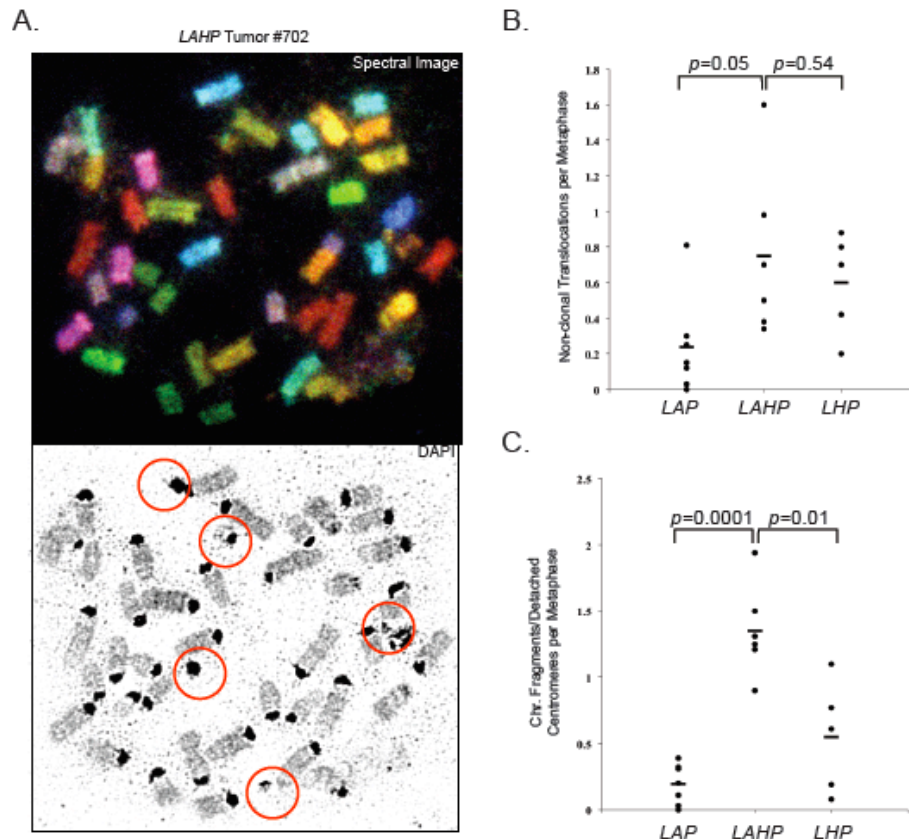


Figure 18. *LAHP* thymic lymphomas exhibit increased genomic instability as compared to *LAP* and *LHP* tumors. A) Spectral and DAPI images of a representative metaphase spread prepared from *LAHP* tumor #702. Circles indicate chromosome fragments and/or detached centromeres. B-C) Quantitative analyses of non-clonal translocations B) or chromosome fragments and detached centromeres C) in *LHP*, *LAP* and *LAHP* thymic lymphomas as analyzed by SKY. Graphs show the average number of each type of chromosome abnormality observed per metaphase in tumors of each genotype. Dots represent the values for each tumor. Lines indicate the mean values for tumors of each genotype.

Chapter IV

Functional Interactions Between ATM and H2AX in Lymphocyte Development, Recombination, and Tumorigenesis

ABSTRACT

The ATM kinase and H2AX, a core histone variant that is phosphorylated by ATM in chromatin around DSBs, are each critical for normal DSB repair, maintenance of genomic stability, and suppression of cancer. Mice with germ line deletions of both factors are early embryonic lethal, and double knockout cells exhibit dramatically increased genomic instability. Deletion or loss of heterozygosity (LOH) of both *ATM* and *H2AFX*, which map to 11q23, occurs in a few types of human tumors. In this part of my thesis, I hypothesized that ATM independent H2AX functions downstream of other kinases are essential for proper DSB repair, genomic stability and tumor suppression. To this end, I have utilized *Atm*^{-/-}*H2ax*^{-/-}, *Atm*^{-/-}, and *H2ax*^{-/-} cell lines and primary T cells to test whether ATM independent H2AX functions prevent DSBs from progressing into translocations, and whether they are important for T cell development and tumor progression. *H2ax* deficiency and haplo-insufficiency cooperates with *p53* loss to enhance cancer predisposition in mice. Based on the interplay between H2AX and p53, which is activated by ATM, and the fact that H2AX functions downstream of other kinases independent of ATM, I also hypothesized that deletion of one or both alleles of *H2ax* will synergize with *Atm* inactivation to increase tumor predisposition. To this end, I have characterized the predisposition of both *Atm*^{-/-} mice and *Atm*^{-/-} mice with conditional inactivation of *H2ax* in thymocytes to thymic lymphomas.

INTRODUCTION

The observation that *Atm*^{-/-} and *H2ax*^{-/-} mice exhibited reduced numbers of developing and mature lymphocytes suggested that ATM and H2AX may function in the repair of RAG-generated DSBs. Subsequent studies showed that ATM kinase activity is required to hold together RAG-generated DNA ends in G1 phase cells (Bredemeyer et al., 2006). In contrast, I showed in Chapter II that H2AX is dispensable for this function in G1 phase *Atm*^{+/+} cells (Yin et al., 2009). However, in case of defective NHEJ, for example in *Artemis*^{-/-} cells, H2AX is required to prevent irreversible separation of unrepaired RAG-induced DSBs ends in G1 phase, as well as antigen receptor loci translocation formation during continued cell cycle progression. Although ATM deficiency does not block NHEJ to the same extent as Artemis deficiency, *Atm*^{-/-} cells are less able to correctly join RAG-induced DSBs in G1 phase, presumably due to destabilized post-synaptic complex. Thus, on the *Atm*^{-/-} background, H2AX may also be important to keep cleavage antigen receptor loci DNA ends in proximity for proper repair and to prevent their progression in to chromosome breaks or translocations during subsequent cell proliferation.

Although ATM is the major kinase that phosphorylates H2AX around RAG-generated DSBs induced in G1 phase cells, DNA-PKcs is also able to phosphorylate H2AX (Savić et al., 2009). In addition, ATM and DNA-PK and, potentially ATR, can phosphorylate H2AX at replication-associated DSBs during S phase, suggesting ATM-independent functions of H2AX (Furuta et al., 2003; Stiff et al., 2004; Ward and Chen, 2001). In *Atm*^{-/-} B cell metaphases, many spontaneous chromosomal abnormalities are

chromosome breaks, which likely are derived from pre-replication, G1 phase, lesions. In contrast, the genetic abnormalities from *H2ax*^{-/-} B cell metaphases are about equally divided between chromosome and chromatid breaks, the later of which generally represent post-replication lesions (Franco et al., 2006). Thus, during the proliferation of *Atm*^{-/-} thymocytes, DNA-PKcs- and ATR-mediated phosphorylation of H2AX at replication-associated DSBs may function to prevent RAG-initiated translocations by suppressing the accumulation of free DNA ends during DNA replication that could be joined with RAG-generated DNA ends.

HR is not required to assemble TCR or Ig genes; however, mice with conditional deletion of BRCA1 or BRCA2 in thymocytes exhibit a complete block at the DN stage, phenotypically similar to NHEJ/p53-deficient mice. The developmental block is rescued through introduction of p53 deficiency or over-expression of the anti-apoptotic Bcl2 protein (Mak et al., 2000; Cheung et al., 2002). Thus, HR is essential for TCR β -triggered proliferation and expansion of DN thymocytes. Combined BRCA1/p53 or BRCA2/p53 deficiency also results in the rapid development of T lineage lymphomas associated with genomic instability that arises from the aberrant repair of replication-associated DSBs. Since H2AX phosphorylation enforces efficient HR and prevents the error-prone deletional repair (Xie et al., 2004), and ATM may modulate HR repair by regulating MRN effector functions (Gatei et al., 2000; Wu et al., 2000; Lim et al., 2000; Matsuoka et al., 2007), I would like to test whether deficiency of H2AX in ATM-null thymocytes would exacerbate the developmental block, and if yes, whether the defects could result from compromised HR repair.

Neither ATM nor H2AX is absolutely required for embryonic development; nonetheless, combined ATM/H2AX loss leads to embryonic lethality and dramatically increased cellular genomic instability compared to loss of either factor alone (Zha et al., 2008). Since ATM suppresses the accumulation of intracellular reactive oxygen species (ROS), ATM/H2AX double knockout embryonic stem (ES) cells and mouse embryonic fibroblasts (MEFs) may fail to repair the oxidative DNA damages in the absence of H2AX, leading to massive genomic instability and cell death.

Atm^{-/-} mice are predisposed to thymic lymphomas with clonal TCR α/δ loci translocations, while *H2ax*^{-/-}*p53*^{-/-} mice only occasionally develop these tumors (Liyanaige et al., 2000; Bassing et al., 2003; Celeste et al., 2003b). The ATM and H2AX genes are very closely linked in both human and mouse and map to a cytogenetic region (11q23) often deleted in some human cancers (Stilgenbauer et al., 1996, 1999), suggesting possible synergistic effects between ATM and H2AX loss in tumor initiation or development. Due to the early embryonic lethality in germ line *Atm*^{-/-}*H2ax*^{-/-} mice, a mouse model that would allow characterization of tumor development is needed. In addition, since DDR mechanisms in embryonic cells may differ from those in somatic cells, I would like to examine the effects of somatic deletion of H2AX on ATM-deficient mice with regard to lymphocyte development, V(D)J recombination and tumorigenesis.

RESULTS

Somatic inactivation of *H2ax* in *Atm*^{-/-} mice leads to impaired lymphocyte

development

To evaluate whether somatic loss of H2AX in $Atm^{-/-}$ mice can avoid the early embryonic lethality in $Atm^{-/-}H2ax^{-/-}$ mice and alter thymocyte development and transformation, I sought to characterize $Atm^{-/-}$ mice with conditional deletion of $H2ax$ in lineage-committed thymocytes. To this end, I generated $Lck-CreH2ax^{F/F}$ (*LH*), $Lck-CreAtm^{-/-}$ (*LA*), and $Lck-CreAtm^{-/-}H2ax^{F/F}$ (*LAH*) mice. All three genotypes of mice survived into adulthood, permitting analysis of their lymphocyte development and tumor predisposition. Cre recombinase-driven deletion of the "floxed" $H2ax$ alleles was confirmed by PCR of genomic DNA from total thymocytes in *LH* and *LAH* mice (Data not shown).

I first characterized lymphocyte development in 4- to 6-week old mice. The percentages of DN, DP, CD4 SP and CD8 SP thymocytes in *LH* mice were similar to previously characterized germ line $H2ax^{-/-}$ and conditional $Lck-CreH2ax^{F/F}p53^{F/F}$ mice (Figure 19A). In the spleen, percentages of CD4 SP and CD8 SP mature T cells were also comparable between *LH* and *LHP* mice, although both were slightly lower than those in wild type mice, suggesting conditional $H2ax$ leads to mild defects in development of mature lymphocytes (Figure 19A). *LA* mice, compared to *LH* mice, showed increased percentages of DN populations and a concomitant decrease in CD4 SP and CD8 SP populations in the thymus, and a dramatic decrease in mature SP T cells in the spleen (Figure 19A), consistent with previously described more severe lymphopenia in $Atm^{-/-}$ than in $H2ax^{-/-}$ mice. Interestingly, conditional knockout of $H2ax$ in *LA* mice did not seem to significantly alter the CD4/CD8 profile in the thymus, or percentages of mature

SP T cells in the spleen, although absolute numbers of total thymocytes in both *LA* and *LAH* mice were significantly lower than those in *LH* mice (Figure 19A, 19B). In addition, total thymocyte numbers in *LAH* mice were significantly reduced, to about 50% of those in *LA* mice (Figure 19B). This is likely due to a significant reduction in the absolute numbers of DP thymocytes in *LAH* mice compared to *LA* mice (Figure 19C). The absolute numbers of DN, CD4 SP and CD8 SP cells did not significantly differ between *LAH* and *LA* thymuses (Figure 19C). Thus, H2AX conditional deletion on the *Atm*^{-/-} background results in further reduction in cellularity, suggesting H2AX loss further exacerbate the developmental defects in *Atm*^{-/-} mice.

Genomic instability in mature *LAH* T cells

Based on known functions of ATM and H2AX in DNA damage response and repair, I hypothesize that the ~50% reduction in total thymocyte and DP thymocyte numbers in *LAH* mice compared to those in *LA* mice results from increased genomic instability and decreased cellular survival. There are several possible underlying mechanisms, which are not necessarily mutually exclusive. First, loss of H2AX in ATM-null lymphocytes may further destabilize the post-cleavage synaptic complex during V(D)J recombination, or allow irreversible separation of cleaved DNA strands. Consequently, more un-repaired V(D)J DSB intermediates or mis-repaired products, such as TCR loci chromosome breaks translocations, would accumulate in *Atm*^{-/-}*H2ax*^{-/-} thymocytes, while successful recombination events would be diminished. Since productive TCR β rearrangement and pre-TCR signals are required for DN-DP transition, the reduction in DP thymocyte numbers could be explained by such a scenario. Second,

since H2AX Ser139 phosphorylation has been shown to enforce efficient homologous recombination and prevent the error-prone deletional repair through SSA, *Atm*^{-/-}*H2ax*^{-/-} thymocytes may be more comprised in HR repair of DNA breaks. Third, *Atm*^{-/-} thymuses exhibit elevated levels of oxidative damage (Barlow et al., 1999), and the inability of *Atm*^{-/-}*H2ax*^{-/-} thymocytes to repair the DNA damages via H2AX-dependent mechanisms would render cell more susceptible to overwhelming genomic instability and subsequent cell death.

To test the hypothesis of increased genomic instability in ATM/H2AX-null thymocytes, I first stimulated splenic T cells from *LAH* mice with IL-2 and ConA for two days, and assayed for genomic instability by SKY (Figure 20A). A total of 98 metaphases were examined, and nearly half of them (45/98=46%) contained at least one type of chromosome aberrations. Approximately 10% metaphases from stimulated splenic T cells of germ line *Atm*^{-/-} mice harbored Chr. 14 abnormalities, most of which likely involve the TCR α/δ locus, reflecting a V(D)J recombination joining defect in the absence ATM. A similar percentage of Chr. 14 abnormalities (8/98=8.2%) was observed in metaphases from stimulated *LAH* splenic T cells. Although more experimental replicates with proper controls from *LA* and *LH* mice are needed to draw a conclusion, this result suggests that conditional ablation of H2AX in *Atm*^{-/-} thymocytes does not lead to more accumulation of chromosome breaks/translocations that result from aberrant V(D)J recombination. Chromosome breaks, chromatid breaks, and both reciprocal and non-reciprocal chromosome translocations were also observed in *LAH* T cells (Figure 20A). It's noteworthy that the incidences of chromosome breaks/fragments and chromatid breaks

are about equal, consistent with the pattern of genomic instability in *Atm*^{-/-}*H2ax*^{-/-} MEFs and ES cells. This observation would be consistent with the model that H2AX loss does not significantly exacerbate the *Atm*^{-/-} defects in pre-replication DNA repair, but causes significant increase in errors of post-replication repair. This is also suggested by the observation that 3/98 (3.1%) metaphases contained quadriradial structures (Figure 20B), similar to those observed in BRCA2-deficient murine cells (Venkitaraman, 2002) but were not observed in *Atm*^{-/-} or *H2ax*^{-/-} cells, suggesting HR might be further compromised in *LAH* peripheral T cells. More independent *LAH* mice together with *LA* and *LH* control mice would be examined by SKY to reach statistically sound conclusions.

Loss of H2AX does not change thymic lymphoma development or phenotype in *Atm*^{-/-} mice

To determine the effect of combined *Atm* and *H2ax* inactivation in thymocytes on tumor development or phenotype, I generated and characterized parallel cohorts of 20 *LA* mice and 35 *LAH* mice for up to 150 days. I also generated and aged approximately 10 *LH* mice, all of which lived without any signs of tumor to over 6 months (Data not shown). In contrast, all *LA* and *LAH* mice succumb to tumors by the age of 5 months. All 20 *LA* cohort mice and 25 of the 27 *LAH* cohort mice died from thymic lymphomas (Table 7). One of the remaining two *LAH* mice was diagnosed with a sarcoma; the other exhibited enlarged lymph nodes and the spleen but not the thymus. *LA* cohort mice survived tumor-free between 70-132 days with a 50% survival time of 89 days (Figure 21A). *LAH* mice survived tumor-free between 73-145 days, with a 50% survival time of 91 days (Figure 21A). The tumor-free survival between *LA* and *LAH* mice was not

significantly different by Log-rank test, indicating that the key events during tumor initiation and progression might be determined by ATM germ line deficiency. This observation differs from what I showed in Chapter III (Figure 16C), where bi-allelic deletion of H2AX in *Artemis*^{-/-}*p53*^{-/-} thymocytes significantly delays thymic lymphomagenesis, suggesting that modification of tumor development by somatic loss of H2AX depends on the cellular context.

Although conditional H2AX ablation did not alter tumor development, it could modify tumor phenotypes such as clonality or patterns of genomic instability. Thus, I determined the developmental stage and clonality of *LA* and *LAH* thymic lymphomas. Most of the *LA* and *LAH* tumors analyzed were TCRβ⁻ and comprised of CD4⁻CD8⁺, CD4⁺CD8⁺, and less frequently CD4⁺CD8⁻ and CD4⁻CD8⁻ cells (Table 7, Table 8). This result suggests that the tumors may have developed through the transformation of TCRβ⁻ thymocytes, or tumor cell surface expression of TCRβ has been down regulated in the transformation process. Since *Atm*^{-/-} mice invariably succumb to thymic lymphomas with clonal TCRα/δ loci translocations that disrupt TCRα chain production, the TCRβ chain on the cells targeted for transformation may be internalized due to lack of TCRα as a pairing partner. Almost all *LA* and *LAH* thymic lymphomas contained two rearranged *Tcrβ* alleles and therefore arose through the clonal expansion of a single thymocyte (Figure 21B). Thus, *LA* and *LAH* tumors each mainly develop from the transformation of a single thymocyte with subsequent genetic or epigenetic changes leading to heterogeneous CD4 and/or CD8 expression.

Thymic lymphomas from *LA* and *LAH* mice display similar clonal translocations

To evaluate whether *LAH* mice develop tumors harboring similar translocations as those in *LA* mice, I conducted SKY on metaphases prepared from 4 *LA* thymic lymphomas and 5 *LAH* thymic lymphomas. All nine tumors analyzed harbor clonal translocations of Chr. 14, likely involving the TCR α/δ loci (Figure 21C). The more frequent clonal translocations observed in these tumors are t(12;14) and t(14;15) (Figure 21C), both of which were seen in thymic lymphomas from *Atm*^{-/-} mice (Liyanage et al., 2000). In Chapter III (Figure 18B), I found that tumors developed from *Artemis*^{-/-}*p53*^{-/-} thymocytes with bi-allelic *H2ax* deletion contained more non-clonal translocations, chromosome breaks and detached centromeres, compared to those originated from *Artemis*^{-/-}*p53*^{-/-} thymocytes. Thus, it remains possible that *LAH* tumors may have accumulated more non-clonal chromosome aberrations than *LA* tumors, due to loss of H2AX-dependent mechanisms of break repair. Therefore, somatic H2AX deletion does not seem to change the patterns of genomic instability, at least for the type of clonal translocations, in tumors that develop in mice with germ line ATM deficiency.

DISCUSSION

Following expression of in-frame VDJ β rearrangements on the cell surface, DN thymocytes are rescued from apoptosis and signal rapid cellular proliferation and differentiation to the DP stage. In DP thymocytes, in-frame VJ α rearrangements generate TCR α chains that associate with TCR β to form the $\alpha\beta$ TCR that rescues DP cells from apoptosis and promote further differentiation to CD4⁺ or CD8⁺ mature SP T cells. In this chapter, I showed that conditional knockout of *H2ax* in *LA* mice did not lead to apparent development block at any particular stage, seem to significantly alter the CD4/CD8 profile in the thymus, or percentages of mature SP T cells in the spleen, although absolute numbers of total thymocytes in both *LA* and *LAH* mice were significantly lower than those in *LH* mice. In addition, total thymocyte numbers in *LAH* mice were significantly reduced, to about 50% of those in *LA* mice. This is likely due to a significant reduction in the absolute numbers of DP thymocytes in *LAH* mice compared to *LA* mice. The absolute numbers of DN, CD4 SP and CD8 SP cells did not significantly differ between *LAH* and *LA* thymuses. Thus, H2AX conditional deletion on the *Atm*^{-/-} background results in further reduction in cellularity, suggesting H2AX loss further exacerbate the developmental defects in *Atm*^{-/-} mice.

Although data currently available suggest that the defects caused by H2AX ablation in lineage committed *Atm*^{-/-} thymocytes are likely depended on the roles of H2AX in post-replication DNA damage repair, the possibility of H2AX collaborating with ATM in NHEJ has neither been proven or ruled out. Mapping of the γ H2AX chromatin domains around induced V(D)J DNA breaks in Abelson cells and HO

recombination sites in yeast by ChIP suggests that H2AX, together with other histones, may be cleared off the very ends of DSBs, while γ H2AX signals extend at least ~500kb along the chromatin fiber (Shroff et al., 2004; Savić et al., 2009). I have proposed a “zipping” model to explain the functional importance of this pattern of γ H2AX distribution around the break sites, that it, to maintain the positional proximity of un-repaired DNA ends by tethering the flanking chromatin. ATM is the major kinase mediating the long range γ H2AX signal propagation in this model, and the contribution of DNA-PKcs to H2AX phosphorylation, albeit much smaller compared to that of ATM, might be evident in the absence of ATM or ATM kinase activity. In addition, *Atm*^{-/-} lymphocytes only show a partial defect in NHEJ of RAG-induced DSBs, suggesting other factors exist to support the joining step. Previously, it was shown that *Atm*^{-/-}:pINV Abelson cells, as compared to *Atm*^{+/+}:pINV cells, exhibited reduced ability to complete successful V(D)J recombination, and accumulated illegitimate repair products (the hybrid joins) and un-repaired RAG-generated DNA ends that physically separated (Bredemeyer et al., 2006). To test the hypothesis that H2AX is needed to suppress antigen receptor loci DNA end separation and subsequent translocation formation in *Atm*^{-/-} cells, I would need to analyze V(D)J recombination in *Atm*^{-/-} and *Atm*^{-/-}*H2ax*^{-/-} Abelson cell lines. To date, I have established several independently derived *Atm*^{-/-}*H2ax*^{F/F} Abelson cell lines, which can be infected with the pINV retroviral substrate and transduced with TAT-Cre to generate *Atm*^{-/-}*H2ax* ^{Δ} cells with single integrants. V(D)J recombination and NHEJ-mediated DSB repair can then be assayed by flow cytometry (FACS) for GFP expression and by Southern blotting with an hCD4 DNA probe, while physical separation of RAG-

generated DNA ends can be assayed by FISH using probes that hybridize to genomic sequences on either side of the pINV integrate site.

Several $Atm^{-/-}H2ax^{\Delta/\Delta}$ cell lines have been generated from $Atm^{-/-}H2ax^{F/F}$ cells, and both lines with similar genetic background have been assayed for V(D)J recombination of the endogenous $Ig\kappa$ locus. I found by Southern blot that $Atm^{-/-}H2ax^{\Delta/\Delta}$ Abelson cells can be induced to undergo similarly robust $Ig\kappa$ recombination as $Atm^{-/-}H2ax^{F/F}$ cells. Thus, a FISH probe pair that flanks the $Ig\kappa$ locus as described above (Figure 7C) will be used to evaluate whether more cleaved $Ig\kappa$ DNA ends separate in G1-arrested $Atm^{-/-}H2ax^{\Delta/\Delta}$ cells than in control $Atm^{-/-}H2ax^{F/F}$ cells. I've also attempted to release these cells from STI571 arrest to test whether H2AX loss leads to more chromosome break/translocation formation in $Atm^{-/-}$ Abelson cells that re-enter the cell cycle. Both before and during STI571 induction, $Atm^{-/-}H2ax^{\Delta/\Delta}$ cells proliferated and survived well in culture without overt cell death, as did $Atm^{-/-}H2ax^{F/F}$ cells. However, while all $Atm^{-/-}H2ax^{F/F}$ lines readily recovered from STI571 treatment as previously shown, all three $Atm^{-/-}H2ax^{\Delta/\Delta}$ lines tested failed to re-start proliferation and showed massive cell death after STI571 withdrawal. Since H2AX is a haplo-insufficient tumor suppressor, $Atm^{-/-}H2ax^{F/\Delta}$ cells have also been generated to test whether a 50% reduction of cellular H2AX can support cell recovery from STI571 treatment and lead to more $Ig\kappa$ -associated genomic instability in $Atm^{-/-}$ cells.

Thymus cellularity in *LAH* mice is significantly reduced compared to that in *LA* mice, while both genotypes of mice develop thymic lymphomas at similar latency and show similar patterns of genomic instability. In this case, the germ line ATM-deficiency may have dictated the transforming events and their cellular target before the excision of *H2ax*, whereas somatic H2AX deletion can contribute to additional genomic aberrations (such as clonal or non-clonal translocations) during tumor progression but is not enough to alter tumor latency. To test this hypothesis, it would be important to monitor and compare tumor predisposition in mice with ATM conditionally depleted at various developmental stages and in different compartments. Importantly, in cases of human B-cell chronic lymphocytic leukemias and mantle cell lymphomas, common somatic deletions within the genomic region 11q22-11q23 may have inactivated the *ATM* (11q22.3) and *H2AFX* (11q23.2-23.3) (Parikh et al., 2007) genes together (Stilgenbauer et al., 1996, 1999). Thus, a clinically relevant mouse model with somatic ablation of both *Atm* and *H2ax* in B cells would be desirable to test whether the two genes collaborate to drive tumorigenesis. These mouse models would also be useful tools to study the functional interactions between ATM and H2AX during CSR, which is comprised in both *Atm*^{-/-} and *H2ax*^{-/-} mice.

Figure 19. Characterization of thymic and splenic T cell development in *LH*, *LA* and *LAH* mice. **A)** Shown are representative anti-CD4 and anti-CD8 flow cytometric analysis of total *LH*, *LA* and *LAH* thymocytes (upper panel), and splenocytes from the same mice (lower panel). The percentage of cells within each quadrant is indicated. **B)** Total thymocyte numbers in *LH*, *LA* and *LAH* mice. Numbers of mice analyzed for each genotype and the *p* value are indicated. **C)** Shown are absolute numbers of DN, DP, CD4 SP and CD8 SP populations in the thymuses of the same mice analyzed in **B**). The *p* value between absolute numbers of *LA* and *LAH* DP populations is indicated. Not significant, *ns*.

A.

Mouse	Total Abnormalities	Chr. 14 Abnormalities	Average Chromosome Translocations per Metaphase		Chromosome Breaks or Fragments per Metaphase	Chromatid Breaks per Metaphase
			21/98=0.214			
LAH 829	45/98=46%	8/98=8.2%	Reciprocal	Non-reciprocal	26/98=0.265	21/98=0.214
			6	15		

B.

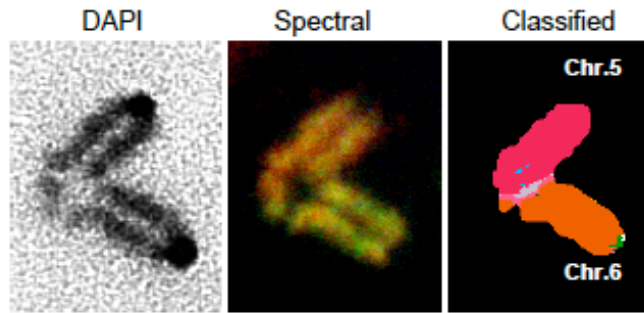
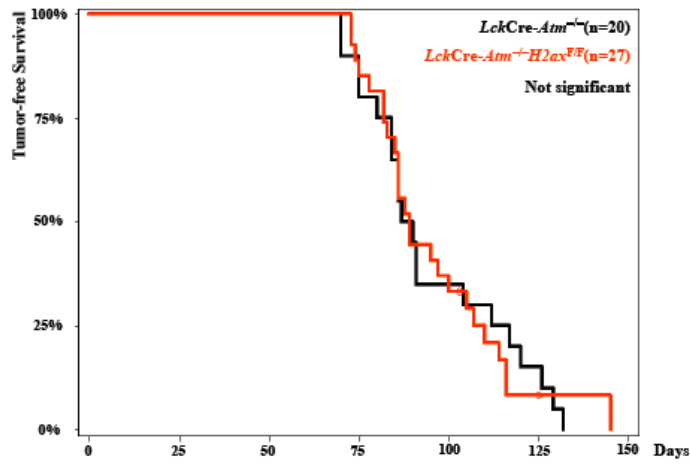


Figure 20. Genomic instability of stimulated splenic T cells from one *LAH* mice

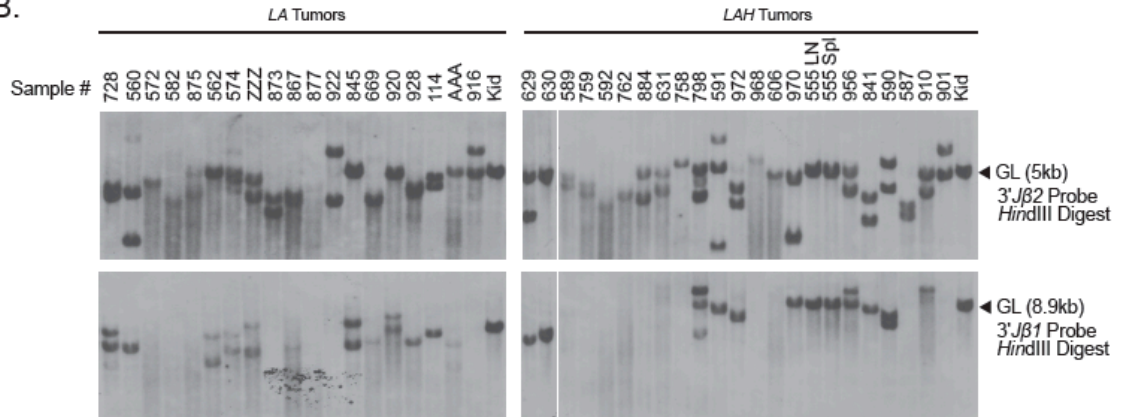
analyzed by SKY. A) In total 98 metaphases were analyzed for stimulated splenic T cells from mouse *LAH*#829. Shown are percentages of metaphases with any chromosome abnormalities (46%), percentage of metaphases with Chr. 14 chromosome abnormalities (8.2%), and average numbers of chromosome translocations (0.214 per metaphase), chromosome breaks (0.265 per metaphase), and chromatid breaks (0.214 per metaphase).

B) A representative quadriradial structure between Chr. 5 and Chr. 6 in *LAH* stimulated splenic T cells. DAPI, spectral and classified images are shown.

A.



B.



C.

<i>LckCre-Atm^{-/-}</i> Tumors		<i>LckCre-Atm^{-/-}H2ax^{F/F}</i> Tumors	
Tumor	Clonal Translocations/Breaks	Tumor	Clonal Translocations/Breaks
560	t(12;15), t(6;14), t(15;6), t(4;15)	589	t(2;1), t(4;5), t(4;15), t(15;4), t(12;2), t(14;15;16)
728	t(14;15)	590	t(14;16), t(4;14), t(14;4), t(14;4;16)
873	t(12;14), t(8;6), t(X;16)	629	t(14;15), t(12;14), t(17;1)
ZZZ	t(14;8), t(12;14), t(14;12)	798	t(14;15), t(12;14)
		884	t(14;15), t(12;14)

Figure 21. Conditional inactivation of *H2ax* in *Atm*-deficient thymocytes does not seem to alter thymic lymphoma development or pattern of genomic instability. **A)** *LAH* mice exhibit similar rate of mortality from thymic lymphomas as *LA* mice. Kaplan-Meier curves showing the percentage of tumor-free survival of *LA* (n=20) and *LAH* (n=27) mice. A drop in the curve represents the sacrifice or death of an animal diagnosed at necropsy with thymic lymphomas. Open circles represent the sacrifice or death of an animal due to other tumors. Log-rank test revealed no significant difference in tumor-free survival. **B)** *LA* and *LAH* tumors arise from the clonal expansion of single thymocytes. Southern blot analyses of *Tcrβ* rearrangements in *HindIII*-digested genomic DNA isolated from *LA* and *LAH* tumor. LN, lymph nodes; Spl, spleen. Kidney (Kid) DNA from non-tumor mice was used as controls. **C)** Summary of clonal chromosome abnormalities in *LA* and *LAH* tumors as shown by SKY. Chromosomes with antigen receptor loci are highlighted.

Table 7: Characterization of *LckCreAtm*^{-/-} Cohort Mice

Mouse	Age at Death (Days)	Cause of Death	FACS Analysis	
			TCR β Stain	CD4/CD8 Stain
26	70	Thymic Lymphoma	TCR β ⁻	CD4 ⁻ CD8 ⁺
922	70	Thymic Lymphoma	TCR β ⁻	CD4 ⁻ CD8 ⁺
114	75	Thymic Lymphoma	TCR β ⁻	CD4 ⁺ CD8 ⁺
875	75	Thymic Lymphoma	TCR β ⁻	CD4 ⁺ CD8 ⁺
845	80	Thymic Lymphoma	TCR β ⁻	CD4 ⁺ CD8 ⁺
928	84	Thymic Lymphoma	TCR β ⁻	CD4 ⁻ CD8 ⁺
920	84	Thymic Lymphoma	TCR β ⁻	CD4 ⁺ CD8 ⁺
116	86	Thymic Lymphoma	n.d.	n.d.
873	86	Thymic Lymphoma	TCR β ⁻	CD4 ⁺ CD8 ⁺
867	87	Thymic Lymphoma	TCR β ⁻	CD4 ⁻ CD8 ⁺
669	90	Thymic Lymphoma	TCR β ⁻	CD4 ⁺ CD8 ⁻ , CD4 ⁺ CD8 ⁺
560	91	Thymic Lymphoma	TCR β ⁻	CD4 ⁺ CD8 ⁻ , CD4 ⁻ CD8 ⁺ , CD4 ⁺ CD8 ⁺
574	91	Thymic Lymphoma	TCR β ⁻	CD4 ⁻ CD8 ⁺ , CD4 ⁺ CD8 ⁺
572	104	Thymic Lymphoma	TCR β ⁻	CD4 ⁺ CD8 ⁻
562	112	Thymic Lymphoma	TCR β ⁺ , TCR β ⁻	CD4 ⁺ CD8 ⁺
728	117	Thymic Lymphoma	TCR β ⁻	CD4 ⁻ CD8 ⁺ , CD4 ⁺ CD8 ⁺
582	120	Thymic Lymphoma	TCR β ⁻	CD4 ⁻ CD8 ⁺
902	126	Thymic Lymphoma	n.d.	n.d.
872	129	Thymic Lymphoma	n.d.	n.d.
877	132	Thymic Lymphoma	TCR β ⁻	CD4 ⁻ CD8 ⁺

Note: n.d., not determined.

Table 8: Characterization of *LckCreAtm^{-/-}H2ax^{F/F}* Cohort Mice

Mouse	Age at Death (Days)	Cause of Death	FACS Analysis	
			TCR β Stain	CD4/CD8 Stain
629	86	Thymic Lymphoma	TCR β^+ , TCR β^-	CD4 $^+$ CD8 $^+$
630	86	Thymic Lymphoma	TCR β^-	CD4 $^+$ CD8 $^+$
589	83	Thymic Lymphoma	TCR β^-	CD4 $^-$ CD8 $^+$, CD4 $^+$ CD8 $^+$
759	82	Thymic Lymphoma	TCR β^{int}	CD4 $^+$ CD8 $^+$
592	86	Thymic Lymphoma	TCR β^-	CD4 $^-$ CD8 $^+$
762	85	Thymic Lymphoma	TCR β^-	CD4 $^+$ CD8 $^+$
884	73	Thymic Lymphoma	TCR β^-	CD4 $^+$ CD8 $^+$
631	73	Thymic Lymphoma	TCR β^-	CD4 $^-$ CD8 $^+$, CD4 $^+$ CD8 $^+$
758	107	Thymic Lymphoma	TCR β^-	CD4 $^+$ CD8 $^-$, CD4 $^+$ CD8 $^+$
798	95	Thymic Lymphoma	TCR β^-	CD4 $^-$ CD8 $^+$, CD4 $^+$ CD8 $^+$
591	75	Thymic Lymphoma	TCR β^-	CD4 $^-$ CD8 $^+$, CD4 $^+$ CD8 $^+$
972	78	Thymic Lymphoma	TCR β^{int}	CD4 $^+$ CD8 $^+$, CD4 $^-$ CD8 $^+$
968	88	Thymic Lymphoma	TCR β^+	CD4 $^+$ CD8 $^+$
606	145	Thymic Lymphoma	TCR β^{int} , TCR β^+	CD4 $^+$ CD8 $^+$, CD4 $^-$ CD8 $^+$
682	100	Thymic Lymphoma	n.d.	n.d.
970	110	Thymic Lymphoma	TCR β^-	CD4 $^+$ CD8 $^+$
555	125	Enlarged Lymph Nodes and Spleen	—	—
956	114	Thymic Lymphoma	TCR β^- , TCR β^+	CD4 $^-$ CD8 $^-$
841	89	Thymic Lymphoma	TCR β^- , TCR β^+	CD4 $^+$ CD8 $^-$
839	89	Thymic Lymphoma	n.d.	n.d.
590	74	Thymic Lymphoma		CD4 $^-$ CD8 $^+$
587	97	Thymic Lymphoma	TCR β^-	CD4 $^+$ CD8 $^+$
983	103	Sarcoma	—	—
590	116	Thymic Lymphoma	TCR β^-	CD4 $^-$ CD8 $^+$
910	82	Thymic Lymphoma	TCR β^-	CD4 $^+$ CD8 $^+$
901	105	Thymic Lymphoma	TCR β^-	CD4 $^+$ CD8 $^+$
911	116	Thymic Lymphoma	n.d.	n.d.

Chapter V

ATM-dependent DNA Damage Signals Prevents Biallelic Igk Chromosome Breaks

Part of this chapter has been published in:

© Hewitt and Yin et al., 2009. *Nat. Immunol.* doi: 10.1038/ni.1735

With permission from the Nature Publishing Group

ABSTRACT

The assembly and expression of functional V(D)J rearrangements is restricted to a single allele, which ensures each lymphocyte expresses antigen receptors of a single specificity. This phenomenon, termed allelic exclusion, may be important for prevention of autoimmunity. Despite intense efforts, the mechanisms of allelic exclusion remain unclear. To explore potential roles of the general DDR machinery in the initiation of allelic exclusion, I have generated cell lines in which Igk locus recombination can be induced in G1 phase cells, and the fates of V(D)J intermediates can be tracked in G1 and during continued cell cycle progression. Although deficiency of the Artemis repair factor leads to accumulation of un-repaired IgL κ locus DNA ends, allelic exclusion is observed in Artemis-null cells. In contrast, Igk double-strand breaks are generated on both alleles in a substantial portion of ATM/Artemis double null cells. DSBs generated on both alleles can persist as chromosome breaks and/or participate in translocations, due to instability of the post-cleavage complex and defective cell cycle checkpoints conferred by ATM deficiency. These data are consistent with the notion that ATM-mediated signals emanating from DSBs generated on one Igk allele prevent initiation of V(D)J recombination at the second allele, to provide a time window to test whether the first VJ κ rearrangement is productive. ATM could orchestrate the signaling pathways enforcing allelic exclusion through its many substrates. I am examining the involvement of H2AX, p53, MDC1, 53BP1, MRE11/RAD50/NBS1 complex components, and possibly the endonuclease complex RAG1/2 that catalyzes V(D)J recombination. In addition, in vivo

model systems are being developed to explore the functions of DDR components in regulating allelic exclusion of the Igκ locus and other antigen receptor loci.

INTRODUCTION

Lymphocyte development is an ordered multi-step process that involves developmentally regulated rearrangement of the antigen receptor gene loci. In T cells, D-to-J β rearrangement occurs before V β -to-DJ β recombination, and production of the TCR β chain in DN thymocytes is necessary to drive cell proliferation and differentiation in to the DP stage, where TCR α region undergoes recombination. Similarly in B cells, at the pro-B cell stage, D_H segments are joined to J_H segments before V_H-to-DJ_H recombination. The light chain genes only rearrange after progression to the pre-B cell stage (Bassing et al., 2002a). Most mature B or T cells that arise through this development process express antigen receptors of only one specificity.

In mammals, monoallelic expression of genes can be either imprinted or random. The expressed allele of imprinted genes is usually determined in the male or female gametes through differential DNA methylation, thus these genes only express the maternal or the paternal alleles in zygotes. In contrast, random monoallelic genes are expressed from the paternal chromosome in some cells and the maternal chromosome in others. Allelic exclusion of the antigen receptor gene loci falls in the category of random monoallelic gene expression, and the mechanisms of its initiation and maintenance are poorly understood (Cedar and Bergman, 2008).

Functional allelic exclusion can be achieved at multiple levels, such as locus accessibility, DNA rearrangement, differential expression and cellular selection. In pro-B cells, the IgH loci are accessible for recombination, while the light chain loci chromatin

remain in a relatively closed conformation and thus do not undergo rearrangement even though the recombinase RAG1/2 is highly expressed. Thus, the choice of which locus undergoes rearrangement can be determined by local chromatin structures, which in turn can be regulated by cis-regulatory elements as well as lineage-specific and development stage-specific trans-acting factors. Analogously, the two homologous alleles may also be differentially epigenetically marked, and/or associate with distinct nuclear environment that determines their accessibility for the recombinase. For example, it has been suggested that the two *Igκ* alleles are differentially marked as early and late replicating alleles (Mostoslavsky et al., 2001). This regulated or deterministic model argues that in pre-B cells the early replicating allele becomes more transcriptionally accessible through DNA demethylation and thus is predisposed to rearrange first (Mostoslavsky et al., 2001). In addition, both *Igκ* alleles are localized to the center of the nucleus in pro-B cells and neither undergoes recombination; however, when cells progress to the pre-B cell stage, the late replicating allele is relocated to the repressive pericentric heterochromatin region and associate with heterochromatin protein 1 (HP1), while the early replicating allele becomes highly enriched with acetylated histones (Kosak et al., 2002; Goldmit et al., 2005; Yang et al., 2005; Fitzsimmons et al., 2007).

Once a productive rearrangement occurs on one allele, feedback signals may prevent recombination of the second allele as well as further rearrangements during later stages of B or T cell development (Jung et al., 2006). For example, the pre-BCR can send feedback signals to suppress simultaneous V_H -to- DJ_H recombination on the remaining allele. In addition, pre-BCR signaling also drives proliferation and differentiation until

the IgL rearrangements, during which further IgH rearrangements need to be suppressed. This suppression could be achieved in a number of possible ways, which are not mutually exclusive. First, feedback signals can downregulate the recombination machinery, including RAG1, RAG2 and TdT (Corcoran, 2005). Second, before IgH rearrangement in pro-B cells, outlying V regions can be brought together with DJ segments into a conformation that favors recombination. This locus “contraction”, or chromatin looping, occurs monoallelically when visualized by 3D FISH (Roldan et al., 2005). Importantly, feedback signals can reverse or prevent looping in a process called “decontraction” (Skok et al., 2007). Third, relocalization of alleles to repressive nuclear periphery or pericentromeric heterochromatic regions is also associated with feedback signaling (Skok et al., 2007). Both chromatin contraction and allele relocalization are likely associated with epigenetic changes of chromatin, but how these changes are initiated and regulated are not fully understood.

Although V(D)J recombination is widely recognized as a physiological DNA damage response, surprisingly, the possibility of DNA damage signals in coordinating bi-allelic V(D)J recombination has never been explored. Intuitively, this intra-nucleus suppressive signal would work faster than the feedback signal following productive rearrangement on one allele. Here, I attempt to uncover roles of the DDR machinery in allelic exclusion. If my hypothesis is true, DNA damage signals emanating from one rearranging allele might prevent initiation of V(D)J recombination on the second allele, providing a time window to test whether the first rearrangement is functional before feedback signals from the cell surface receptors are available.

RESULTS

ATM prevents biallelic RAG-mediated cleavage

Treatment of v-Abl-transformed (Abl) pre-B cell lines deficient in nonhomologous end-joining with the Abl kinase inhibitor STI571 leads to G1 arrest, expression of *Rag1* and *Rag2* and accumulation of unrepaired RAG-generated breaks, which activate ATM-dependent signals. To directly evaluate whether ATM prevents biallelic RAG-mediated cleavage, I treated *Rag2*^{-/-}, *Artemis*^{-/-} and *Artemis*^{-/-}*Atm*^{-/-} cells for 1-7 days with STI571 and analyzed the Igκ locus by Southern blot of DNA isolated from these cells (Figure 22A). Artemis is a nonhomologous end-joining factor required for opening coding ends so that RAG-generated DSBs are repaired. The germline Jκ band was retained in the control *Rag2*^{-/-} cells, whereas in *Artemis*^{-/-} cells, I found 30-50% less of the germline Jκ band and correspondingly more Jκ coding-end bands (Figure 22A). These data demonstrate that RAG-mediated cleavage occurred on half of the Igκ alleles in these cells. In contrast, I found 80% less of the germline Jκ band and correspondingly more Jκ coding-end bands in *Artemis*^{-/-}*Atm*^{-/-} cells, which indicated that RAG-mediated cleavage occurred on more than half of the Igκ alleles in these cells (Figure 22A). I obtained similar results with independently derived cell lines. These data suggest that cleavage activates ATM signals that prevent RAG-mediated cleavage of the other Igκ allele until nonhomologous end-joining-mediated formation of VκJκ coding joints.

ATM prevents the biallelic dissociation of *Igκ* coding ends and biallelic chromosome breaks or translocations

During V(D)J recombination, ATM maintains coding ends in repair complexes and prevents RAG-initiated genomic instability (Bredemeyer et al., 2006). To investigate whether ATM prevents the biallelic dissociation of *Igκ* coding ends and biallelic chromosome breaks or translocations involving *Igκ*, I did two-color DNA FISH with the 5' V κ BAC RP24-243E11 probe and the 3' C κ BAC RP23-341D5 probe on G1 nuclei prepared from STI57-treated *Artemis*^{-/-} pre-B cells also deficient in the tumor suppressor p53 and *Artemis*^{-/-}*Atm*^{-/-} pre-B cells (Figure 22B). I used *Artemis*^{-/-}*p53*^{-/-} cells rather than *Artemis*^{-/-} cells so that the ATM/p53-dependent G1/S checkpoint was impaired, as in *Artemis*^{-/-}*Atm*^{-/-} cells. I found coincident (< 1.0 μ m) probe signals on both alleles in 85% of *Artemis*^{-/-}*p53*^{-/-} nuclei, with noncoincident probe signals on one allele in 15% and both alleles in less than 1% of nuclei (Figure 22B). I found coincident probe signals on both alleles in 50% of *Artemis*^{-/-}*Atm*^{-/-} nuclei, with noncoincident probe signals on one allele in 41% and on both alleles in 10% of nuclei (Figure 22B). The difference between noncoincident signals in 1% of *Artemis*^{-/-}*p53*^{-/-} nuclei and 10% of *Artemis*^{-/-}*Atm*^{-/-} nuclei was statistically significant ($p = 0.005$). Next I did FISH with the V κ and C κ BACs and a chromosome-6 'paint' on metaphase spreads prepared from untreated cells or cells that had been released back into cycle by removal of STI571. I found chromosome-6 translocations in less than 3% of metaphases prepared from untreated cells (data not shown). I found RAG-induced *Igκ* chromosome breaks or translocations in 4% of *Artemis*^{-/-}*p53*^{-/-} cells, whereby lesions arose from a single *Igκ* allele (Figure 22C). In contrast, I found *Igκ* chromosome breaks or translocations in 66% of *Artemis*^{-/-}*Atm*^{-/-} cells, with 30% of cells containing lesions arising from both *Igκ* alleles (Figure 22C). The

difference between the absence of biallelic *Igκ* abnormalities in *Artemis*^{-/-}*p53*^{-/-} nuclei and 30% of *Artemis*^{-/-}*Atm*^{-/-} nuclei was statistically significant ($p = 0.004$). Collectively, these data demonstrate that ATM regulates monoallelic RAG-mediated cleavage of homologous *Igκ* loci to prevent biallelic V(D)J recombination.

No single ATM substrates tested fully recapitulates the *Atm*^{-/-} phenotype

ATM is a versatile kinase that has many known and potentially even more unknown substrates (Matsuoka et al., 2007). To delineate which substrates mediate the ATM-dependent signals in restricting recombination to only one allele, I took a candidate approach and tested several well-established ATM substrates. These factors include: the major phospho-H2AX epitope binding protein in mammalian cells, MDC1; NBS1, a component of the MRN complex, which can function both upstream and downstream of ATM; and the methylated histone binding protein 53BP1. Since *Nbs1*^{-/-} mice are early embryonic lethal, a mutant NBS1 allele *Nbs1*^{m/m} was used to generate *Artemis*^{-/-}*Nbs1*^{m/m} Abelson cell lines (Kang et al., 2002); all other *Artemis*^{-/-} cells were generated from crosses of germ line deficient mice. I analyzed the *Igκ* locus by Southern blot of DNA isolated from *Artemis*^{-/-}*Mdc1*^{-/-}, *Artemis*^{-/-}*Nbs1*^{m/m}, and *Artemis*^{-/-}*53bp1*^{-/-} cells treated for 1-7 days with STI571. In three independent *Artemis*^{-/-}*Mdc1*^{-/-} and *Artemis*^{-/-}*53bp1*^{-/-} lines each, and one *Artemis*^{-/-}*Nbs1*^{m/m} line, I found the *Igκ* germ line band intensity decreased to around 50% of that of the untreated cells (Figure 23). Although in the cases of *Artemis*^{-/-}*Nbs1*^{m/m} and *Artemis*^{-/-}*53bp1*^{-/-} cells, the remaining germ line band intensity could be slightly less than 50% of control, none of three genotypes of cells fully recapitulated the >80% loss of the germline *Igκ* band in *Artemis*^{-/-}*Atm*^{-/-} cells (Figure

23). Since at 96 hours in STI571 treatment, none of *Artemis*^{-/-}*H2ax*^{-/-} lines resembled *Artemis*^{-/-}*Atm*^{-/-} lines in the loss of germ line band, it is unlikely that H2AX is the sole factor that mediates ATM-dependent DDR signal to prevent bi-allelic Igκ cleavage.

DISCUSSION

In this chapter, I took advantage of the inducible V(D)J recombination system, created persistent DNA DSBs on one of the two Igk alleles using *Artemis*^{-/-} cells, and assayed the recombination status of the remaining allele. Although the prolonged G1 arrest in Abelson cells treated with STI571 resembles the G0/G1 phase of slowly cycling immature lymphocytes, the *Rag1/Rag2* genes are continuously expressed while primary lymphocytes may turn off the recombinase expression periodically, thus restrict its cutting on one allele instead of two. In addition, DNA damage signals emanating from one rearranging allele of the antigen receptor loci in vivo may be too transient to regulate RAG-cleavage on the other allele.

Expression of two different BCRs/TCRs by one cell (dual receptor) is a potential mechanism underlying autoimmunity. Since loss of ATM allows biallelic RAG-induced cleavage, in theory, ATM-deficiency in mice and humans should allow two potentially productive antigen receptor rearrangements, one on each allele. No overt autoimmune symptoms have been observed in young *Atm*^{-/-} mice, and work from our lab has shown *IgH* allelic exclusion is maintained in *Atm*^{-/-} mice containing allotypically marked *IgH* alleles by flow cytometry analysis of surface and cytoplasmic IgH expression (Hewitt et al., 2009). However, *Atm*^{-/-} mice die from aggressive thymic lymphomas by the age of 5 months, preventing the study of autoimmunity that might develop in aged *Atm*^{-/-} mice. In addition, recently deficiency in ATM was found to lead to attrition of naive T cells and an autoimmune-biased T cell repertoire in rheumatoid arthritis (RA) (Shao et al., 2009). Thus, how relevant is dual receptor production to autoimmune diseases such as RA

remains to be determined, and whether ATM contributes to the suppression of TCR β and Ig κ allelic inclusion in vivo and subsequent development of autoimmunity is still an open question.

Although there is not yet direct evidence linking my results to autoimmune diseases, the implications to the maintenance of genomic stability is more apparent. In experiments where large, often times overwhelming, dosages of DNA damage were used, the role of ATM signaling from one break to suppress break induction at other genomic loci was never observed. Nonetheless, ATM-dependent phosphorylation of KAP-1 is essential for the localized and genome-wide chromatin decondensation, which is particularly important for heterochromatic DNA DSB repair (Ziv et al., 2006; Goodarzi et al., 2008), suggesting ATM-mediated DNA damage signals may alter chromatin dynamics to coordinate break repair. Furthermore, my result provides the first evident that at physiological DNA damage levels (1-2 breaks per cell), ATM signaling also coordinates break induction on homologous Ig alleles. Moreover, a recent report suggests that ATM-dependent mechanisms may also orchestrate break induction and repair on different antigen receptor gene loci. T cell progenitors frequently rearrange the IgH D_H and J_H segments, although V_H to DJ_H recombination is restricted to B cells. Thus in wild type mice, rearranging IgH locus may activate ATM to forestall simultaneous TCR α/δ rearrangement, or vice versa; in contrast, *Atm*^{-/-} lymphocytes may accumulate unrepaired IgH and TCR α/δ breaks within the same cells where chimeric IgH/TCR α/δ translocations can form. An increase in potential chimeric TCR γ /TCR α/δ translocations was also observed in this study (Callén et al., 2009). Crosstalk between different

rearranging antigen receptor loci through ATM-dependent mechanisms might better explain why clonal translocations that juxtapose IgH and TCR α/δ loci are frequently seen in *Atm*^{-/-} mice thymic lymphomas as well as lymphoid malignancies from A-T patients.

The mechanisms by which different genomic loci cross talk through ATM signaling are largely unknown. Based on recent reports highlighting ATM functions in genomic relaxation after break induction and in heterochromatic DNA break repair, it is possible that ATM alters the global nuclear heterochromatin landscape or localization of antigen receptor gene loci relative to repressive or permissive nuclear compartments, the latter of which has been suggested by 3D FISH experiments examining the Ig loci nuclear dynamics during lymphocyte development. In addition to these more general mechanisms, it was proposed that the two homologous immunoglobulin loci could undergo RAG1-mediate homologous pairing, and the physical proximity may contribute to the coordinated rearrangement. Importantly, both RAG1/2 are putative ATM substrates and their phosphorylation status may control the degradation, deposition and activity of the recombinase machinery. Last but not least, it remains possible that the multiple ATM substrates, such as NBS1 and 53BP1, among many others, collectively mediate the ATM function in a redundant manner to ensure mono-allelic recombination.

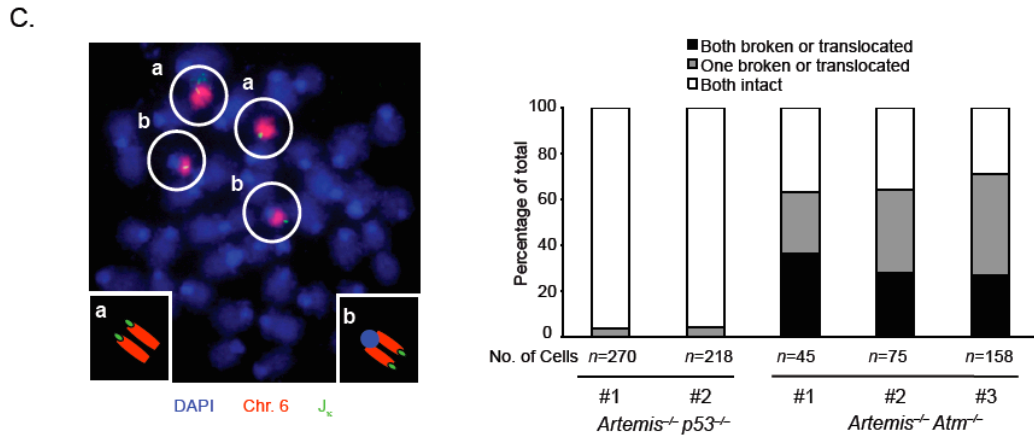
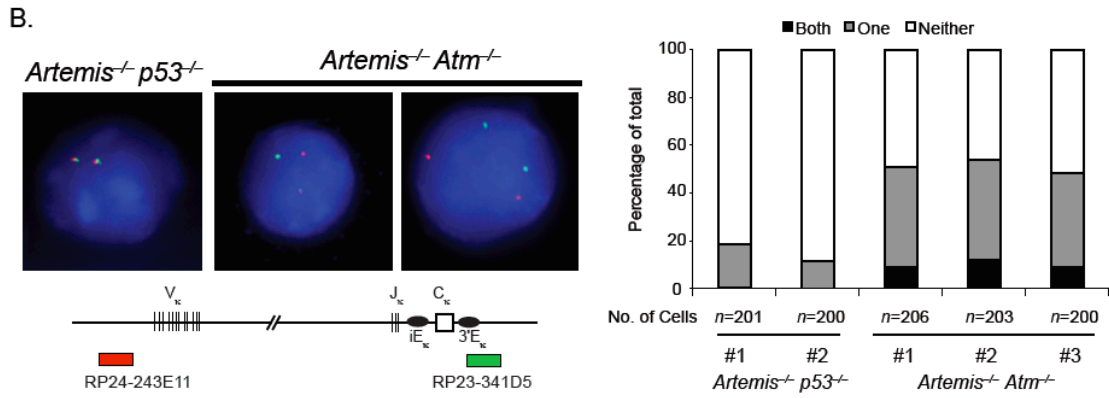
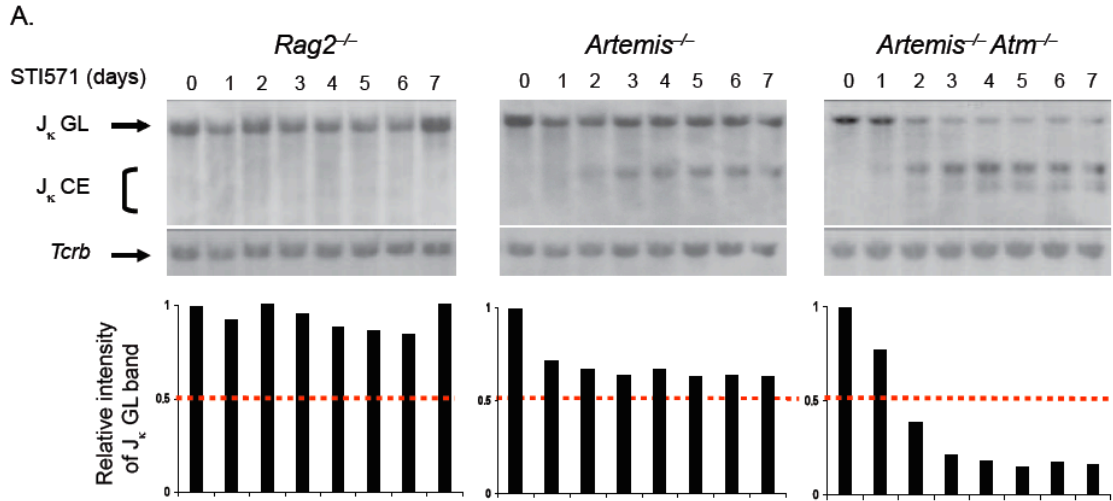


Figure 22. ATM prevents the biallelic cleavage and dissociation of *Igκ* coding ends and biallelic chromosome breaks or translocations. **A)** Southern blot analysis of the *Igκ* locus of *Bam*HI-digested genomic DNA isolated from *Rag2*^{-/-}, *Artemis*^{-/-} and *Artemis*^{-/-} *Atm*^{-/-} Abelson pre-B cell lines treated with STI571 (time, above lanes). Top, hybridization to a 3' Jκ probe; arrows and bracket (left margin), bands corresponding to germline *Igκ* (Jκ GL) and unrepaired Jκ coding ends (Jκ CE). Below, blots stripped and rehybridized to a probe for the *Tcrβ* locus (loading and normalization control). Bottom, RAG-mediated *Igκ* cutting, presented as the intensity of the germline Jκ band relative to that of the *Tcrβ* band. **B)** RAG-induced *Igκ* genomic instability during V(D)J recombination in pre-B cell lines. Left, light microscopy of two-color FISH of G1-phase nuclei of STI571-treated *Artemis*^{-/-} *p53*^{-/-} and *Artemis*^{-/-} *Atm*^{-/-} pre-B cells with a 5' Vκ BAC (red) and 3' Cκ BAC (green), and the DNA-intercalating dye DAPI to visualize DNA. Right, *Artemis*^{-/-} *p53*^{-/-} and *Artemis*^{-/-} *Atm*^{-/-} pre-B cells with coincident (< 1.0 μm) and noncoincident (> 1.0 μm) hybridization of the 5' Vκ and 3' Cκ signals. Both, FISH signals separate on both *Igκ* alleles; One, FISH signals separate on only one *Igκ* allele; Neither, FISH signals coincide on both *Igκ* alleles. *P* = 0.005, *Artemis*^{-/-} *p53*^{-/-} and *Artemis*^{-/-} *Atm*^{-/-} pre-B cells with separated signals on both alleles (Student's equal variation). **C)** RAG-induced *Igκ* chromosome breaks or translocations during V(D)J recombination in pre-B cell lines. Left, light microscopy of painting of whole chromosome 6 (red) and FISH analysis of metaphases prepared from STI571-treated and released *Artemis*^{-/-} *Atm*^{-/-} pre-B cells, stained with the 5' Vκ and 3' Cκ BACs (green) and DAPI (blue). Insets (bottom left and right), chromosomes fragments broken at the *Igκ* locus; main image, B outlines the two centromeric fragments and A outlines the two

telomeric fragments. Right, pre-B cell lines with *Igκ* chromosome breaks or translocations on one or both copies of chromosome 6. Original magnification, × 1,000 **B)** or × 600 **C)**. Exp, experiment number. Data are representative of at least three independent experiments.

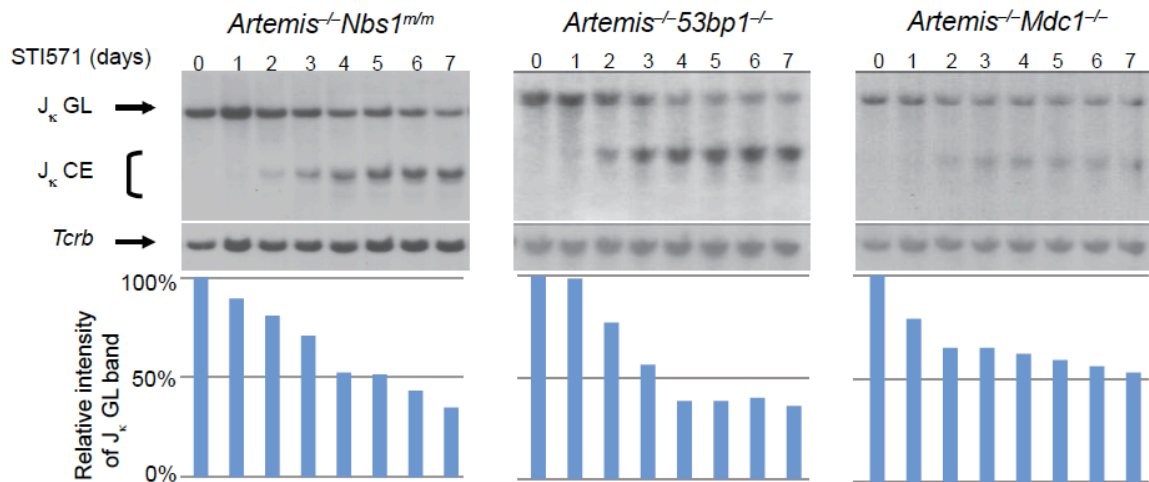


Figure 23. No single ATM substrates tested fully recapitulates the *Atm*^{-/-} phenotype.

Southern blot analysis of the Ig κ locus of *Bam*HI-digested genomic DNA isolated from *Artemis*^{-/-}*Nbs1*^{m/m}, *Artemis*^{-/-}*53bp1*^{-/-} and *Artemis*^{-/-}*Mdc1*^{-/-} Abelson pre-B cell lines treated with STI571 (time, above lanes). Top, hybridization to a 3' J κ probe; arrows and bracket (left margin), bands corresponding to germline J κ (GL) and unrepaired J κ coding ends (J κ CE). Below, blots stripped and re-hybridized to a probe for the *Tcr β* locus (loading and normalization control). Bottom, RAG-mediated Ig κ cutting, presented as the intensity of the germline J κ band relative to that of the *Tcr β* band.

Chapter VI
Summary and Discussion

Highly sophisticated and often redundant DNA damage surveillance and repair mechanisms evolved very early in life since they are at work even in present day prokaryotic cells. It is suggested that V(D)J recombination may have evolved from an ancient transposable DNA element (Zhou et al., 2004), therefore DNA damage response and repair is an integral part of this genetically programmed antigen receptor diversification process in developing lymphocytes of higher organisms. In the previous chapters, I have utilized V(D)J recombination as a model system for physiological DNA double strand break repair, and elucidated novel mechanisms by which the chromatin component histone H2AX and the chromatin-associated kinase ATM coordinately regulate the recombination reaction, maintain lymphocyte genomic stability and suppress lymphoma predisposition. I will conclude by discussing important unanswered questions, and the implications of the novel functions of H2AX and ATM in the context of general cellular DNA damage response and cancer progression.

Is the DNA strand zipping function of H2AX dependent on Ser139 phosphorylation?

By using either germ line or conditional H2AX-deficient lymphocytes, I have demonstrated that while H2AX is not essential for the NHEJ repair of chromosomally integrated substrates, it is necessary to suppress irreversible separation of RAG-cleaved un-repaired DNA strands in G1 phase Abelson cells. Consistent with the increase in end separation, loss of H2AX protein also allows more antigen receptor loci chromosome breaks and translocations to form during continued cell proliferation. In vivo, H2AX also suppresses formation of chromosome breaks emanating from un-repaired TCR α/δ loci. Based on the observation that large γ H2AX domains flank the DSB sites but are absent at

the cleaved DNA ends, I propose that γ H2AX and associated factors can zip the flanking chromatin within the higher order chromatin structure to promote positional proximity of the un-repaired DNA ends. In addition to being phosphorylated, H2AX also becomes acetylated by the acetyltransferase Tip60 and ubiquitylated by the E3 ubiquitin ligases RNF8 and RNF168 following DSB induction (van Attikum and Gasser, 2009). Moreover, the C-terminal Tyr142 was recently identified as a phosphorylation site; Tyr142 is phosphorylated before DNA damage, and its dephosphorylation precedes and is required for Ser139 phosphorylation upon break induction (Xiao et al., 2009; Cook et al., 2009). Although current evidences suggest that both Tip60 and RNF8/RNF168 function downstream of γ H2AX formation, Tyr142 phosphorylation can clearly recruit the pro-apoptotic kinase JNK1 independent of Ser139 phosphorylation. Thus, it remains to be determined whether H2AX Ser139 phosphorylation is the primary event that contributes to H2AX's end stabilization role. To this end, mice and Abelson cells with non-phosphorylatable 139S->A mutations, or phosphorylation mimicking 139S->E/D mutations would be needed.

Is there functional redundancy among RAGs, ATM and H2AX in end stabilization?

H2ax^{-/-} cells exhibit increased sensitivity to agents that induce DSBs, elevated levels of spontaneous genomic instability, and defective NHEJ and HR repair of chromosomal DSBs. In particular, about 50% of stimulated *H2ax*^{-/-} splenic T cells exhibit spontaneous chromosome abbreviations, including about equal numbers of pre-replicative chromosome breaks and post-replicative chromatid breaks. In addition, *H2ax*^{-/-} B cells are severely defective in CSR when stimulated in vitro, since H2AX is

required for long-range switch region synapsis and to prevent AID-dependent DNA breaks from progressing into chromosome breaks/translocations. In postreplicative repair, γ H2AX domain formation also allows binding of the cohesin machinery that is necessary for sister chromatid cohesion to ensure proper homologous recombination. Therefore, H2AX is clearly important for general DSB repair and the observation that V(D)J recombination is not affected in *H2ax*^{-/-} Abelson cells came as a surprise. V(D)J recombination NHEJ is unique in that both RAG proteins bind DNA and form a large protein complex that can accommodate and shepherd the DSB intermediates during the joining step. Moreover, the RAG1/2 complex may also cooperate with other DDR mediators and effectors, such as ATM/MRN and DNA-PK, and together form a larger complex to tether cleavage DNA ends and funnel them into NHEJ, thus diminishing the need for γ H2AX domains to zip the flanking chromatin. If this is the case, RAG1 K980A and RAG1 R838A/K839A/R840A mutants that display joining defects due to unstable post-cleavage complexes could be used to uncover the role of H2AX (Lee et al., 2004). Furthermore, NHEJ products by these two RAG1 mutations are characterized by short sequence homologies and excessive deletions, indicative of an alternative NHEJ repair. NBS1 is required for alternative NHEJ of hairpin coding ends and promotes proper resolution of inversional recombination intermediates, but which other factors are involved has not been determined. By preventing irreversible separation of the DNA ends released from the unstable post-synaptic complex, H2AX may also be important for the alternative NHEJ pathways.

In addition, the RING domain of RAG1 has been shown to bind to and mono-ubiquitylate histone H3 and this ubiquitin ligase activity of RAG1 is important for V(D)J recombination efficiency both in vitro and in vivo (Grazini et al., 2010). Since at general double strand breaks, H2AX and H2A have been shown to be ubiquitylated by RNF8 and this ubiquitylation signal is further amplified by RNF168, it would be curious to determine the spatial and stoichiometric relationship between these two types of histone modifications around RAG-induced DSBs, and their relative contributions to V(D)J recombination efficiency.

Does γ H2AX recruit cohesin-like complexes to regulate V(D)J recombination?

In yeast, phosphorylation of the H2AX homologue at S/G2 phase DSBs promotes re-localization of cohesins around broken DNA ends. This process is likely important for stabilizing broken DNA strands along the undamaged sister chromatid, shuttling DNA ends away from SSA into SCR and preventing chromatid breaks. Recently it was found that cohesin is recruited to CCCTC-binding factor (CTCF) sites throughout immunoglobulin loci during B lymphocyte development in a developmental stage-specific manner (Degner et al., 2009). CTCF is a transcription factor that regulates gene expression by long-range chromosomal looping. The differential binding of cohesin to CTCF sites may promote formation of multiple loops and thus effective V(D)J recombination. It is important to note that even in wild type Abelson cells induced to undergo Igk recombination, large γ H2AX chromatin domains form around the breaks as assayed by ChIP, albeit the amplitude is lower than those in *Artemis*^{-/-} cells (Savić et al., 2009). Based on these evidences, I hypothesize that in the G0/G1 phase of cycling

immature lymphocytes, γ H2AX domains formed around rearranging antigen receptor loci may recruit the cohesins or similar complexes to tether the flanking chromatin in proximity. The chromatin “zipping” may or may not coincide with the cohesin-CTCF-mediated chromatin looping. One intriguing possibility is that the developmental stage-regulated chromatin looping can position the V, D, and J segments in a pattern that facilitates RAG deposition, cleavage and γ H2AX chromatin zipper formation.

Do other DDR factors have structural functions similar to H2AX?

In a current model, γ H2AX is central for the propagation of DDR factors along chromatin and amplification of DNA damage signals. The hierarchal assembly of factors in chromatin around DSBs can be illustrated by the observations that H2AX is required for normal DSB-induced foci of MDC1, RNF8/RNF168, 53BP1, and BRCA1; MDC1 is required for normal DSB-induced foci of RNF8/RNF168, 53BP1, and BRCA1; whereas, RNF8 is required for normal DSB-induced foci of RNF168, 53BP1 and BRCA1. Recent reports suggest that MDC1 is the major γ H2AX-binding protein in mammals, and MDC1 mediates chromatin retention of at least two groups of proteins: NBS1-containing complex (MRN) and RNF8-containing complexes. The RNF8-containing complexes may include RNF168, BRAC1/Rap80, and 53BP1, all of which involve the ubiquitin pathway (Stewart, 2009). The MRN components have been shown to function in the same pathway as ATM during NHEJ of RAG-induced breaks, but none of the other aforementioned factors have been characterized as to their involvement in the NHEJ pathway. First, given the intrinsic complexity and diversity of protein functions, it is of great interest to examine the NHEJ roles of the individual factors in G1-arrested Abelson

cells. Based on phenotypes of mutant mice and known molecular interactions, I anticipate MDC1 and 53BP1 loss to phenocopy H2AX deficiency. Although 53BP1 or MDC1 might not be critical for chromosomal end joining *per se*, given their presence in DNA damage foci and the ability of 53BP1 to oligomerize (Zgheib et al., 2009), it could be critical for end stability and suppression of translocations when un-repaired breaks persist in G1 phase or beyond. To test this hypothesis, *Artemis*^{-/-} *53bp1*^{-/-} *p53*^{-/-} and *Artemis*^{-/-} *Mdc1*^{-/-} *p53*^{-/-} Abelson cells may be utilized as described for studying H2AX functions in Chapter II. Consistent with a possible role of 53BP1 in NHEJ, it was recently found that 53BP1 is required for usage of distal V gene rearrangements by promoting chromatin dynamics, and loss of 53BP1 protein leads to increased antigen receptor loci DNA end degradation and micro-homology mediated repair instead of normal NHEJ.

Does H2AX function in signaling cell cycle checkpoint activation and cell death?

Although *H2ax*^{-/-} cells display normal activation of cell cycle checkpoints and apoptotic responses upon induction of large numbers of DSBs, *H2ax*^{-/-} cells are defective in the G2/M checkpoint following induction of only a few DSBs, possibly due to an inability to assemble signaling complexes in chromatin around DSBs and amplify DDR signals. In addition, when induced to undergo V(D)J recombination, *Artemis*^{-/-} *H2ax*^{-/-} Abelson cells fail to upregulate the anti-apoptotic factors such as Pim2 and Bcl3 as robustly as *Artemis*^{-/-} cells. If this mechanism holds true in primary T cells in vivo, it can at least in part explain the delayed tumor development in *LAHP* than in *LAP* mice, as well as the altered pattern of genomic instability (Figure 24).

One potentially relevant signaling pathway is the mitogen-activated protein kinase (MAPK) p38 pathway. ATM and ATR Ser/Thr protein kinases orchestrate multiple aspects of the DNA damage response via phosphorylation of effectors such as Chk1 and Chk2 protein kinases. MAPK p38 also regulates cell cycle checkpoints in response to DNA damage. The p38-mediated G2/M checkpoint mechanism is essential to prevent catastrophic mitosis entry in the absence of p53 (Reinhardt et al., 2007). MAPK p38 directly phosphorylates and activates MK2, which, like Chk1 and Chk2, phosphorylates and inactivates Cdc25B and Cdc25C, thus preventing cell cycle progression. However, how p38 is activated by DNA damage is not known, although ATM/ATR might directly phosphorylate and activate the thousand and one amino acid (TAO) kinases, leading to p38 activation down the cascade (Raman et al., 2007). Curiously, mice lacking either H2AX or 53BP1, but not Chk2, manifest a G2/M checkpoint defect close to that observed in *Atm*^{-/-} cells after exposure to low, but not high, doses of IR. In V(D)J recombination the amount of DNA damage is analogous to low doses of IR. In DN3 thymocytes, activation of p38 leads to the phosphorylation and accumulation of p53, resulting in the G2/M checkpoint induction. Thus, it is important to test whether RAG-generated breaks can activate p38 and whether H2AX is required for this checkpoint activation.

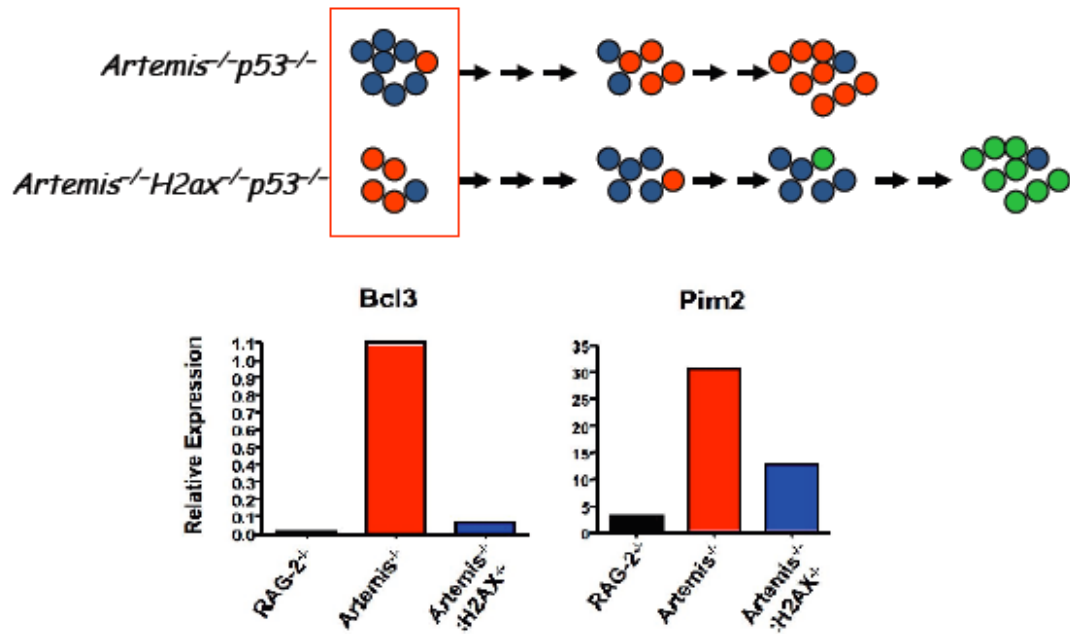


Figure 24. Proposed model to explain delayed tumor development in *LAHP* mice

compared to *LAP* mice. Upper panel, bi-allelic deletion of H2AX results in higher

percentages of thymocytes with un-repaired TCR α/δ locus chromosome breaks (cells

shown in red). However, the survival of thymocytes with persistent un-repaired breaks is

compromised in the absence of H2AX, thus during subsequent transformation *LAP* mice

succumb to tumors with clonal TCR α/δ locus chromosome translocations faster than

LAHP mice. Instead, *LAHP* thymocytes need to acquire other oncogenic hits (cells shown

in green) to be fully transformed. Lower panel, *Artemis*^{-/-}*H2ax*^{-/-} Abelson cells fail to

upregulate the anti-apoptotic factors such as Pim2 and Bcl3 as robustly as *Artemis*^{-/-}

cells.

Concluding Remarks

DSBs could be resolved as oncogenic chromosome breaks or translocations if improperly repaired. Yet DSBs are purposely induced within G1 phase of the cell cycle by the site-specific RAG1/2 endonuclease complex during V(D)J recombination, and subsequently repaired to generate the large repertoire of antigen receptor specificities. In mice, both the core histone variant H2AX and kinase ATM are required for proper DSB repair, maintenance of genomic stability, and suppression of tumors, including lymphomas with translocations involving the antigen receptor loci. ATM and H2AX are also required for checkpoint activation in response to low doses of IR, which is similar to the amount of DNA damage during V(D)J recombination. In this thesis, I have elucidated that H2AX, in collaboration with ATM, maintains genomic stability in developing lymphocytes by holding RAG-generated DNA ends in proximity to facilitate repair. In addition, H2AX may have additional functions in signaling to checkpoint activation and/or cell death to coordinate the timing of DSB repair and cell cycle progression. My results suggest that H2AX functions in lymphoma suppression may depend on the cellular context. Moreover, I have uncovered a novel function of the extensively studied kinase ATM in regulating mono-allelic V(D)J recombination of the immunoglobulin loci. My results provide the first evidence that DNA damage signals mediated by ATM can contribute to the long-standing question of the initiation and maintenance of allelic exclusion. Future efforts would include developing corresponding animal models to test whether the mechanisms that I discovered in cell line based systems hold true in vivo, and whether they can be exploited in prevention and therapies for diseases such as cancer and autoimmune diseases.

Chapter VII
Materials and Methods

Mice

All mice were bred and maintained under specific pathogen-free conditions within the Laboratory Animal Facility of the Children's Hospital of Philadelphia. All mouse experiments were performed in accordance with relevant institutional and national regulations and guidelines and were approved by the Children's Hospital of Philadelphia Institutional Animal Care and Use Committee. $H2ax^{-/-}$, $H2ax^{F/F}$, $Artemis^{-/-}$, $p53^{F/F}$, $Lck-Cre$ transgene, and $E\mu-Bcl-2$ transgene mice were previously described (Strasser et al., 1991; Jonkers et al., 2001; Lee et al., 2001; Bassing et al., 2002b, 2003; Rooney et al., 2002). Generation of the $Lck-CreH2ax^{F/F}p53^{F/F}$, $Lck-CreArtemis^{-/-}p53^{F/F}$ and $Lck-CreArtemis^{-/-}H2ax^{F/F}p53^{F/F}$ mice were performed on the 129SvEv background.

Flow Cytometry

Single cell suspensions from primary thymuses and spleens of 4-6 week old mice or thymic lymphomas when they arose were stained with antibodies in PBS with 2% FBS. For analyses of CD4, CD8, and TCR β expression, cells were stained with FITC-conjugated anti-TCR β , PE-conjugated anti-CD8, and APC-conjugated anti-CD4 (BD Pharmingen). For analyses of DN thymocyte subsets, cells were stained with a mixture of PE-conjugated antibodies for TCR β , TCR δ , CD8 α , CD45R, CD19, CD11c, CD11b, Ter119, and NK1.1, as well as PE-Cy7-conjugated anti-CD25 and allophycocyanin-conjugated anti-c-kit antibodies (BD Pharmingen). Data was acquired on a FACSCalibur (BD Biosciences, San Jose, CA) using CellQuest software (BD Biosciences) and analyzed using FlowJo software (Tree Star).

Generation and culture of abl pre-B cell lines

Bone marrow from 3-5 week-old $H2ax^{-/-}$, $H2ax^{F/F}$, $H2ax^{F/F}p53^{F/F}$, $Artemis^{-/-}H2ax^{F/F}$, $Artemis^{-/-}p53^{F/F}$, or $Artemis^{-/-}H2ax^{F/F}p53^{F/F}$ mice harboring the $E\mu$ -Bcl-2 transgene were cultured and infected with the pMSCV v-abl retrovirus to generate abl pre-B cell lines of each genotype as previously described (Bredemeyer et al., 2006). Generation of the $Artemis^{-/-}Rag2^{-/-}$ abl pre-B cells was previously described (Savić et al., 2009). $H2ax^{-/-}$, $H2ax^{F/F}$, $H2ax^{F/F}p53^{F/F}$ and $Artemis^{-/-}H2ax^{F/F}$ abl pre-B cells (10^6 /mL) were transduced with pMX-DEL^{CJ} retroviral recombination substrate by co-centrifugation at 1800 rpm for 90 minutes. Limiting dilution into 96 well plates and Southern blot analysis was used to isolate clonal cell lines with single pMX-DEJ^{CJ} integrants. Cells were treated with 3 μ M STI571 for the indicated times at a density of 10^6 cells/ml. For STI571 release experiments, cells were collected, washed, and then plated into media without STI571 and cultured for approximately 10-14 days prior to metaphase preparation.

Southern blot analysis

Genomic DNA (20-30 μ g) of Abelson cells, primary thymocytes, tumors, or kidney controls was digested with 100 units of the indicated restriction enzymes (New England Biolabs). Digested DNA was separated on a 1.0% TAE agarose gel, transferred onto Zeta-probe membrane (BioRad), and hybridized with ³²P-labeled DNA probes as previously described (Sleckman et al., 1997). The Southern blot probes used are as follows: C4 probe for pMX-DEL^{CJ}, the 3' Jk probe for Igk loci, and a TCR β VDJ probe for loading control (Bassing et al., 2000; Bredemeyer et al., 2006; Helmink et al., 2009). The extent of Jk cleavage was calculated by the following formula:

$$\text{Percentage of J}\kappa \text{ Cleavage} = \left[1 - \left(\frac{\text{Ig}\kappa \text{ GL}^{+\text{STI}}}{\text{TCR}\beta \text{ GL}^{+\text{STI}}} \right) \middle/ \left(\frac{\text{Ig}\kappa \text{ GL}^{-\text{STI}}}{\text{TCR}\beta \text{ GL}^{-\text{STI}}} \right) \right] \times 100\%$$

where the Ig κ germline hybridization intensity using the 3' J κ probe before or after STI571 treatment (Ig κ GL^{-STI} and Ig κ GL^{+STI}, respectively) was normalized to the corresponding TCR β germline hybridization intensity using the VDJ probe (TCR β GL^{-STI} and TCR β GL^{+STI}, respectively). The H2AX probe was generated via PCR with primers 5'-CTCTGGATCCCGTAGAGGGCAGAAGG-3' and 5'-GCGCGGATCCTGATTTCAAACTGTATGCCAGGG-3'. The p53 probe has previously been described (Jonkers et al., 2001). The 3'*J* β 1 and 3'*J* β 2 probes have been previously described (Khor and Sleckman, 2005).

Western Blot Analysis

Lysates of primary thymocytes were prepared as previously described (Savić et al., 2009). Samples were separated on a denaturing SDS gel and transferred to Immobilon membrane (Millipore). Membranes were first incubated with an anti-H2AX antibody (Upstate Biotech) in 5% milk overnight, the same membrane were then stripped and probed in the same manner with an anti-tubulin antibody (Fischer 05829MI) as a loading control. Western blots were visualized as previously described (Bassing et al., 2008).

Chromatin immunoprecipitation

All data points represent average values with standard deviation error bars obtained from experiments conducted three times on cells of two independently derived *Artemis*^{-/-} pre-B cell lines. ChIP assays were conducted and data analyzed exactly as described previously

(Savić et al., 2009). The sequences of the primers used for qPCR analysis of each genomic location relative to Jk1 were either described (Savić et al., 2009) are as follows: -250 kb, 5'-CCATCATCAGAACCCAGCATT-3' and 5'-GCCCTTCTTGACATCCTCTATCA-3'; -650 kb, 5'AATGGCACAATCCTAGAGGTACAAG-3' and 5'-CCCTGCTGACTCACTCTCACAT-3'; -1 Mb, 5' GACCCAAAGAAACAAAACAAT AAGG-3' and 5'-CCCCATCCCCCTCCTAGTT-3'; -1.3 Mb, 5'-AAATGGACATCTTACCGAA AGCA-3' and 5'-CCTGGGTTTCTTGTTATTCCAAA-3'; -1.6 Mb, 5'-AGCCAGGTTGGATGT GCTATAAA-3' and 5'-CACCCAGTCTCCAGCAATCA-3'.

Cytogenetic analyses

Kits for spectral karyotyping (SKY) and whole chromosome painting were used for metaphase analysis according to manufacturers' instructions (Applied Spectral Imaging, Vista, CA). BAC FISH probes were labeled with Biotin (Biotin-Nick Translation Mix, Roche), and were applied to G1 phase nuclei or metaphase spreads prepared as previously described (Hewitt et al., 2009). The 5' V κ (RP24-243E11) and 3' C κ (RP23-341D5) BACs used for 2C-FISH analysis were previously described (Hewitt et al., 2009). The TCRC β -164G11, TCRV β 17a-23N16, TCRC α -232F19, TCRV δ 3/V α 6-46G9, and 5'IgH BAC207 BACs used for FISH analysis of translocations in primary thymocytes were previously described (Liyanage et al., 2000; Franco et al., 2006). The *c-myc* BAC 454G15 was a gift from Dr. Kevin D. Mills, The Jackson Laboratory. All images were

captured and analyzed on a SKY workstation using Case Data Manager Version 5.5, installed and configured by Applied Spectral Imaging. The 2C-FISH experiments to assay for DSB positional stability were conducted independently on three different lines of *Rag2^{-/-}*, *Artemis^{-/-}*, and *Artemis^{-/-}H2ax^{-/-}* abl pre-B cells. To avoid observer bias, these data of these experiments were conducted and obtained blind of the genotypes, with the exception of one *Artemis^{-/-}* line that was not scored blind.

OP9-DL1 co-culture

Bone marrow cells from 4-6 week old mice were harvested and red blood cell lysed. Progenitor cells were enriched using MACS purification columns (Miltenyi Biotech, Bergisch Gladbach, Germany) and antibodies specific for mature hematopoietic lineages (CD24, B220, Mac-1, Gr-1, NK1.1, CD11c, and Thy1.2). Approximately 2 million cells were cultured per well using 24 well plates. Cultures were otherwise treated as described (Schmitt and Zúñiga-Pflücker, 2002), except for supplementation with 5 ng/mL of murine IL-7 and human Flt-3L (R&D Systems, Minneapolis, MN).

Statistical analysis.

The Kaplan-Meier curves were generated in SAS Version 9 (SAS Institute Inc.). All other statistical analysis was performed with two-tailed unpaired Student's t tests in Excel (Microsoft). $p < 0.05$ was considered to be statistically significant.

Chapter VIII

References

1. Agrawal, A., and D.G. Schatz. 1997. RAG1 and RAG2 form a stable postcleavage synaptic complex with DNA containing signal ends in V(D)J recombination. *Cell*. 89:43–53.
2. Ahnesorg, P., P. Smith, and S.P. Jackson. 2006. XLF interacts with the XRCC4-DNA ligase IV complex to promote DNA nonhomologous end-joining. *Cell*. 124:301–313.
3. Allman, D., A. Sambandam, S. Kim, J.P. Miller, A. Pagan, D. Well, A. Meraz, and A. Bhandoola. 2003. Thymopoiesis independent of common lymphoid progenitors. *Nat. Immunol.* 4:168–174.
4. Andegeko, Y., L. Moyal, L. Mittelman, I. Tsarfaty, Y. Shiloh, and G. Rotman. 2001. Nuclear retention of ATM at sites of DNA double strand breaks. *J. Biol. Chem.* 276: 38224–38230.
5. Anderson, D.E., K.M. Trujillo, P. Sung, and H.P. Erickson. 2001. Structure of the Rad50/Mre11 DNA repair complex from *Saccharomyces cerevisiae* by electron microscopy. *J. Biol. Chem.* 276:37027–37033.
6. Armstrong, S.A., and A.T. Look. 2005. Molecular genetics of acute lymphoblastic leukemia. *J. Clin. Oncol.* 23:6306–6315.
7. Bakkenist, C.J., and M.B. Kastan. 2003. DNA damage activates ATM through intermolecular autophosphorylation and dimer dissociation. *Nature*. 421:499–506.
8. Barlow, C., S. Hirotsune, R. Paylor, M. Liyanage, M. Eckhaus, F. Collins, Y. Shiloh, J.N. Crawley, T. Ried, D. Tagle, and A. Wynshaw-Boris. 1996. Atm-deficient mice: a paradigm of ataxia telangiectasia. *Cell*. 86:159–171.
9. Barlow, C., P.A. Dennery, M.K. Shigenaga, M.A. Smith, J.D. Morrow, L.J. Roberts, 2nd, A. Wynshaw-Boris, and R.L. Levine. 1999. Loss of the ataxia-telangiectasia gene product causes oxidative damage in target organs. *Proc. Natl. Acad. Sci. USA*. 96:9915–9919.
10. Bartek, J., and J. Lukas. 2007. DNA damage checkpoints: from initiation to recovery or adaptation. *Curr. Opin. Cell Biol.* 19:238–245.
11. Bassing, C.H., F.W. Alt, M.M. Hughes, M. D'Auteuil, T.D. Wehrly, B.B. Woodman, F. Gärtner, J.M. White, L. Davidson, and B.P. Sleckman. 2000. Recombination signal sequences restrict chromosomal V(D)J recombination beyond the 12/23 rule. *Nature*. 405:583–586.
12. Bassing, C.H., W. Swat, and F.W. Alt. 2002. The mechanism and regulation of chromosomal V(D)J recombination. *Cell*. 109:S45–S55.
13. Bassing, C.H., K.F. Chua, J. Sekiguchi, H. Suh, S.R. Whitlow, J.C. Fleming, B.C. Monroe, D.N. Ciccone, C. Yan, K. Vlasakova, D.M. Livingston, D.O. Ferguson, R. Scully, and F.W. Alt. 2002. Increased ionizing radiation sensitivity and genomic instability in the absence of histone H2AX. *Proc. Natl. Acad. Sci. USA*. 99:8173–8178.
14. Bassing, C.H., H. Suh, D.O. Ferguson, K.F. Chua, J. Manis, M. Eckersdorff, M. Gleason, R. Bronson, C. Lee, and F.W. Alt. 2003. Histone H2AX: a dosage-dependent suppressor of oncogenic translocations and tumors. *Cell*. 114:359–370.
15. Bassing, C.H., and F.W. Alt. 2004. H2AX may function as an anchor to hold broken chromosomal DNA ends in close proximity. *Cell Cycle*. 3:149–153.

16. Bassing, C.H., S. Ranganath, M. Murphy, V. Savić, M. Gleason, and F.W. Alt. 2008. Aberrant V(D)J recombination is not required for rapid development of H2ax/p53 deficient thymic lymphomas with clonal translocations. *Blood*. 111:2163–2169.
17. Beucher, A., J. Birraux, L. Tchouandong, O. Barton, A. Shibata, S. Conrad, A.A. Goodarzi, A. Krempler, P.A. Jeggo, and M. Lobrich. 2009. ATM and Artemis promote homologous recombination of radiation-induced DNA double-strand breaks in G2. *EMBO J*. 28:3413–3427.
18. Bewersdorf, J., B.T. Bennett, and K.L. Knight. 2006. H2AX chromatin structures and their response to DNA damage revealed by 4Pi microscopy. *Proc. Natl. Acad. Sci. USA*. 103:18137–18142.
19. Bhandoola, A., H. von Boehmer, H.T. Petrie, and J.C. Zúñiga-Pflücker. 2007. Commitment and developmental potential of extrathymic and intrathymic T cell precursors: plenty to choose from. *Immunity*. 26:678–689.
20. Bhaskara, V., A. Dupre, B. Lengsfeld, B.B. Hopkins, A. Chan, J.H. Lee, X. Zhang, J. Gautier, V. Zakian, and T.T. Paull. 2007. Rad50 adenylate kinase activity regulates DNA tethering by Mre11/Rad50 complexes. *Mol. Cell*. 25:647–661.
21. Bonner, W.M., C.E. Redon, J.S. Dickey, A.J. Nakamura, O.A. Sedelnikova, S. Solier, and Y. Pommier. 2008. Gamma-H2AX and cancer. *Nat. Rev. Cancer*. 8:957–967.
22. Borghesani, P.R., F.W. Alt, A. Bottaro, L. Davidson, S. Aksoy, G.A. Rathbun, T.M. Roberts, W. Swat, R.A. Segal, and Y. Gu. 2000. Abnormal development of Purkinje cells and lymphocytes in *Atm* mutant mice. *Proc. Natl. Acad. Sci. USA*. 97:3336–3341.
23. Bosma, G.C., R.P. Custer, and M.J. Bosma. 1983. A severe combined immunodeficiency mutation in the mouse. *Nature*. 301:527–530.
24. Bredemeyer, A.L., G.G. Sharma, C.Y. Huang, B.A. Helmink, L.M. Walker, K.C. Khor, B. Nuskey, K.E. Sullivan, T.K. Pandita, C.H. Bassing, and B.P. Sleckman. 2006. ATM stabilizes DNA double-strand-break complexes during V(D)J recombination. *Nature*. 442:466–470.
25. Bredemeyer, A.L., B.A. Helmink, C.L. Innes, B. Calderon, L.M. McGinnis, G.K. Mahowald, E.J. Gapud, L.M. Walker, J.B. Collins, B.K. Weaver, L. Mandik-Nayak, R.D. Schreiber, P.M. Allen, M.J. May, R.S. Paules, C.H. Bassing, and B.P. Sleckman. 2008. DNA double-strand breaks activate a multi-functional genetic program in developing lymphocytes. *Nature*. 456:819–823.
26. Brown, D.T. 2001. Histone variants: are they functionally heterogeneous? *Genome Biol*. 2:REVIEWS0006.
27. Bryant, H.E., N. Schultz, H.D. Thomas, K.M. Parker, D. Flower, E. Lopez, S. Kyle, M. Meuth, N.J. Curtin, and T. Helleday. 2005. Specific killing of BRCA2-deficient tumours with inhibitors of poly(ADP-ribose) polymerase. *Nature*. 434:913–917.
28. Buck, D., L. Malivert, R. de Chasseval, A. Barraud, M.C. Fondanèche, O. Sanal, A. Plebani, J.L. Stéphan, M. Hufnagel, F. le Deist, A. Fischer, A. Durandy, J.P. de Villartay, and P. Revy. 2006. Cernunnos, a novel nonhomologous end-joining

- factor, is mutated in human immunodeficiency with microcephaly. *Cell*. 124:287–299.
29. Burma, S., B.P. Chen, M. Murphy, A. Kurimasa, and D.J. Chen. 2001. ATM phosphorylates histone H2AX in response to DNA double-strand breaks. *J. Biol. Chem.* 276:42462–42467.
 30. Callén, E., M. Jankovic, S. Difilippantonio, J.A. Daniel, H.T. Chen, A. Celeste, M. Pellegrini, K. McBride, D. Wangsa, A.L. Bredemeyer, B.P. Sleckman, T. Ried, M. Nussenzweig, and A. Nussenzweig. 2007. ATM prevents the persistence and propagation of chromosome breaks in lymphocytes. *Cell*. 130:63–75.
 31. Callén, E., S. Bunting, C.Y. Huang, M.J. Difilippantonio, N. Wong, B. Khor, G. Mahowald, M.J. Kruhlak, T. Ried, B.P. Sleckman, and A. Nussenzweig. 2009. Chimeric IgH-TCRalpha/delta translocations in T lymphocytes mediated by RAG. *Cell Cycle*. 8:2408–2412.
 32. Carpenter, A.C., K.S. Yang-Iott, L.H. Chao, B. Nuskey, S. Whitlow, F.W. Alt, and C.H. Bassing. 2009. Assembled DJ beta complexes influence TCR beta chain selection and peripheral V beta repertoire. *J. Immunol.* 182:5586–5595.
 33. Carson, C.T., R.A. Schwartz, T.H. Stracker, C.E. Lilley, D.V. Lee, and M.D. Weitzman. 2003. The Mre11 complex is required for ATM activation and the G2/M checkpoint. *EMBO J.* 22:6610–6620.
 34. Cedar, H., and Y. Bergman. 2008. Choreography of Ig allelic exclusion. *Curr. Opin. Immunol.* 20:308–317.
 35. Celeste, A., S. Petersen, P.J. Romanienko, O. Fernandez-Capetillo, H.T. Chen, O.A. Sedelnikova, B. Reina-San-Martin, V. Coppola, E. Meffre, M.J. Difilippantonio, C. Redon, D.R. Pilch, A. Oлару, M. Eckhaus, R.D. Camerini-Otero, L. Tessarollo, F. Livak, K. Manova, W.M. Bonner, M.C. Nussenzweig, and A. Nussenzweig. 2002. Genomic instability in mice lacking histone H2AX. *Science*. 296:922–927.
 36. Celeste, A., O. Fernandez-Capetillo, M.J. Kruhlak, D.R. Pilch, D.W. Staudt, A. Lee, R.F. Bonner, W.M. Bonner, and A. Nussenzweig. 2003. Histone H2AX phosphorylation is dispensable for the initial recognition of DNA breaks. *Nat. Cell Biol.* 5:675–679.
 37. Celeste, A., S. Difilippantonio, M.J. Difilippantonio, O. Fernandez-Capetillo, D.R. Pilch, O.A. Sedelnikova, M. Eckhaus, T. Ried, W.M. Bonner, and A. Nussenzweig. 2003. H2AX haploinsufficiency modifies genomic stability and tumor susceptibility. *Cell*. 114:371–383.
 38. Chapman, J.R., and S.P. Jackson. 2008. Phospho-dependent interactions between NBS1 and MDC1 mediate chromatin retention of the MRN complex at sites of DNA damage. *EMBO Rep.* 9:795–801.
 39. Chaudhuri, J., U. Basu, A. Zarrin, C. Yan, S. Franco, T. Perlot, B. Vuong, J. Wang, R.T. Phan, A. Datta, J. Manis, and F.W. Alt. 2007. Evolution of the immunoglobulin heavy chain class switch recombination mechanism. *Adv. Immunol.* 94:157–214.
 40. Chen, H.T., A. Bhandoola, M.J. Difilippantonio, J. Zhu, M.J. Brown, X. Tai, E.P. Rogakou, T.M. Brotz, W.M. Bonner, T. Ried, and A. Nussenzweig. 2000. Response to RAG-mediated VDJ cleavage by NBS1 and gamma-H2AX. *Science*.

290:1962–1965.

41. Cheung, A.M., M.P. Hande, F. Jalali, M.S. Tsao, B. Skinnider, A. Hirao, J.P. McPherson, J. Karaskova, A. Suzuki, A. Wakeham, A. You-Ten, A. Elia, J. Squire, R. Bristow, R. Hakem, and T.W. Mak. 2002. Loss of Brca2 and p53 synergistically promotes genomic instability and deregulation of T-cell apoptosis. *Cancer Res.* 62:6194–6204.
42. Chowdhury, D., M.C. Keogh, H. Ishii, C.L. Peterson, S. Buratowski, and J. Lieberman. 2005. Gamma-H2AX dephosphorylation by protein phosphatase 2A facilitates DNA double-strand break repair. *Mol. Cell.* 20:801–809.
43. Corcoran, A.E. 2005. Immunoglobulin locus silencing and allelic exclusion. *Semin. Immunol.* 17:141–154.
44. Corneo, B., R.L. Wendland, L. Deriano, X. Cui, I.A. Klein, S.Y. Wong, S. Arnal, A.J. Holub, G.R. Weller, B.A. Pancake, S. Shah, V.L. Brandt, K. Meek, and D.B. Roth. 2007. Rag mutations reveal robust alternative end joining. *Nature.* 449:483–486.
45. Cook, P.J., B.G. Ju, F. Telese, X. Wang, C.K. Glass, and M.G. Rosenfeld. 2009. Tyrosine dephosphorylation of H2AX modulates apoptosis and survival decisions. *Nature.* 458:591–596.
46. Daley, J.M., P.L. Palmbo, D. Wu, and T.E. Wilson. 2005. Nonhomologous end joining in yeast. *Annu. Rev. Genet.* 39:431–451.
47. D'Amours, D., and S.P. Jackson. 2002. The Mre11 complex: at the crossroads of DNA repair and checkpoint signalling. *Nat. Rev. Mol. Cell Biol.* 3:317–327.
48. Dasika, G.K., S.C. Lin, S. Zhao, P. Sung, A. Tomkinson, and E.Y. Lee. 1999. DNA damage-induced cell cycle checkpoints and DNA strand break repair in development and tumorigenesis. *Oncogene.* 18:7883–7899.
49. de Jager, M., J. van Noort, D.C. van Gent, C. Dekker, R. Kanaar, and C. Wyman. 2001. Human Rad50/Mre11 is a flexible complex that can tether DNA ends. *Mol. Cell.* 8:1129–1135.
50. Degner, S.C., T.P. Wong, G. Jankevicius, and A.J. Feeney. 2009. Developmental stage-specific recruitment of cohesin to CTCF sites throughout immunoglobulin loci during B lymphocyte development. *J. Immunol.* 182:44–48.
51. Deriano, L., T.H. Stracker, A. Baker, J.H. Petrini, and D.B. Roth. 2009. Roles for NBS1 in alternative nonhomologous end-joining of V(D)J recombination intermediates. *Mol. Cell.* 34:13–25.
52. Difilippantonio, S., A. Celeste, O. Fernandez-Capetillo, H.T. Chen, B. Reina San Martin, F. Van Laethem, Y.P. Yang, G.V. Petukhova, M. Eckhaus, L. Feigenbaum, K. Manova, M. Kruhlak, R.D. Camerini-Otero, S. Sharan, M. Nussenzweig, and A. Nussenzweig. 2005. Role of Nbs1 in the activation of the Atm kinase revealed in humanized mouse models. *Nat. Cell Biol.* 7:675–685.
53. Difilippantonio, S., A. Celeste, M.J. Kruhlak, Y. Lee, M.J. Difilippantonio, L. Feigenbaum, S.P. Jackson, P.J. McKinnon, and A. Nussenzweig. 2007. Distinct domains in Nbs1 regulate irradiation-induced checkpoints and apoptosis. *J. Cell Biol.* 204:1003–1011.
54. Difilippantonio, S., E. Gapud, N. Wong, C.Y. Huang, G. Mahowald, H.T. Chen, M.J. Kruhlak, E. Callén, F. Livak, M.C. Nussenzweig, B.P. Sleckman, and A.

- Nussenzweig. 2008. 53BP1 facilitates long-range DNA end-joining during V(D)J recombination. *Nature*. 456:529–533.
55. Dimitrova, N., Y.C. Chen, D.L. Spector, and T. de Lange. 2008. 53BP1 promotes non-homologous end joining of telomeres by increasing chromatin mobility. *Nature*. 456:524–528.
 56. Dinkelmann, M., E. Spehalski, T. Stoneham, J. Buis, Y. Wu, J.M. Sekiguchi, and D.O. Ferguson. 2009. Multiple functions of MRN in end-joining pathways during isotype class switching. *Nat. Struct. Mol. Biol.* 16:808–813.
 57. Doil, C., N. Mailand, S. Bekker-Jensen, P. Menard, D.H. Larsen, R. Pepperkok, J. Ellenberg, S. Panier, D. Durocher, J. Bartek, J. Lukas, and C. Lukas. RNF168 binds and amplifies ubiquitin conjugates on damaged chromosomes to allow accumulation of repair proteins. *Cell*. 136:435–446.
 58. Dominski, Z. 2007. Nucleases of the metallo-beta-lactamase family and their role in DNA and RNA metabolism. *Crit. Rev. Biochem. Mol. Biol.* 42:67–93.
 59. Downs, J.A., M.C. Nussenzweig, and A. Nussenzweig. 2007. Chromatin dynamics and the preservation of genetic information. *Nature*. 447:951–958.
 60. Dujka, M.E., N. Puebla-Osorio, O. Tavana, M. Sang, and C. Zhu. 2010. ATM and p53 are essential in the cell-cycle containment of DNA breaks during V(D)J recombination in vivo. *Oncogene*. 29:957–965.
 61. Elson, A., Y. Wang, C. J. Daugherty, C. C. Morton, F. Zhou, J. Campos-Torres, and P. Leder. 1996. Pleiotropic defects in ataxia-telangiectasia protein-deficient mice. *Proc. Natl. Acad. Sci. USA*. 93:13084–13089.
 62. Farmer, H., N. McCabe, C.J. Lord, A.N. Tutt, D.A. Johnson, T.B. Richardson, M. Santarosa, K.J. Dillon, I. Hickson, C. Knights, N.M. Martin, S.P. Jackson, G.C. Smith, and A. Ashworth. 2005. Targeting the DNA repair defect in BRCA mutant cells as a therapeutic strategy. *Nature*. 434:917–921.
 63. Fernandez-Capetillo, O., H.T. Chen, A. Celeste, I. Ward, P.J. Romanienko, J.C. Morales, K. Naka, Z. Xia, R.D. Camerini-Otero, N. Motoyama, P.B. Carpenter, W.M. Bonner, J. Chen, and A. Nussenzweig. 2002. DNA damage-induced G2-M checkpoint activation by histone H2AX and 53BP1. *Nat. Cell Biol.* 4:993–997.
 64. Ferrando, A.A., D.S. Neuberg, J. Staunton, M.L. Loh, C. Huard, S.C. Raimondi, F.G. Behm, C.H. Pui, J.R. Downing, D.G. Gilliland, E.S. Lander, T.R. Golub, and A.T. Look. 2002. Gene expression signatures define novel oncogenic pathways in T cell acute lymphoblastic leukemia. *Cancer Cell*. 1:75–87.
 65. Fitzsimmons, S.P., R.M. Bernstein, E.E. Max, J.A. Skok, and M.A. Shapiro. 2007. Dynamic changes in accessibility, nuclear positioning, recombination, and transcription at the Ig kappa locus. *J. Immunol.* 179:5264–5273.
 66. Franco, S., M. Gostissa, S. Zha, D.B. Lombard, M.M. Murphy, A.A. Zarrin, C. Yan, S. Tepsuporn, J.C. Morales, M.M. Adams, Z. Lou, C.H. Bassing, J.P. Manis, J. Chen, P.B. Carpenter, and F.W. Alt. 2006. H2AX prevents DNA breaks from progressing to chromosome breaks and translocations. *Mol. Cell*. 21:201–214.
 67. Fugmann, S.D., A.I. Lee, P.E. Shockett, I.J. Villey, and D.G. Schatz. 2000. The RAG proteins and V(D)J recombination: complexes, ends, and transposition. *Annu. Rev. Immunol.* 18:495–527.
 68. Furuta, T., H. Takemura, Z.Y. Liao, G.J. Aune, C. Redon, O.A. Sedelnikova, D.R.

- Pilch, E.P. Rogakou, A. Celeste, H.T. Chen, A. Nussenzweig, M.I. Aladjem, W.M. Bonner, and Y. Pommier. 2003. Phosphorylation of histone H2AX and activation of Mre11, Rad50, and Nbs1 in response to replication-dependent DNA double-strand breaks induced by mammalian DNA topoisomerase I cleavage complexes. *J. Biol. Chem.* 278:20303–20312.
69. Gatei, M., D. Young, K.M. Cerosaletti, A. Desai-Mehta, K. Spring, S. Kozlov, M.F. Lavin, R.A. Gatti, P. Concannon, and K. Khanna. 2000. ATM-dependent phosphorylation of nibrin in response to radiation exposure. *Nat. Genet.* 25:115–119.
 70. Gao, Y., J. Chaudhuri, C. Zhu, L. Davidson, D.T. Weaver, and F.W. Alt. 1998. A targeted DNA-PKcs-null mutation reveals DNA-PK-independent functions for KU in V(D)J recombination. *Immunity.* 9:367–376.
 71. Gladdy, R.A., M.D. Taylor, C.J. Williams, I. Grandal, J. Karaskova, J.A. Squire, J.T. Rutka, C.J. Guidos, and J.S. Danska. 2003. The RAG-1/2 endonuclease causes genomic instability and controls CNS complications of lymphoblastic leukemia in p53/Prkdc-deficient mice. *Cancer Cell.* 3:37–50.
 72. Gladdy, R.A., L.M. Nutter, T. Kunath, J.S. Danska, and C.J. Guidos. 2006. p53-Independent apoptosis disrupts early organogenesis in embryos lacking both ataxia-telangiectasia mutated and Prkdc. *Mol. Cancer Res.* 4:311–318.
 73. Godfrey, D.I., J. Kennedy, T. Suda, and A. Zlotnik. 1993. A developmental pathway involving four phenotypically and functionally distinct subsets of CD3⁻CD4⁻CD8⁻ triple-negative adult mouse thymocytes defined by CD44 and CD25 expression. *J. Immunol.* 150:4244–4252.
 74. Goldmit, M., Y. Ji, J. Skok, E. Roldan, S. Jung, H. Cedar, and Y. Bergman. 2005. Epigenetic ontogeny of the κ locus during B cell development. *Nat. Immunol.* 6:198–203.
 75. Gong, Z., Y.W. Cho, J.E. Kim, K. Ge, and J. Chen. 2009. Accumulation of Pax2 transactivation domain interaction protein (PTIP) at sites of DNA breaks via RNF8-dependent pathway is required for cell survival after DNA damage. *J. Biol. Chem.* 284:7284–7293.
 76. Goodarzi, A.A., A.T. Noon, D. Deckbar, Y. Ziv, Y. Shiloh, M. Löbrich, and P.A. Jeggo. 2008. ATM signaling facilitates repair of DNA double-strand breaks associated with heterochromatin. *Mol. Cell.* 31:167–177.
 77. Grabher, C., H. von Boehmer, and A.T. Look. 2006. Notch 1 activation in the molecular pathogenesis of T-cell acute lymphoblastic leukaemia. *Nat. Rev. Cancer.* 6:347–359.
 78. Grazini, U., F. Zanardi, E. Citterio, S. Casola, C.R. Goding, and F. McBlane. 2010. The RING domain of RAG1 ubiquitylates histone H3: a novel activity in chromatin-mediated regulation of V(D)J joining. *Mol. Cell.* 37:282–293.
 79. Hakem, R. 2008. DNA-damage repair: the good, the bad, and the ugly. *EMBO J.* 27:589–605.
 80. Harrison, J.C., and J.E. Haber. 2006. Surviving the Breakup: The DNA damage checkpoint. *Annu. Rev. Genet.* 40:209–235.
 81. Harper, J.W., and S.J. Elledge. 2007. The DNA damage response: ten years after. *Mol. Cell.* 28:739–745.

82. Helmink, B.A., A.L. Bredemeyer, B.S. Lee, C.Y. Huang, G.G. Sharma, L.M. Walker, J.J. Bednarski, W.L. Lee, T.K. Pandita, C.H. Bassing, and B.P. Sleckman. 2009. MRN complex function in the repair of chromosomal Rag-mediated DNA double-strand breaks. *J. Exp. Med.* 206:669–679.
83. Hewitt, S.L., B. Yin, Y. Ji, J. Chaumeil, K. Marszalek, J. Tenthorey, G. Salvagiotto, N. Steinel, L.B. Ramsey, J. Ghysdael, M.A. Farrar, B.P. Sleckman, D.G. Schatz, M. Busslinger, C.H. Bassing, and J.A. Skok. 2009. RAG-1 and ATM coordinate monoallelic recombination and nuclear positioning of immunoglobulin loci. *Nat. Immunol.* 10:655–664.
84. Hoeijmakers, J.H. 2001. Genome maintenance mechanisms for preventing cancer. *Nature.* 411:366–374.
85. Hollstein, M., D. Sidransky, B. Vogelstein, and C.C. Harris. 1991. p53 mutations in human cancers. *Science.* 253:49–53.
86. Hopfner, K.P., L. Craig, G. Moncalian, R.A. Zinkel, T. Usui, B.A. Owen, A. Karcher, B. Henderson, J.L. Bodmer, C.T. McMurray, J.P. Carney, J.H. Petrini, and J.A. Tainer. 2002. The Rad50 zinc-hook is a structure joining Mre11 complexes in DNA recombination and repair. *Nature.* 418:562–566.
87. Horejsí, Z., J. Falck, C.J. Bakkenist, M.B. Kastan, J. Lukas, and J. Bartek. 2004. Distinct functional domains of Nbs1 modulate the timing and magnitude of ATM activation after low doses of ionizing radiation. *Oncogene.* 23:3122–3127.
88. Hsieh, C.L., C.F. Arlett, and M.R. Lieber. 1993. V(D)J recombination in ataxia telangiectasia, Bloom's syndrome, and a DNA ligase I-associated immunodeficiency disorder. *J. Biol. Chem.* 268:20105–20109.
89. Huen, M.S., R. Grant, I. Manke, K. Minn, X. Yu, M.B. Yaffe, and J. Chen. 2007. RNF8 transduces the DNA-damage signal via histone ubiquitylation and checkpoint protein assembly. *Cell.* 131:901–914.
90. Jackson, S.P., and J. Bartek. 2009. The DNA-damage response in human biology and disease. *Nature.* 461:1071–1078.
91. Jankovic, M., A. Nussenzweig, and M.C. Nussenzweig. 2007. Antigen receptor diversification and chromosome translocations. *Nat. Immunol.* 8:801–808.
92. Jia, J., M. Kondo, and Y. Zhuang. 2007. Germline transcription from T-cell receptor Vbeta gene is uncoupled from allelic exclusion. *EMBO J.* 26:2387–2399.
93. Jonkers, J., R. Meuwissen, H. van der Gulden, H. Peterse, M. van der Valk, and A. Berns. 2001. Synergistic tumor suppressor activity of BRCA2 and p53 in a conditional mouse model for breast cancer. *Nat. Genet.* 29:418–425.
94. Jung, D., C. Giallourakis, R. Mostoslavsky and F.W. Alt. 2006. Mechanism and control of V(D)J recombination at the immunoglobulin heavy chain locus. *Annu. Rev. Immunol.* 24:541–570.
95. Kang, J., R.T. Bronson, and Y. Xu. 2002. Targeted disruption of NBS1 reveals its roles in mouse development and DNA repair. *EMBO J.* 21:1447–1455.
96. Khanna, K.K., and S.P. Jackson. 2001. DNA double-strand breaks: signalling, repair and the cancer connection. *Nature Genet.* 27:247–254.
97. Khor, B., and Sleckman, B.P. 2005. Intra- and inter-allelic ordering of T cell receptor beta chain gene assembly. *Eur. J. Immunol.* 35:964–970.
98. Kinner, A., W. Wu, C. Staudt, and G. Iliakis. 2008. Gamma-H2AX in recognition

- and signaling of DNA double-strand breaks in the context of chromatin. *Nucleic Acids Res.* 36:5678–5694.
99. Kolas, N.K., J.R. Chapman, S. Nakada, J. Ylanko, R. Chahwan, F.D. Sweeney, S. Panier, M. Mendez, J. Wildenhain, T.M. Thomson, L. Pelletier, S.P. Jackson, and D. Durocher. 2007. Orchestration of the DNA-damage response by the RNF8 ubiquitin ligase. *Science.* 318:1637–1640.
 100. Kosak, S.T., J.A. Skok, K.L. Medina, R. Riblet, M.M. Le Beau, A.G. Fisher, and H. Singh. 2002. Subnuclear compartmentalization of immunoglobulin loci during lymphocyte development. *Science.* 296:158–162.
 101. Lee, G.S., M.B. Neiditch, S.S. Salus, and D.B. Roth. 2004. RAG proteins shepherd double-strand breaks to a specific pathway, suppressing error-prone repair, but RAG nicking initiates homologous recombination. *Cell.* 117:171–184.
 102. Lee, J., and S. Desiderio. 1999. Cyclin A/CDK2 regulates V(D)J recombination by coordinating RAG-2 accumulation and DNA repair. *Immunity.* 11:771–781.
 103. Lee, J.H., and T.T. Paull. 2004. Direct activation of the ATM protein kinase by the Mre11/Rad50/Nbs1 complex. *Science.* 304:93–96.
 104. Lee, J.H., and T.T. Paull. 2005. ATM activation by DNA double-strand breaks through the Mre11-Rad50-Nbs1 complex. *Science.* 308:551–554.
 105. Lee, P.P., D.R. Fitzpatrick, C. Beard, H.K. Jessup, S. Lehar, K.W. Makar, M. Perez-Melgosa, M.T. Sweetser, M.S. Schlissel, S. Nguyen, S.R. Cherry, J.H. Tsai, S.M. Tucker, W.M. Weaver, A. Kelso, R. Jaenisch, and C.B. Wilson. 2001. A critical role for Dnmt1 and DNA methylation in T cell development, function, and survival. *Immunity.* 15:763–774.
 106. Liao, M.J., X.X. Zhang, R. Hill, J. Gao, M.B. Qumsiyeh, W. Nichols, and T. van Dyke. 1998. No requirement for V(D)J recombination in p53-deficient thymic lymphoma. *Mol. Cell Biol.* 18:3495–3501.
 107. Lieber, M.R. 2008. The mechanism of human nonhomologous DNA end joining. *J. Biol. Chem.* 283:1–5.
 108. Lieber, M.R., Y. Ma, U. Pannicke, and K. Schwarz. 2003. Mechanism and regulation of human non-homologous DNA end-joining. *Nat. Rev. Mol. Cell Biol.* 4:712–720.
 109. Lim, D.S., S.T. Kim, B. Xu, R.S. Maser, J. Lin, J.H. Petrini, and M.B. Kastan. 2000. ATM phosphorylates p95/nbs1 in an S-phase checkpoint pathway. *Nature.* 404:613–617.
 110. Lindahl, T., and D.E. Barnes. 2000. Repair of endogenous DNA damage. *Cold Spring Harb. Symp. Quant. Biol.* 65:127–134.
 111. Linker, C., L. Damon, C. Ries, and W. Navarro. 2002. Intensified and shortened cyclical chemotherapy for adult acute lymphoblastic leukemia. *J. Clin. Oncol.* 20:2464–2471.
 112. Liyanage, M., Z. Weaver, C. Barlow, A. Coleman, D.G. Pankratz, S. Anderson, A. Wynshaw-Boris, and T. Ried. 2000. Abnormal rearrangement within the alpha/delta T-cell receptor locus in lymphomas from Atm-deficient mice. *Blood* 96:1940–1946.
 113. Lou, Z., K. Minter-Dykhouse, S. Franco, M. Gostissa, M.A. Rivera, A. Celeste, J.P. Manis, J. van Deursen, A. Nussenzweig, T.T. Paull, F.W. Alt, and J. Chen.

2006. MDC1 maintains genomic stability by participating in the amplification of ATM-dependent DNA damage signals. *Mol. Cell*. 21:187–200.
114. Ma, Y., U. Pannicke, K. Schwarz, and M.R. Lieber. 2002. Hairpin opening and overhang processing by an Artemis/DNA-dependent protein kinase complex in nonhomologous end joining and V(D)J recombination. *Cell*. 108:781–794.
115. Mahaney, B.L., K. Meek, and S.P. Lees-Miller. 2009. Repair of ionizing radiation-induced DNA double-strand breaks by non-homologous end-joining. *Biochem. J*. 417:639–650.
116. Mailand, N., S. Bekker-Jensen, H. Faustrup, F. Melander, J. Bartek, C. Lukas, and J. Lucas. 2007. RNF8 ubiquitylates histones at DNA double-strand breaks and promotes assembly of repair proteins. *Cell*. 131:887–900.
117. Mak, T.W., A. Hakem, J.P. McPherson, A. Shehabeldin, E. Zabolcki, E. Migon, G.S. Duncan, D. Bouchard, A. Wakeham, A. Cheung, J. Karaskova, I. Sarosi, J. Squire, J. Marth, and R. Hakem. 2000. Brcal required for T cell lineage development but not TCR loci rearrangement. *Nat. Immunol*. 1:77–82.
118. Matei, I.R., R.A. Gladdy, L.M. Nutter, A. Canty, C.J. Guidos, and J.S. Danska. 2007. ATM deficiency disrupts Tcr locus integrity and the maturation of CD4⁺CD8⁺ thymocytes. *Blood*. 109:1887–1896.
119. Matsuoka, S., B.A. Ballif, A. Smogorzewska, E.R. McDonald, 3rd, K.E. Hurov, J. Luo, C.E. Bakalarski, Z. Zhao, N. Solimini, Y. Lerenthal, Y. Shiloh, S.P. Gygi, and S.J. Elledge. 2007. ATM and ATR substrate analysis reveals extensive protein networks responsive to DNA damage. *Science*. 316:1160–1166.
120. Melander, F., S. Bekker-Jensen, J. Falck, J. Bartek, N. Mailand, and J. Lukas. 2008. Phosphorylation of SDT repeats in the MDC1 N terminus triggers retention of NBS1 at the DNA damage-modified chromatin. *J. Cell Biol*. 181:213–226.
121. Mills, K.D., D.O. Ferguson, and F.W. Alt. 2003. The role of DNA breaks in genomic instability and tumorigenesis. *Immunol. Rev*. 194:77–95.
122. Moreno-Herrero, F., M. de Jager, N.H. Dekker, R. Kanaar, C. Wyman, and C. Dekker. 2005. Mesoscale conformational changes in the DNA-repair complex Rad50/Mre11/Nbs1 upon binding DNA. *Nature*. 437:440–443.
123. Moshous, D., I. Callebaut, R. de Chasseval, B. Corneo, M. Cavazzana-Calvo, F. Le Deist, I. Tezcan, O. Sanal, Y. Bertrand, N. Philippe, A. Fischer, and J.P. de Villartay. 2001. Artemis, a novel DNA double-strand break repair/V(D)J recombination protein, is mutated in human severe combined immune deficiency. *Cell*. 105:177–186.
124. Mostoslavsky, R., N. Singh, T. Tenzen, M. Goldmit, C. Gabay, S. Elizur, P. Qi, B.E. Reubinoff, A. Chess and H. Cedar, and Y. Bergman. 2001. Asynchronous replication and allelic exclusion in the immune system. *Nature*. 414:221–225.
125. Muljo, S.A., and M.S. Schlissel. 2003. A small molecule Abl kinase inhibitor induces differentiation of Abelson virus-transformed pre-B cell lines. *Nat. Immunol*. 4:31–37.
126. Nakada, S., G.I. Chen, A.C. Gingras, and D. Durocher. 2008. PP4 is a gamma-H2AX phosphatase required for recovery from the DNA damage checkpoint. *EMBO Rep*. 9:1019–1026.
127. Nick McElhinny, S.A., and D.A. Ramsden. 2004. Sibling rivalry: competition

- between Pol X family members in V(D)J recombination and general double strand break repair. *Immunol. Rev.* 200:156–164.
128. O’Driscoll, M., A.R. Gennery, J. Seidel, P. Concannon, and P.A. Jeggo. 2004. An overview of three new disorders associated with genetic instability: LIG4 syndrome, RS-SCID and ATR-Seckel syndrome. *DNA Repair. (Amst.)*. 3:1227–1235.
 129. Oeffinger, K.C., A.C. Mertens, C.A. Sklar, T. Kawashima, M.M. Hudson, A.T. Meadows, D.L. Friedman, N. Marina, W. Hobbie, N.S. Kadan-Lottick, C.L. Schwartz, W. Leisenring, and L.L. Robison; Childhood Cancer Survivor Study. 2006. Chronic health conditions in adult survivors of childhood cancer. *N. Engl. J. Med.* 355:1572–1582.
 130. Orban, P.C., D. Chui, and J.D. Marth. 1992. Tissue- and site-specific DNA recombination in transgenic mice. *Proc. Natl. Acad. Sci. USA.* 89:6861–6865.
 131. Parikh, R.A., J.S. White, X. Huang, D.W. Schoppy, B.E. Baysal, R. Baskaran, C.J. Bakkenist, W.S. Saunders, L.C. Hsu, M. Romkes, and S.M. Gollin. 2007. Loss of distal 11q is associated with DNA repair deficiency and reduced sensitivity to ionizing radiation in head and neck squamous cell carcinoma. *Genes Chromosomes Cancer.* 46:761–775.
 132. Park, E.J., D.W. Chan, J.H. Park, M.A. Oettinger, and J. Kwon. 2003. DNA-PK is activated by nucleosomes and phosphorylates H2AX within the nucleosomes in an acetylation-dependent manner. *Nucleic Acids Res.* 31: 6819–6827.
 133. Paull, T.T., E.P. Rogakou, V. Yamazaki, C.U. Kirchgessner, M. Gellert, and W.M. Bonner. 2000. A critical role for histone H2AX in recruitment of repair factors to nuclear foci after DNA damage. *Curr. Biol.* 10:886–895.
 134. Pedraza-Alva, G., M. Koulunis, C. Charland, T. Thornton, J.L. Clements, M.S. Schlissel, and M. Rincon. 2006. Activation of p38 MAP kinase by DNA double-strand breaks in V(D)J recombination induces a G2/M cell cycle checkpoint. *EMBO J.* 25:763–773.
 135. Perkins, E.J., A. Nair, D.O. Cowley, T. van Dyke, Y. Chang, and D.A. Ramsden. 2002. Sensing of intermediates in V(D)J recombination by ATM. *Genes Dev.* 16:159–164.
 136. Petiniot, L.K., Z. Weaver, C. Barlow, R. Shen, M. Eckhaus, S.M. Steinberg, T. Ried, A. Wynshaw-Boris, and R.J. Hodes. 2000. Recombinase-activating gene (RAG) 2-mediated V(D)J recombination is not essential for tumorigenesis in Atm-deficient mice. *Proc. Natl. Acad. Sci. USA.* 97:6664–6669.
 137. Petiniot, L.K., Z. Weaver, M. Vacchio, R. Shen, D. Wangsa, C. Barlow, M. Eckhaus, S.M. Steinberg, A. Wynshaw-Boris, T. Ried, and R.J. Hodes. 2002. RAG-mediated V(D)J recombination is not essential for tumorigenesis in Atm-deficient mice. *Mol. Cell Biol.* 22:3174–3177.
 138. Poinsignon, C., D. Moshous, I. Callebaut, R. de Chasseval, I. Villey, and J.P. de Villartay. 2004. The metallo-beta-lactamase/beta-CASP domain of Artemis constitutes the catalytic core for V(D)J recombination. *J. Exp. Med.* 199:315–321.
 139. Pui, C.H., and W.E. Evans. 2006. Treatment of acute lymphoblastic leukemia. *N. Engl. J. Med.* 354:166–178.

140. Pui, C.H., L.L. Robison, and A.T. Look. 2008. Acute lymphoblastic leukaemia. *Lancet*. 371:1030–1043.
141. Raman, M., S. Earnest, K. Zhang, Y. Zhao, and M.H. Cobb. 2007. TAO kinases mediate activation of p38 in response to DNA damage. *EMBO J*. 26:2005–2014.
142. Ramiro, A.R., M. Jankovic, E. Callén, S. Difilippantonio, H.T. Chen, K.M. McBride, T.R. Eisenreich, J. Chen, R.A. Dickins, S.W. Lowe, A. Nussenzweig, and M.C. Nussenzweig. 2006. Role of genomic instability and p53 in AID-induced c-myc-IgH translocations. *Nature*. 440:105–109.
143. Rass, E., A. Grabarz, I. Plo, J. Gautier, P. Bertrand, and B.S. Lopez. 2009. Role of Mre11 in chromosomal nonhomologous end joining in mammalian cells. *Nat. Struct. Mol. Biol*. 16:819–824.
144. Raulet, D.H., D.M. Spencer, Y.H. Hsiang, J.P. Goldman, M. Bix, N.S. Liao, M. Zijstra, R. Jaenisch, and I. Correa. 1991. Control of gamma/delta T-cell development. *Immunol. Rev*. 120:185–204.
145. Raval, P., A.N. Kriatchko, S. Kumar, and P.C. Swanson. 2008. Evidence for Ku70/Ku80 association with full-length RAG1. *Nucleic Acids Res*. 36:2060–2072.
146. Reina-San-Martin, B., S. Difilippantonio, L. Hanitsch, R.F. Masilamani, A. Nussenzweig, and M.C. Nussenzweig. 2003. H2AX is required for recombination between immunoglobulin switch regions but not for intra-switch region recombination or somatic hypermutation. *J. Exp. Med*. 197:1767–1778.
147. Reinhardt, H.C., A.S. Aslanian, J.A. Lees, and M.B. Yaffe. 2007. p53-deficient cells rely on ATM- and ATR-mediated checkpoint signaling through the p38MAPK/MK2 pathway for survival after DNA damage. *Cancer Cell*. 11:175–89.
148. Revy, P., D. Buck, F. le Deist, and J.P. de Villartay. 2005. The repair of DNA damages/modifications during the maturation of the immune system: lessons from human primary immunodeficiency disorders and animal models. *Adv. Immunol*. 87:237–295.
149. Riballo, E., M. Kühne, N. Rief, A. Doherty, G.C. Smith, M.J. Recio, C. Reis, K. Dahm, A. Fricke, A. Krempler, A.R. Parker, S.P. Jackson, A. Gennery, P.A. Jeggo, and M. Löbrich. 2004. A pathway of double-strand break rejoining dependent upon ATM, Artemis, and proteins locating to gamma-H2AX foci. *Mol. Cell*. 16:715–724.
150. Rogakou, E.P., D.R. Pilch, A.H. Orr, V.S. Ivanova, and W.M. Bonner. 1998. DNA double-stranded breaks induce histone H2AX phosphorylation on serine 139. *J. Biol. Chem*. 273:5858–5868.
151. Rogakou, E.P., C. Boon, C. Redon, and W.M. Bonner. 1999. Megabase chromatin domains involved in DNA double-strand breaks in vivo. *J. Cell. Biol*. 146:905–916.
152. Roldan, E., M. Fuxa, W. Chong, D. Martinez, M. Novatchkova, M. Busslinger, and J.A. Skok. 2005. Locus ‘decontraction’ and centromeric recruitment contribute to allelic exclusion of the immunoglobulin heavy-chain gene. *Nat. Immunol*. 6:31–41.
153. Rooney, S., J. Sekiguchi, C. Zhu, H.L. Cheng, J. Manis, S. Whitlow, J. DeVido,

- D. Foy, J. Chaudhuri, D. Lombard, and F.W. Alt. 2002. Leaky Scid phenotype associated with defective V(D)J coding end processing in Artemis-deficient mice. *Mol. Cell.* 10:1379–1390.
154. Rooney, S., F.W. Alt, D. Lombard, S. Whitlow, M. Eckersdorff, J. Fleming, S. Fugmann, D.O. Ferguson, D.G. Schatz, and J. Sekiguchi. 2003. Defective DNA repair and increased genomic instability in Artemis-deficient murine cells. *J. Exp. Med.* 197:553–565.
155. Rooney, S., J. Sekiguchi, S. Whitlow, M. Eckersdorff, J.P. Manis, C. Lee, D.O. Ferguson, and F.W. Alt. 2004. Artemis and p53 cooperate to suppress oncogenic N-myc amplification in progenitor B cells. *Proc. Natl. Acad. Sci. USA.* 101:2410–2415.
156. Rooney, S., J. Chaudhuri, and F.W. Alt. 2004. The role of the non-homologous end-joining pathway in lymphocyte development. *Immunol. Rev.* 200:115–131.
157. Rouse, J., and S.P. Jackson. 2002. Interfaces between the detection, signaling, and repair of DNA damage. *Science.* 297:547–551.
158. Savić, V., B. Yin, N.L. Maas, A.L. Bredemeyer, A.C. Carpenter, B.A. Helmink, K.S. Yang-Iott, B.P. Sleckman, and C.H. Bassing. 2009. Formation of dynamic gamma-H2AX domains along broken DNA strands is distinctly regulated by ATM and MDC1 and dependent upon H2AX densities in chromatin. *Mol. Cell.* 34:298–310.
159. Schmitt, T.M., and J.C. Zúñiga-Pflücker. 2002. Induction of T cell development from hematopoietic progenitor cells by delta-like-1 in vitro. *Immunity.* 17:749–756.
160. Shao, L., H. Fujii, I. Colmegna, H. Oishi, J.J. Goronzy, and C.M. Weyand. 2009. Deficiency of the DNA repair enzyme ATM in rheumatoid arthritis. *J. Exp. Med.* 206:1435–1449.
161. Shroff, R., A. Arbel-Eden, D. Pilch, G. Ira, W.M. Bonner, J.H. Petrini, J.E. Haber, and M. Lichten. 2004. Distribution and dynamics of chromatin modification induced by a defined DNA double-strand break. *Curr. Biol.* 14:1703–1711.
162. Silverman, L.B., R.D. Gelber, V.K. Dalton, B.L. Asselin, R.D. Barr, L.A. Clavell, C.A. Hurwitz, A. Moghrabi, Y. Samson, M.A. Schorin, S. Arkin, L. Declerck, H.J. Cohen, and S.E. Sallan. 2001. Improved outcome for children with acute lymphoblastic leukemia: results of Dana-Farber Consortium Protocol 91-01. *Blood.* 97:1211–1218.
163. Skok, J.A., R. Gisler, M. Novatchkova, D. Farmer, W. de Laat, and M. Busslinger. 2007. Reversible contraction by looping of the Tcr α and Tcr β loci in rearranging thymocytes. *Nat. Immunol.* 8:378–387.
164. Sleckman, B.P., C.G. Bardon, R. Ferrini, L. Davidson, and F.W. Alt. 1997. Function of the TCR alpha enhancer in alpha/beta and gamma/delta T cells. *Immunity.* 7:505–515.
165. Soutoglou, E., J.F. Dorn, K. Sengupta, M. Jasin, A. Nussenzweig, T. Ried, G. Danuser, and T. Misteli. 2007. Positional stability of single double-strand breaks in mammalian cells. *Nat. Cell Biol.* 9:675–682.
166. Spycher, C., E.S. Miller, K. Townsend, L. Pavic, N.A. Morrice, P. Janscak, G.S. Stewart, and M. Stucki. 2008. Constitutive phosphorylation of MDC1 physically

- links the MRE11-RAD50-NBS1 complex to damaged chromatin. *J. Cell Biol.* 181:227–240.
167. Stewart, G.S., S. Panier, K. Townsend, A.K. Al-Hakim, N.K. Kolas, E.S. Miller, S. Nakada, J. Ylanko, S. Olivarius, M. Mendez, C. Oldreive, J. Wildenhain, A. Tagliaferro, L. Pelletier, N. Taubenheim, A. Durandy, P.J. Byrd, T. Stankovic, A.M. Taylor, and D. Durocher. 2009. The RIDDLE syndrome protein mediates a ubiquitin-dependent signaling cascade at sites of DNA damage. *Cell.* 136:420–434.
 168. Stewart, G.S. 2009. Solving the RIDDLE of 53BP1 recruitment to sites of damage. *Cell Cycle.* 8:1532–1538.
 169. Stiff, T., M. O'Driscoll, N. Rief, K. Iwabuchi, M. Lobrich, and P.A. Jeggo, 2004. ATM and DNA-PK function redundantly to phosphorylate H2AX after exposure to ionizing radiation. *Cancer Res.* 64:2390–2396.
 170. Stilgenbauer, S., P. Liebisch, M.R. James, M. Schröder, B. Schlegelberger, K. Fischer, M. Bentz, P. Lichter P, and H. Döhner. 1996. Molecular cytogenetic delineation of a novel critical genomic region in chromosome bands 11q22.3-923.1 in lymphoproliferative disorders. *Proc. Natl. Acad. Sci. USA.* 93:11837–11841.
 171. Stilgenbauer, S., D. Winkler, G. Ott, C. Schaffner, E. Leupolt, M. Bentz, P. Möller, H.K. Müller-Hermelink, M.R. James, P. Lichter, and H. Döhner. 1999. Molecular characterization of 11q deletions points to a pathogenic role of the ATM gene in mantle cell lymphoma. *Blood.* 94:3262–3264.
 172. Stracker, T.H., J.W. Theunissen, M. Morales, and J.H. Petrini. 2004. The Mre11 complex and the metabolism of chromosome breaks: the importance of communicating and holding things together. *DNA Repair (Amst.).* 3:845–854.
 173. Stracker, T.H., M. Morales, S.S. Couto, H. Hussein, and J.H. Petrini. 2007. The carboxy terminus of NBS1 is required for induction of apoptosis by the MRE11 complex. *Nature.* 447:218–221.
 174. Strahl, B.D., and C.D. Allis. 2000. The language of covalent histone modifications. *Nature.* 403:41–45.
 175. Strasser, A., A.W. Harris, and S. Cory. 1991. Bcl-2 transgene inhibits T cell death and perturbs thymic self-censorship. *Cell.* 67:889–899.
 176. Stucki, M., and S.P. Jackson. 2006. Gamma-H2AX and MDC1: anchoring the DNA-damage-response machinery to broken chromosomes. *DNA Repair (Amst.).* 5:534–543.
 177. Taccioli, G.E., A.G. Amatucci, H.J. Beamish, D. Gell, X.H. Xiang, M.I. Torres Arzayus, A. Priestley, S.P. Jackson, A. Marshak Rothstein, P.A. Jeggo, and V.L. Herrera. 1998. Targeted disruption of the catalytic subunit of the DNA-PK gene in mice confers severe combined immunodeficiency and radiosensitivity. *Immunity.* 9:355–366.
 178. Theunissen, J.W., M.I. Kaplan, P.A. Hunt, B.R. Williams, D.O. Ferguson, F.W. Alt, and J.H. Petrini. 2003. Checkpoint failure and chromosomal instability without lymphomagenesis in Mre11(ATLD1/ATLD1) mice. *Mol. Cell.* 12:1511–1523.

179. Thompson, L.H., and D. Schild. 2002. Recombinational DNA repair and human disease. *Mutat. Res.* 509:49–78.
180. Unal, E., A. Arbel-Eden, U. Sattler, R. Shroff, M. Lichten, J.E. Haber, and D. Koshland. 2004. DNA damage response pathway uses histone modification to assemble a double-strand break-specific cohesin domain. *Mol. Cell.* 16:991–1002.
181. Uziel, T., Y. Lerenthal, L. Moyal, Y. Andegeko, L. Mittelman, and Y. Shiloh. 2003. Requirement of the MRN complex for ATM activation by DNA damage. *EMBO J.* 22:5612–5621.
182. Vacchio, M.S., A. Olaru, F. Livak, and R.J. Hodes. 2007. ATM deficiency impairs thymocyte maturation because of defective resolution of T cell receptor alpha locus coding end breaks. *Proc. Natl. Acad. Sci. USA.* 104:6323–6328.
183. van Attikum, H., and S.M. Gasser. 2009. Crosstalk between histone modifications during the DNA damage response. *Trends Cell Biol.* 19:207–217.
184. van der Burg, M., H. Ijspeert, N.S. Verkaik, T. Turul, W.W. Wiegant, K. Morotomi-Yano, P.O. Mari, I. Tezcan, D.J. Chen, M.Z. Zdzienicka, J.J. van Dongen, and D.C. van Gent. 2009. A DNA-PKcs mutation in a radiosensitive T⁺B⁻ SCID patient inhibits Artemis activation and nonhomologous end-joining. *J Clin. Invest.* 119:91–98.
185. van Gent, D.C., J.H. Hoeijmakers, and R. Kanaar. 2001. Chromosomal stability and the DNA double-stranded break connection. *Nat. Rev. Genet.* 2:196–206.
186. Vanasse, G.J., J. Halbrook, S. Thomas, A. Burgess, M.F. Hoekstra, C.M. Disteché, and D.M. Willerford. 1999. Genetic pathway to recurrent chromosome translocations in murine lymphoma involves V(D)J recombinase. *J. Clin. Invest.* 103:1669–1675.
187. Venkitaraman, A.R. 2002. Cancer susceptibility and the functions of BRCA1 and BRCA2. *Cell.* 108(2):171–182.
188. von Boehmer, H. 2004. Selection of the T-cell repertoire: receptor-controlled checkpoints in T-cell development. *Adv. Immunol.* 84:201–238.
189. Wang, B., and S.J. Elledge. 2007. Ubc13/Rnf8 ubiquitin ligases control foci formation of the Rap80/Abraxas/Brcal/Brc36 complex in response to DNA damage. *Proc. Natl. Acad. Sci. USA.* 104:20759–20763.
190. Ward, I.M., and J. Chen. 2001. Histone H2AX is phosphorylated in an ATR-dependent manner in response to replicational stress. *J. Biol. Chem.* 276:47759–47762.
191. Wiltzius, J.J., M. Hohl, J.C. Fleming, and J.H. Petrini. 2005. The Rad50 hook domain is a critical determinant of Mre11 complex functions. *Nat. Struct. Mol. Biol.* 12:403–407.
192. Wood, J.L., N. Singh, G. Mer, and J. Chen. 2007. MCPH1 functions in an H2AX-dependent but MDC1-independent pathway in response to DNA damage. *J. Biol. Chem.* 282:35416–35423.
193. Wu, X., V. Ranganathan, D.S. Weisman, W.F. Heine, D.N. Ciccone, T.B. O'Neill, K.E. Crick, K.A. Pierce, W.S. Lane, G. Rathbun, D.M. Livingston, and D.T. Weaver. 2000. ATM phosphorylation of Nijmegen breakage syndrome protein is required in a DNA damage response. *Nature.* 405:477–482.

194. Wyman, C., D. Ristic, and R. Kanaar. 2004. Homologous recombination-mediated double-strand break repair. *DNA Repair (Amst.)*. 3:827–833.
195. Xiao, A., H. Li, D. Shechter, S.H. Ahn, L.A. Fabrizio, H. Erdjument-Bromage, S. Ishibe-Murakami, B. Wang, P. Tempst, K. Hofmann, D.J. Patel, S.J. Elledge, and C.D. Allis. 2009. WSTF regulates the H2A.X DNA damage response via a novel tyrosine kinase activity. *Nature*. 457:57–62.
196. Xie, A., N. Puget, I. Shim, S. Odate, I. Jarzyna, C.H. Bassing, F.W. Alt, and R. Scully. 2004. Control of sister chromatid recombination by histone H2AX. *Mol. Cell*. 16:1017–1025.
197. Xie, A., A. Kwok, and R. Scully. 2009. Role of mammalian Mre11 in classical and alternative nonhomologous end joining. *Nat. Struct. Mol. Biol.* 16:814–818.
198. Xu, Y., T. Ashley, E.E. Brainerd, R.T. Bronson, M.S. Meyn, and D. Baltimore. 1996. Targeted disruption of ATM leads to growth retardation, chromosomal fragmentation during meiosis, immune defects, and thymic lymphoma. *Genes Dev.* 10:2411–2422.
199. Yang, Q., R. Riblet, and C.L. Schildkraut. 2005. Sites that direct nuclear compartmentalization are near the 5' end of the mouse immunoglobulin heavy-chain locus. *Mol. Cell Biol.* 25: 6021–6030.
200. Yin, B., V. Savić, M.M. Juntilla, A.L. Bredemeyer, K.S. Yang-Iott, B.A. Helmink, G.A. Koretzky, B.P. Sleckman, and C.H. Bassing. 2009. Histone H2AX stabilizes broken DNA strands to suppress chromosome breaks and translocations during V(D)J recombination. *J. Exp. Med.* 206:2625–2639.
201. Zgheib, O., K. Pataky, J. Brugger, and T.D. Halazonetis. 2009. An oligomerized 53BP1 tudor domain suffices for recognition of DNA double-strand breaks. *Mol. Cell Biol.* 29:1050–1058.
202. Zha, S., J. Sekiguchi, J.W. Brush, C.H. Bassing, and F.W. Alt. 2008. Complementary functions of ATM and H2AX in development and suppression of genomic instability. *Proc. Natl. Acad. Sci. USA*. 105:9302–9306.
203. Zhang, X., J. Succi, Z. Feng, S. Prithivirajasingh, M.D. Story, and R.J. Legerski. 2004. Artemis is a phosphorylation target of ATM and ATR and is involved in the G2/M DNA damage checkpoint response. *Mol. Cell Biol.* 24:9207–9220.
204. Zhou, L., R. Mitra, P.W. Atkinson, A.B. Hickman, F. Dyda, and N.L. Craig. 2004. Transposition of hAT elements links transposable elements and V(D)J recombination. *Nature*. 432:995–1001.
205. Ziv, Y., D. Bielopolski, Y. Galanty, C. Lukas, Y. Taya, D.C. Schultz, J. Lukas, S. Bekker-Jensen, J. Bartek, and Y. Shiloh. 2006. Chromatin relaxation in response to DNA double-strand breaks is modulated by a novel ATM- and KAP-1 dependent pathway. *Nat. Cell Biol.* 8:870–876.
206. Zou, L., and S.J. Elledge. 2003. Sensing DNA damage through ATRIP recognition of RPA-ssDNA complexes. *Science*. 300:1542–1548.